Unione Europea

PON Ricerca e Innovazione 2014- 2020

Ministero dell'Istruzione, dell'Università e della Ricerca

Dottorato di Ricerca in Ingegneria dei Prodotti e dei Processi Industriali

Rigid polyurethanes foaming with CO_2 as physical blowing agent

Maria Rosaria Di Caprio

PhD in *Industrial Product and Process Engineering* (XXX Cycle)

Department of Chemical, Material and Industrial Production Engineering

University of Naples FEDERICO II

PhD Supervisors: Prof. Ernesto Di Maio, Ing. Salvatore Iannace

PhD Coordinator: Prof. Giuseppe Mensitieri

Contents

Abstract

There is significant industrial interest in the development of innovative and efficient materials for thermal insulation applications. Indeed, the energy issues are becoming more and more important because of possible energy shortage in the future compounded by global warming. Moreover, regulations on thermal insulation in the household sector, building trade, aeronautics and gas transport are becoming ever stricter. One of the solutions to these issues is to fabricate materials with very low thermal conductivity. Many cellular materials are used in thermal insulation to take advantage of the good insulation capacity of some gases, in particular rigid polyurethane foams. The thermal conductivity of these polymers can become lower than the relevant gas, because of the Knudsen effect that limits the heat conduction via a confined gaseous phase. Fabrication of low density material within which the gas mobility is restricted is a challenge in terms of obtaining a very low thermal conductivity material.

In this dissertation, the foaming of rigid polyurethanes by using high pressure carbon dioxide (CO_2) as physical blowing agent was investigated starting from the knowledge of the behavior of the whole system in the presence of CO_2. The study of CO_2 sorption in the polymeric precursors of rigid polyurethane foam (polyol and isocyanate), by using a coupled gravimetry-Axisymmetric Drop Shape Analysis, was conducted to design the process and the equipment and to optimize the foaming. In particular, to address the recent interest in combining the gas (physical) foaming with the classical (chemical) polyurethane foaming, a novel instrumented pressure vessel was designed for studying: i) gas sorption under high pressure on the different reactants, kept separate and ii) synthesis under high gas pressure, upon mixing, by spectroscopic investigation and iii) foaming upon release of the pressure. In the literature, no papers addressed the use of CO_2 as a physical blowing agent in polyurethane foams (as well as in other thermosetting polymers), where CO_2 solubilization is conducted in both the reactants before mixing in lab-scale. Furthermore, in industrial processes, typically liquid CO_2 is mechanically mixed (not solubilized) under pressure in polyurethane foam reactants to froth the mixture by release pressure.

The two novelties, shown in this thesis, are the possibility to solubilize the gas (1) as physical blowing agent (2) in both the reactants of a polyurethane foam before the mixing.

As results, from sorption measurements the maximum value of CO_2 pressure usable for foaming experiments was defined, in order to avoid extraction of low molecular weight fractions of the polymeric precursors in CO_2. Rigid polyurethane foams obtained during this Ph.D. are described in terms of their morphology.

In conclusion, the developed lab-scale apparatus allows to obtain rigid polyurethane foams by solubilizing CO_2, as physical blowing agent, both in polyol and isocyanate. By optimizing some chemical and processing parameters is possible to control the morphology and so the thermal conductivity of the final foam.

In the first part of this thesis, an overview of the current chemistry and foaming processes used in the production of rigid polyurethane foam are reported. The main part will be occupied by the description of CO_2 solubility measurements, of the new equipment to study sorption, synthesis and foaming of rigid polyurethane foams and of experimental results.

Chapter 1: Introduction

This chapter introduces concepts, which will be used in Chapter 2-5 to describe the current state of the art in the production of rigid polyurethane foams and the results achieved during the Ph.D. by using CO_2 as physical blowing agent. The reader will be introduced to the rigid polyurethane foaming science focusing the attention on their insulation properties and the possibility to improve it. Moreover, the objective will be fully clarified in the second paragraph and a general overview of the all manuscript will be given in the end of this chapter.

1.1. Rigid polyurethane foams

Rigid polyurethane foams (PURs) are closed-cell foamed plastic materials with excellent thermal insulating properties, used as a factory made material in the form of insulation boards or blocks, or in combination with various rigid facings for appliances as a construction and domestic material. In addition to the low thermal conductivity, PURs are stable and durable, which is an important feature to guarantee the stability of the insulating properties. In fact, in building applications, these materials must work for as long as the building stands and should have a useful life beyond 50 years [1]. The thermal insulation properties of PURs are due to the presence of closed micro-cells, filled with inert gases, which work, at micron scale, as insulated glazing do at macroscopic scale in reducing heat transfer in buildings. Figure 1a,b shows typical microstructures of closed-cell rigid and open cell flexible polyurethane foams, as seen in a scanning electron microscope (SEM). These cell structures present flat faces and straight edges that are defined by struts and windows and could be connected by continuous closed space where the compartments are isolated from each other (Figure 1a) or void spaces where air can pass freely (Figure 1b).

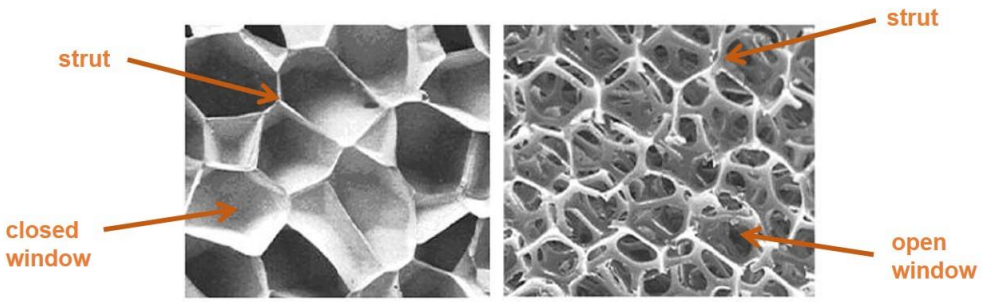

Figure 1: SEM micrograph of (a) a closed-cell rigid polyurethane foam and (b) of an open-cell flexible polyurethane foam.

Thermal conductivities, depending on the total gas content (void volume fraction), on the pore topology (foam morphology) and on the thermal conductivities of both the polymer matrix and the gas, may reach values as low as 18 mW/(m K) [2]. Until recently, the inert gas most commonly used in polyurethane foams was R-11 (trichlorofluoromethane, CFC-11). However, the Montreal Protocol on substances that deplete the ozone layer has called for the phasing out of the use of chlorofluorocarbons (CFCs) and their replacement with hydrocarbons (HCs) and hydrofluorocarbons (HFCs).

The foamed structure of PURs is obtained by the simultaneous polymerization (gelling) reaction between polymeric precursors (polyol and isocyanate) and gas generation, which can result from a physical, chemical or mechanical process. In physical foaming, a fluid such as hydrocarbons (mainly cyclopentane) or hydrofluorocarbons, is first solubilized at high pressure in the polymeric precursors at ambient temperature and then it is allowed to evolve from the solution by pressure quench (in this case, no chemical reaction involves the blowing process and the fluid is called physical blowing agent (PBA)). In chemical foaming, the blowing agent is generated from a chemical reaction. Typically, the addition of water in the formulation allows for the reaction of water with isocyanate, to give unstable carbamic acid that decomposes to amine and CO_2 as a by-product, which blows the polymer [2]. In mechanical foaming, the gas, most commonly air, is dispersed into the starting components by vigorous agitation, which leaves entrapped air bubbles within the polymeric matrix. Most commonly, both PBA and water are used, in a combined chemical and physical foaming manner, The addition of water has to be finely controlled, as its reaction with the isocyanate may give polyurea as a by-product, which has detrimental effects on some physical and mechanical properties of the final foamed products, such as the stiffness and the strength, and has negative effects on processability [3].

1.2. Objective of the thesis

In the field of PURs, there is a large interest to improve their thermal insulation properties in order to reduce the energy consumption in appliances as building and domestic households. Currently typical PURs are characterized by cell size higher than 100 μm, thermal conductivity around 18 mW/m K at 10°C and density 0.1-0.2 g/cm^3. Furthermore, due to the restrictions imposed by the Montreal Protocol on ozone-depleting substances (e.g. chlorofluorocarbon (CFC) and the necessity to replace flammable hydrocarbon (HC) (e.g. cyclopentane), the use of CO_2 as PBA could be a possible alternative.

Therefore, in the context to reduce thermal conductivity of the PURs and to meet the environmental requests, the aim of this thesis has been to generate know–how on the foaming of rigid polyurethane by using CO_2 at high pressure, as PBA, through the two following points:

-the study of CO_2 solubility in the polymeric precursor (polyol and isocyanate) of the PURs in order to design the process and the equipment and to optimize the foaming.

-the design of an experimental setup for the study of rigid polyurethane foaming process by using CO_2 at high pressure, in order to obtain foams with reduced thermal conductivity and density in comparison to the current PURs.

Actually, CO_2 is the most favorable foaming agent because of its unique properties. In particular, CO_2 is environmentally friendly and offers a long-term sustainable solution, due to its zero Ozone Depletion Potential (ODP) and its lowest Global Warming Potential (GWP), set equal to 1 as reference to other Green-House-Gases (GHG). Furthermore, CO_2 is non-flammable and is inexpensive, as it is readily available in the atmosphere and other natural sources [1]. Even if CO_2 is characterized by a thermal conductivity higher than other PBAs, its use at high pressures allows to reduce the thermal conductivity of a foam by decreasing the cell size (Knudsen effect for cell size < 10 μm). High pressure CO_2 was extensively already used to create thermoplastic microfoams whether in continuous or in batch processes, as reported in many papers. Considerable effort has been made to optimize the foaming process to decrease the cell size and increase the cell density [4,5]. Park et al. [6,7] studied the effects of processing pressure when the maximum amount of CO_2 was injected into a high impact polystyrene (HIPS) melt at each processing pressure. Cell density was found to increase nearly linearly with pressure drop, pressure drop rate, and CO_2 content. Foaming of PMMA has been studied by Goel and Beckman [8–10], while Kumar and coworkers have studied foaming in the polycarbonate–CO_2 system [11]. McCarthy and coworkers [12] have recently reported on microcellular polystyrene foams processed in supercritical CO_2 ($scCO_2$); they studied the effects of cell size and orientation on the yield stress. Foaming of polypropylene has also been studied extensively [13,14], with the most recent report by Liang and Wang [15], who highlighted the effect of temperature drop during depressurization of the polymer in equilibrium with high-pressure CO_2. An interesting development in this field made by Handa and coworkers [16] was the preparation of a very fine structure of foamed PMMA with an average cell size of 0.35 microns and cell density of 4.4×10^{13} cells/g. The authors utilized the phenomenon of retrograde vitrification documented earlier

by Condo and Johnston [17,18]. Handa and Kumar [19] have also recently reported the analysis of foaming glycol-modified PET (PETG) with $scCO_2$. Another approach to create microcellular materials was demonstrated recently by Beckman and coworkers [20]. First, they synthesized a number of chemicals soluble in $scCO_2$ or liquid CO_2. These chemicals comprise a number of "monomers" containing one or two urea groups and fluorinated "tail" groups that enhance solubility of these compounds in CO_2. When these compounds were dissolved in CO_2, their self-association led to the formation of gels. The removal of CO_2 via depressurization resulted in the formation of foams with cells with an average diameter of less than 1 μm. CO_2-assisted foaming of biodegradable polymers, such as poly(lactide- *co*-glycolide) (PLGA) copolymer [21], represents an exciting opportunity in the formation of sponge scaffolds for medical applications. Indeed, this approach was used to generate high-surface-area fibrillar scaffolds that were then used to generate liver tissue [22]. In thermosetting foams, CO_2 has been successfully adopted as a PBA to produce epoxy foams [23-25]. In these cases, CO_2 was solubilized at high pressure in the pre-mixed reactants of the epoxy formulation (*after* reactants mixing), kept at low temperature to avoid curing before a sufficient amount of the PBA was solubilized. At the end of the solubilization stage, a temperature increase activated the catalysts for the initiation of the resin curing. The CO_2 pressure release allowed the formation of the bubbles, in turn stabilized by the completion of the curing process. CO_2 was also used as PBA to obtain polyurethane foams (PUFs), starting from a formulation characterized by a very slow curing reaction [26]. Also in this case, CO_2 pressurization was performed *after* mixing of the reactants (namely, a polyol and an isocyanate), the slow curing allowing for sufficient solubilization of the PBA, eventually released for foaming [26]. In the literature, no papers addressed the use of CO_2 as a PBA in PUFs (as–well as in other thermosetting polymers), where CO_2 solubilization is conducted *before* reactants mixing. This would be useful when starting from a formulation characterized by a fast curing reaction, where no time is allowed for PBA solubilization after mixing. Nor it has been reported a method to use PBAs in thermosetting polymers whose reactivity cannot be halted at will. In the case of polyurethanes, in fact, the typical processing temperatures utilized in the industry to conduct PUFs synthesis are in the range 25-35°C and cooling would be required to slow down the curing. As an alternative, a change in the catalysts to slow down the curing would also be possible, as it has been done previously [23-26], but this would considerably alter the current formulations and methods and would be of limited scientific and industrial interest.
In this context, in the field of PURs, liquid CO_2 is nowadays used in the so-called frothing process, where it is mechanically mixed (not solubilized) under pressure with the PUFs reactants during their chemical reaction and the mixture is then frothed by pressure release [27]. In the latter case, CO_2 does

not behave as a PBA, but as a dispersed phase that expands upon pressure release. Foam morphologies, in this case, are controlled by the dispersion efficiency and not by the numerous variables and methods available to the gas foaming process.

An analysis of the influence of process parameters on the final morphology of rigid polyurethane foam, in the physical foaming with CO_2, was conducted in this thesis. Furthermore, a possible CO_2 effect on the reaction kinetics of the polymerization reaction was studied. These investigations give the possibility to design the material and the process to drive the foam to the desire final morphology. In this dissemination, CO_2 derives from the blowing reaction between isocyanate and water was referred to as CO_2 (water), has been distinguished from CO_2 solubilized under pressure, as PBA, in either the polyol or the isocyanate component.

This project was conducted in collaboration with DOW Chemical Italy s.r.l. that kindly has supplied a model formulation for PURs on which all the experiments of this dissertation were conducted.

1.3. Overview of the thesis

The first chapter is an introduction to the current world of PURs in insulation appliances. The use of CO_2 as PBA is described in many polymer systems present in the literature and the objective of the thesis is explained.

In the second Chapter 2 the fundamentals of polyurethane foam formation are reported, in terms of its general chemistry, followed by the theory of bubble formation and the nucleation process. The theory of thermal insulation is reviewed highlighting the current problems facing industry with regards to rigid polyurethane foam as an insulation material.

Chapter 3 concerns the study of CO_2 solubilization at high pressure in the two components of a rigid polyurethane foam (polyol and isocyanate), by using a modified Magnetic Suspension Balance based on coupled sorption-Axisymmetric Drop Shape Analysis (ADSA) for fully experimentally and concurrently measurement of solubility, mutual diffusivity, specific volume and interfacial tension of polyol/CO_2 and isocyanate/CO_2 solutions at 35°C.

The design of experimental setups for the study of gas sorption and polyurethane synthesis and foaming process of rigid polyurethane by using CO_2 as PBA are described in Chapter 4. Furthermore, experimental results obtained with this new apparatus are shown.

In Chapter 5, a focus box on the study of the effect of CO_2 pressure on the reaction kinetics of the polymerization reaction by spectroscopy investigation is reported.

In the “Conclusions e future developments” Chapter are resumed all the main results of the current Ph.D. and possible future works.

1.4. References

[1] D. Randall, S. Lee. The Polyurethanes Book, J. Wiley, New York, 2002.

[2] K. H. Choe, D. S. Lee, W. J. Seo, W.N. Kim. Properties of rigid polyurethane foams with blowing agents and catalysts. *Polym. J.* 36 (2004) 368.

[3] E. Occhiello, P. Golini. Process for producing rigid polyurethane foams and finished articles obtained therefrom. U.S. Patent 20,040,092,616, May 13, 2004.

[4] D. L. Tomasko, H. Li, D. Liu, X. Han, M. J. Wingert. L. J. Lee, K. W. Koelling. A Review of CO_2 Applications in the Processing of Polymers. *Ind. Eng. Chem. Res.* 42 (2003) 6431.

[5] S. G. Kazarian. Polymer Processing with Supercritical Fluids. *Polym. Sci. Ser. C*, 42 (2000) 78.

[6] C. B. Park, D. F. Baldwin, N. P. Suh. Effect of the pressure drop rate on cell nucleation in continuous processing of microcellular polymers. *Polym. Eng. Sci.* 35 (1995) 432.

[7] C. B. Park, N. P. Suh, D. F. Baldwin. Method for Providing Continuous Processing of Microcellular and Supermicrocellular Foamed Materials. U.S. Patent 5,866,053, Apr 18, 1999.

[8] S. K. Goel, E. J. Beckman. Generation of microcellular polymeric foams using supercritical carbon dioxide. II: Cell growth and skin formation. *Polym. Eng. Sci.* 34 (1994) 1148.

[9] S. K. Goel, E. J. Beckman. Generation of microcellular polymeric foams using supercritical carbon dioxide. I: Effect of pressure and temperature on nucleation. *Polym. Eng. Sci.* 34 (1994) 1137.

[10] S. K. Goel, E. J. Beckman. Nucleation and growth in microcellular materials: Supercritical CO_2 as foaming agent. *AIChE J.* 41 (1995) 357.

[11] V. Kumar, J. E. Weller. Microcellular polycarbonate. Part I. Experiments on bubble nucleation and growth. *ANTEC*, 1991, 1401.

[12] K. A. Arora, A. J. Lesser, T. J. McCarthy. Compressive behavior of microcellular polystyrene foams processed in supercritical carbon dioxide. *Polym. Eng. Sci.* 38 (1998) 2055.

[13] C. B. Park, L. K. Cheung. A study of cell nucleation in the extrusion of polypropylene foams *Polym. Eng. Sci.* 37 (1997) 1.

[14] J. S. Colton, N. P. Suh. Nucleation of microcellular foam: Theory and practice. *Polym. Eng. Sci.* 27 (1987) 500.

[15] M. T. Liang, C. M. Wang. Production of Very Low Density Microcellular Polypropylene by Supercritical Carbon Dioxide. Proceedings of the 6th Meeting on Supercritical Fluids: Chemistry and Materials, Nottingham (UK), 1999, 151.

[16] Y. P. Handa, Z. Zhang. A new technique for measuring retrograde vitrification in polymer–gas systems and for making ultramicrocellular foams from the retrograde phase. *Polym. Sci., Part B: Polym. Phys.* 38 (2000) 716.

[17] P. D. Condo, K. P. Johnston. In situ measurement of the glass transition temperature of polymers with compressed fluid diluents. *J. Polym. Sci., Part B: Polym. Phys.* 32 (1994) 523.

[18] P. D. Condo, I. C. Sanchez, C. G. Panayiotou, K. P. Johnston. Glass Transition Behavior Including Retrograde Vitrification of Polymers with Compressed Fluid Diluents *Macromolecules* 25 (1992) 6119.

[19] Y. P. Handa, B. Wong, Z. Zhang, V. Kumar, S. Eddy, K. Khemani. Some thermodynamic and kinetic properties of the system PETG-CO_2, and morphological characteristics of the CO_2-blown PETG foams. *Polym. Eng. Sci.* 39 (1999) 55.

[20] C. Shi, Z. Huang, S. Kilic, J. Xu, R. M. Enick, E. J. Beckman, A. J. Carr, R. E. Melendez, A. D. Hamilton. The gelation of CO_2: a sustainable route to the creation of microcellular materials. *Science* 286 (1999) 1540.

[21] D. Sparacio, E. J. Beckman. Generation of Microcellular Biodegradable Polymers Using Supercritical Carbon Dioxide. *Polym. Prepr.* 38 (1997) 422.

[22] J. A. Hubbell, R. Langer. Tissue engineering *Chem. Eng. News* 73 (1995) 42.

[23] L. M. Bonnaillie, R. P. Wool. Thermosetting foam with a high bio-based content from acrylated epoxidized soybean oil and carbon dioxide. *J. Appl. Polym. Sci.*105 (2007) 1042.

[24] A. Ito, T. Semba, K. Taki, M. Ohshima. Effect of the Molecular Weight between Crosslinks of Thermally Cured Epoxy Resins on the CO_2-Bubble Nucleation in a Batch Physical Foaming Process. *J. Appl. Polym. Sci*. 131 (2014) 40407.

[25] Q. Ren, S. Zhu. One-Pack Epoxy Foaming with CO_2 as Latent Blowing Agent. *ACS Macro Lett.* 4 (2015) 693.

[26] K. L. Parks, E. J. Beckman. Generation of microcellular polyurethane foams via polymerization in carbon dioxide. II: Foam formation and characterization. *Polym. Eng. Sci.* 36 (1996) 2417.

[27] C. Fiorentini, A. C. Murray Griffiths. Froth process for continuous manufacture of polyurethane foam slab-stocks, U.S. Patent 5,665,287, Sep 9, 1997.

Chapter 2: Principle and chemistry of rigid polyurethane foams

This chapter introduces basic concepts, which will be used in the following Chapters, in order to introduce the reader to the rigid polyurethane foaming science.

2.1. Basic chemistry

The production of a rigid polyurethane foam is a complex process involving many components and at least two competing reactions [1]:

1) The polymerization reaction (addressed to, typically, as “gelling” or “curing” reaction) which occurs between an isocyanate and a polyol according to a polyaddition reaction to give polyurethane polymer as follows:

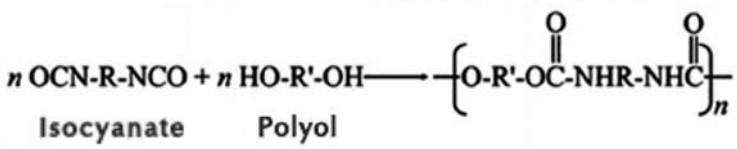

(2.1)

2) The blowing reaction which occurs between isocyanate and water (typically added in little percentage in the polyol) to give a thermally unstable carbamic acid that spontaneously decomposes to amine and CO_2 as a by-product, eventually inflating the polymer.

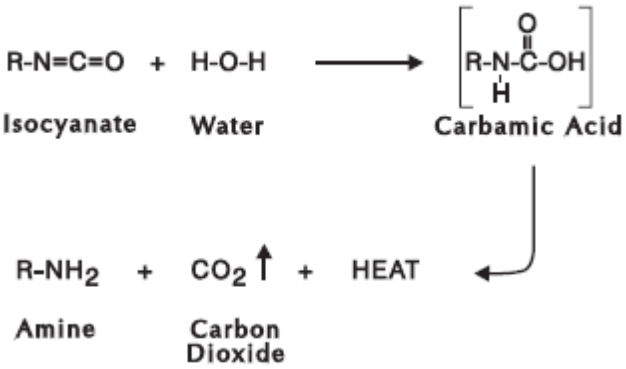

(2.2)

These two exothermic reactions take place simultaneously in presence of catalysts, surfactants and blowing agents.

Furthermore, side reactions occur in the chemical system in presence of an excess of isocyanate. The reaction of the amine with isocyanate gives a disubstituted urea.

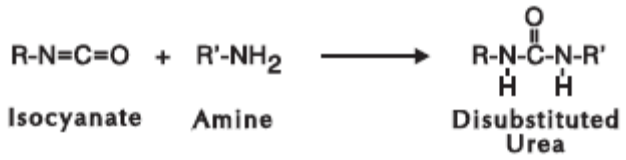

(2.3)

The isocyanate can also reacts with a disubstituted urea to form biuret (2.4) and with urethane to give allophanate (2.5)

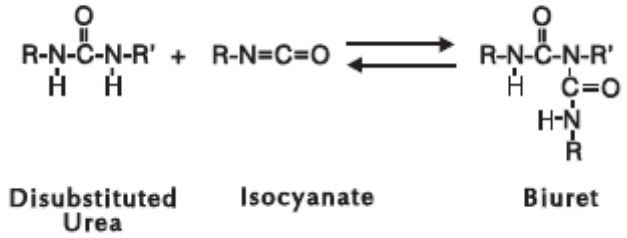

(2.4)

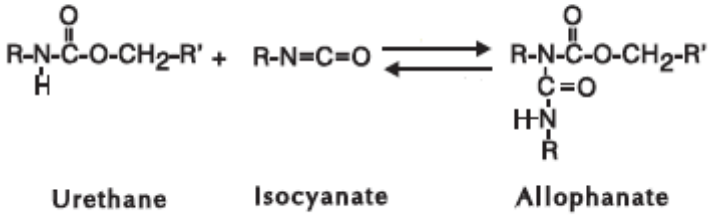

(2.5)

Isocyanate also can undergo to dimerization (2.6) and trimerization (2.7) reactions:

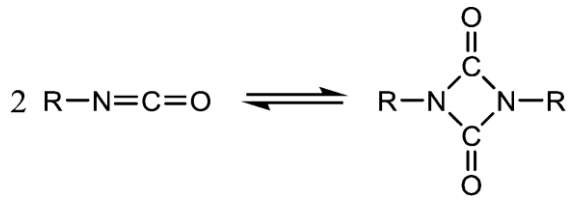

(2.6)

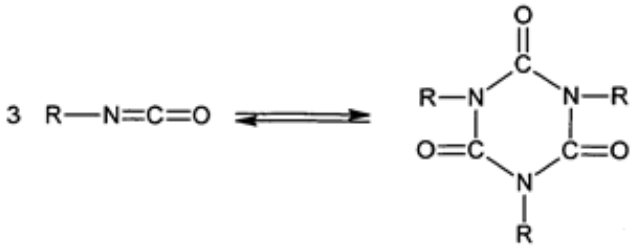

(2.7)

2.2. Principal polyurethane foam components

Rigid polyurethane foam recipes normally contain a host of ingredients selected to aid in achieving the desired final properties of foam. Following the common chemicals used in the production of rigid polyurethane foam are described.

2.2.1. Polyols

Polyols are a source of hydroxyl (OH) or other isocyanate reactive groups. Processing and properties of the resultant foam can be markedly influenced by the choice of starting polyol structure. Polyols mainly used for PURs are low molecular weight hydroxyl terminated polyethers, polyesters and natural products (e.g. castor oil) [2]. Polyether polyols are produced by addition of 1,2-propylene oxide (PO) and ethylene oxide (EO) to the hydroxyl group (or amino groups) of low molecular weight molecules, usually by anionic chain mechanism. Polyester polyols are prepared by the polycondensation reaction of di-, or polycarbonic acid or their anhydrides (e.g. phthalic acid, phthalic anhydride) with di- and polyalcohols (e.g. ethylene glycol) [3].

2.2.2. Isocyanates

The isocyanate provides the source of NCO groups to react with functional groups from the polyol, water and other ingredients in the formulation. All the isocyanates used in the industry today contain at least two isocyanate groups per molecule. The phosgenation of amines represents the most commercially viable method of producing isocyanates as illustrate following:

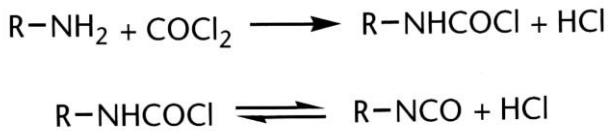

(2.8)

During the past toluene diisocyanate (TDI) (1 and 2) was used in field of PURs. Due to its high isocyanate content and high vapour pressure it was replace and, nowadays, polymeric isocyanates such as methylene diphenyl diisocyanate (PMDI) (3) are mainly used (Fig. 1) [2].

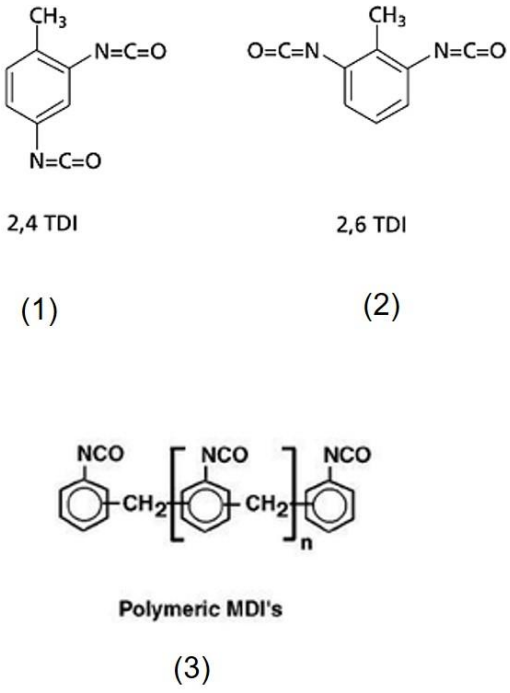

Fig. 1. Chemical structure of TDI isomers (1), (2) and of polymeric MDI's.

The amount of isocyanate required to react with a polyol is calculated in terms of stoichiometric equivalents:

$$Isocyanate\ Index = \frac{Actual\ amount\ of\ isocyanate\ used}{Theoretical\ amount\ of\ isocyanate\ required} \times 100 \quad (2.9)$$

Typically for PURs the recipes provides an excess of isocyanate in order to obtain the desired final properties.

2.2.3. Catalysts

All the commercially manufactured PURs are made with the aid of at least one catalyst. Of the many classes of compounds investigated, the amines and the organometallics have been found most useful. Various combinations of catalysts are used in order to establish an optimum balance between the polymerization and the blowing reaction. The polymer and gas formation rates must be balanced so that the gas is entrapped efficiently in the gelling polymer and the cell-walls develop sufficient strength to maintain their structure without collapse or shrinkage. Catalysts are also important for assuring completeness of reaction or "cure" in the finished foam.

The catalysts most commonly used are tertiary amines such as triethylamine, and alkali metal salts, e.g. potassium acetate. Some catalysts such as tertiary amines affect both the polymerization and the blowing reaction, while others like dibutyltin dilaurate promote primarily the polymerization reaction and chain propagation [4].

2.2.4. Blowing agents

Blowing agents are substances capable of producing a cellular structure in polymeric matrix via a foaming process. During the polymerization reaction they give rise to gas bubbles which inflate the polymer. According to the mechanisms of bubbles formation, blowing agents can be classified as follows:

- *Chemical blowing agents* produce gas by a chemical reaction, which involves some components of the polyurethane formulation. Azodicarbimides are used extensively in many plastics where the processing temperature causes chemical breakdown of the blowing agent to form gases, for instance nitrogen in this case [4]. This type of chemical blowing agent is

not often used in polyurethane process where foams are at least partially blown with CO_2 derives from the blowing reaction which occurs between isocyanate and water [5].

- *Physical blowing agents* are soluble additives (liquid or gas). They are not involved in chemical reactions and are mostly liquids with low boiling points, e.g. chlorofluorocarbons (CFCs), hydrochlorofluorocarbons (HCFCs), hydrofluorocarbon (HCFs) and hydrocarbons (HCs) (e.g. cyclopentane). They evaporate by the heat derives from the exothermic polymerization and blowing reactions.
  In the field of PURs, key factors for the choice of the PBAs are following listed [4]:

  - the gas thermal conductivity, which have to be very low in insulation applications;

  - ease of handling. The specific properties of blowing agents lead to different machine requirement. Flammable blowing agent, such as pentane, require suitable explosion-proof equipment, which has a higher cost than a conventional equipment, tougher with an appropriate extraction system. Blowing agent with boiling points lower than room temperature require special cooling or pressure feature;

  -the solubility of blowing agents in the foam matrix, which varies considerably, should be as low as possible since the combined effect of matrix plasticization and lowered cell gas pressure can also cause dimensional stability problems. The diffusivity rate out of the foam is low, but differs slightly for the different blowing agents;

  -cost effectiveness.

2.2.5. Surfactants

Polyurethane foams are made with the aid of nonionic, silicone-based surfactants. In broad terms, surfactants perform several functions. They:

- Lower surface tension;
- Emulsify incompatible formulation ingredients;
- Promote nucleation of bubbles during mixing;
- Stabilize the rising foam by reducing stress concentrations in thinning cell-walls;
- Counteract the defoaming effect of any solids added to or formed; e.g., precipitated polyurea structures, during the foam reaction.

Among these functions, stabilization of the cell-walls is the most important. By doing this, the surfactant prevents the coalescence of rapidly growing cells until those cells have attained sufficient strength through polymerization to become self-supporting. Without this effect, continuing cell coalescence would lead to total foam collapse. Surfactants also help to control the precise timing and the degree of cell-opening. Within each foam formulation, a minimum level of surfactant is needed to produce commercially acceptable foam.

In the absence of a surfactant, a foaming system will normally experience catastrophic coalescence and exhibit the event known as boiling. With addition of a small amount of surfactant, stable yet imperfect foams can be produced. With increasing surfactant concentration, a foam system will show improved stability and cell-size control. At optimum concentrations, stable open-cell foams may be produced. At higher surfactant levels, the cell windows become overstabilized and the resulting foams are tighter with diminished physical properties [1].

Two of the more common surfactants used in polyurethane foams are dimethyl polysiloxane [6] and dimethylpolysiloxanepolyalkylene oxide copolymer [7], the latter being primarily used.

2.2.6. Lab-scale preparation of rigid polyurethane foams

Typically, the two components of PURs, the formulated polyol (contains catalysts, surfactants, blowing agents and water) and the PMDI, are mixed and simultaneously a stopwatch is starting in order to measure the following characteristic time intervals [4]:

1. Cream time: start of volume increase.
2. Gel time: the foam has developed enough gel strength due to the polymerization extension and corresponds to time when strings of polymer can be withdrawn by dipping a pointer into the foam mix.
3. Rise Time: end of increase in volume.
3. Tack-free time: the surface of the foam is no longer adhesive.
5. Curing: foaming is complete and the polyaddition product gels and solidifies.

2.3. Physical foaming: basic principle of foam formation

Most foamed polymers are produced by solubilizing a gas throughout a fluid polymer phase. The foaming process occurs through four stages following discussed [2]:

1. The gas dissolution stage
2. The cell nucleation / bubble formation stage
3. The foam growth stage
4. The bubble stability stage

2.3.1. The gas dissolution stage

The first step of the foaming process is to form a gas/polymer solution. There are two factors that need to be taken into account for this process: the maximum amount of gas soluble in the polymer at given conditions of temperature and pressure and the time the system takes to reach the equilibrium state (also, addressed to as "saturation" state). The amount of gas required to saturate a polymer is defined as the solubility of the gas in the polymer and may be expressed in terms of the concentration defined as the moles of gas divided by the volume of the polymer/gas solution or, alternatively in terms of the mass fraction defined as the mass of gas divided by the mass of the polymer/gas solution. The actual concentration of gas in a polymer is a critical variable in determining the cell morphology and it depends by the temperature and pressure and the couple polymer/gas. Attainment of the equilibrium state (gas saturation of the polymer) depends on the time allowed for the sorption process to reach equilibrium. Fick 's law is useful in the analysis of the gas dissolution process:

$$\bar{J} = -D\,\nabla C \tag{2.10}$$

which in scalar form, for component *x*, reads:

$$J_x = -D\frac{\partial C}{\partial x} \tag{2.11}$$

J_x is the mass flux in the x direction, D is the diffusion coefficient, C is the concentration of the dissolved gas and x is the space coordinate. As a consequence of the mass flux, the concentration may change and its time derivative is described by Fick's second law:

$$\frac{\partial C}{\partial t} = \frac{\partial}{\partial x}\left(D\frac{\partial C}{\partial x}\right) \tag{2.12}$$

2.3.2. The cell nucleation /bubble formation stage

The driving force for cell nucleation in a polymer is thermodynamic metastability, which is a sudden solubility change of the dissolved gas typically by saturation pressure or temperature change. If the bubbles are formed in an initial single phase the process is called *self-nucleation* or *homogeneous nucleation.* In the presence of a second phase such as additives (e.g. solid nucleating agents) or interface between two not miscible liquids, heterogeneous nucleation also occurs. The second phase plays the role of nucleation sites and reduces the nucleation energy while increasing the rate of nucleation [8]. The nucleation process is one of the most important in determining the morphology of the foam. The number and distribution of the nuclei can affect immensely the properties of the foam.

2.3.2.1. Classical nucleation theory

In the classical nucleation theory [9], nucleation presumably occurs in the new phase in the form of nucleus with a critical radius r_{cr}. In fact, only the nuclei whose radius is greater than the critical radius value spontaneously grow, otherwise they tend to coalesce.

The system free energy ΔG is the other main parameter, together r_{cr}, involved in the cell nucleation formation.

Homogeneous nucleation: At room temperature, the polymer/gas system tends to minimize its free energy:

$$\Delta G = \frac{-4\pi r^3 \Delta P}{3} + 4\pi r^2 \gamma \tag{2.13}$$

where r is the cell radius; γ the surface tension; ΔP the level of super-saturation i.e. pressure difference between the metastable solution and the nucleated phase of pure gas. The free energy reaches a maximum value when r = r_{cr} (ΔG(r_{cr})). The system tends to reduce its free energy: nuclei whose radius is lower than r_{cr} resorb, whereas those whose radius is larger than r_{cr} grow. When r=r_{cr}, the free energy derivative tends to zero, giving the following relation:

$$r_{cr} = \frac{2\gamma}{\Delta P} \qquad (2.14)$$

Therefore, the nucleation occurs when the energy barrier ΔG(r_{cr}) is crossed:

$$\Delta G_{hom} = \frac{16\pi\gamma^3}{\Delta P^2} \qquad (2.15)$$

Thermodynamic destabilization during the nucleation stage provides additional energy to the polymer/gas system, decreasing the ΔG(r_{cr}) and allowing cell formation. The highest reduction of free energy of critical nucleus formation is obtained when the cell surface curvature is low, i.e. a flat surface would be optimal.

Heterogonous nucleation: As previously described, the presence of fillers, impurities or spherulites in polymers give rise to another nucleation phenomenon, heterogeneous nucleation which appears in addition to homogeneous nucleation. In this case, due to a reduction factor *f* (*critical energy reduction factor*), the free energy ΔG(r_{cr}) decreases as follows:

$$\Delta G_{het} = \frac{\Delta G_{hom} f_{(m,w)}}{2} \qquad (2.16)$$

Factor f is correlated to the to the surface curvature; in particular it depends from $m=\cos\theta=(\gamma_{13}-\gamma_{23})/\gamma_{12}$ and $w=r/r_{cr}$ (relative curvature) where r is the radius of the particles, γ_{13},γ_{23} and γ_{12} are the interfacial tensions of polymer–nanoparticle, gas–nanoparticle and polymer-gas respectively and θ is the contact angle between the nucleated bubble, particles and polymer surface (Fig. 2).

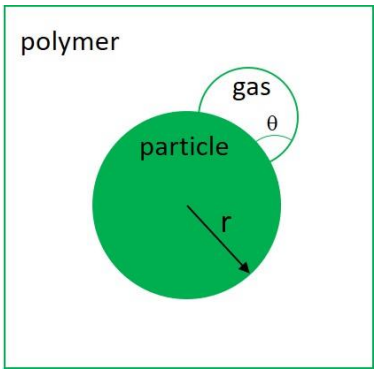

Fig. 2. Scheme of gas bubble nucleation on a particle with radius r .

According to the classical nucleation theory, the heterogeneous rate depends on the concentration of heterogeneous nucleation sites and the nucleation efficiency depends on the dispersion of filler inside the polymeric matrix which can be controlled through filler type, size and surface chemistry. Heterogeneous nucleation also happens when two liquids are not miscible. In this kind of chemical system, interfaces (where the formation of nuclei are easier) are generated when the two liquids get in contact due to the mixing.

2.3.3. The bubble growth stage

A bubble, once formed, may grow by diffusion of gas from liquid phase into bubble phase. An important consequence of the existence of a free surface energy in gas bubbles is the presence of a pressure difference across the curved gas-liquid interface. This pressure difference under a concave curved meniscus gives rise to the well-known capillary elevation effect on a liquid in a small tube. If the curved liquid surface fully encloses a volume of gas, a bubble results. The pressure excess of the gas in the bubble is given by the Laplace equation:

$$\Delta P = \frac{2\gamma}{r} \qquad (2.17)$$

where γ is the surface tension of the liquid and r the radius of the bubble. From this equation, it is evident that the pressure inside a bubble is inversely proportional to the radius of the bubble. In real foams there is always a distribution of bubble sizes, hence the pressures in different bubbles will

not be the same. This will lead to the diffusion of gas molecules from regions of higher pressure (the small bubbles) to regions of lower pressure (the large bubbles). The rate at which diffusion proceeds will be proportional to the pressure difference, the permeability and the thickness of the liquid film separating bubbles of unequal size. Therefore, all bubbles will grow or shrink depending on their diameter and the diameter of the bubbles in their environment. Initially, each large bubble is surrounded by many smaller ones and one concept for bubble growth would be the diffusion of gas from the smaller to the larger bubbles. A simplified case of one large and one small bubble is presented in Fig. 3.

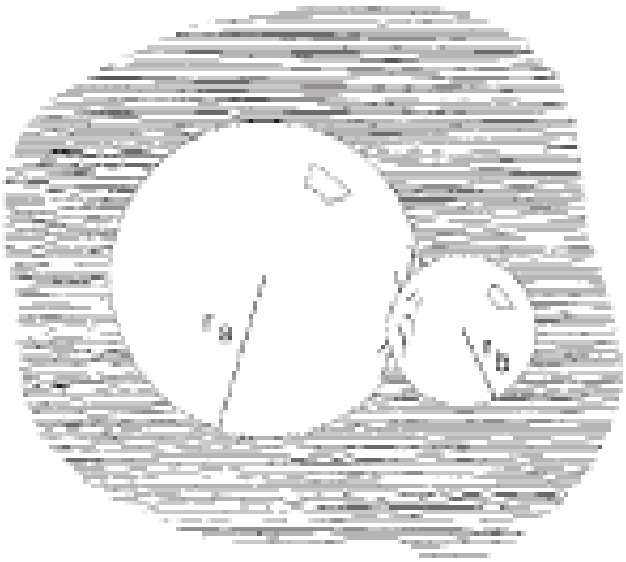

Fig. 3. Two different size bubbles [1].

The pressure difference between the gas in a small bubble and that of an adjacent larger bubble is given by:

$$\Delta P = P_b - P_a = 2\gamma \left[\frac{1}{r_b} - \frac{1}{r_a}\right] \qquad (2.18)$$

where r_b is the radius of the small bubble and r_a is the radius of the large bubble. Again, γ is the surface tension of the liquid. The radius of the large bubble, r_a, will be many times as large as that of the small bubble, r_b, and, for a first approximation, the term $1/r_a$ may be neglected. The pressure difference causing gas diffusion is then proportional to the pressure excess in the small bubble. The

rate at which a small bubble shrinks and disappears is then dependent mainly on its own radius and the permeability of the gas through the liquid separating adjacent bubbles [1].

2.3.4. The bubble stability stage

Bubble stability during growth is a complex function of surfactant effects, rate of gas evolution, viscosity, pressures and the presence of cell-disrupting agents. As the growing spherical cells are squeezed into polyhedra, the liquid phase is initially redistributed between the tetrahedral interstices and the bubble surfaces [1]. When a cell expands, the concentration of gas solubilized is reduced. This concentration may be restored by one of two processes: The surface layer can flow from areas of low surface tension to those of high surface tension (low concentration), or surfactant in the interior of the liquid can diffuse to the surface. In the first case, called the *Marangoni Effect*, the surface flow is believed to drag underlying layers of liquid along with it, thus restoring film thickness. This process thus enhances film elasticity and resilience. The second process, known as the *Gibbs Effect* replenishes surfactant concentration at the surface, but does not restore liquid to the film, hence it is not selfhealing. The temperature of the foam can also affect the stability. An increase in temperature reduces both viscosity and surface tension, making the thinning of membranes easier, and potentially leading to the rupture of membranes (cell walls) that are too thin to withstand existing stress. Conversely, a rise in temperature also increases reaction rates, which can be favorable in those foams where ultimate stabilization depends on further polymerization. Cell walls may be thinned by drainage due to gravity and capillary action, which sometimes can lead to excessive thinning, followed by rupture. In some cases the surfaces o f a very thin film attract each other by van der Waals forces, also favoring continuing thinning [10].

Polymeric foams are also stabilized by a rapid increase in viscosity. In polymerizing foam systems, polymerization proceeds at the same time as foaming, and reaction rates are catalyzed to give at least moderate molecular weight and viscosity by the time the foam rise is complete. Successful closed-cell foams are produced when the cell membranes are sufficiently strong (elastic) to withstand rupture at the maximum foam rise, and the modulus of the polymer is increased rapidly to a high level so that the cells are dimensionally stable in spite of the development of a partial vacuum within the cells. This is achieved most easily in relatively high-density foams or in highly cross-linked foams [11].

2.4. Thermal insulation of cellular materials

Thermal insulation is a feature of all expanded materials, in particular cellular structures with closed cells [12].

The factors that contribute to limit the thermal flux are:

-low volumetric fraction of solid phase;

-reduced cell dimensions;

-small conductivity of the gas trapped into the cell.

Thermal conductivity is defined by Fourier's law:

$$q = -\lambda \cdot \nabla T \tag{2.19}$$

where q is the thermal flux (heat amount passing through a unitary surface in a unitary time interval), λ is the thermal conductivity, T is temperature.

The thermal conductivity of a polymeric foam is given by four contributions [12-14]:

$$\lambda = \lambda_s + \lambda_g + \lambda_c + \lambda_r \tag{2.20}$$

in which:

-λs corresponds to the conduction through the solid phase;

-λg corresponds to the conduction through the gas-filled interior;

-λc corresponds to the convention within the cells;

-λr corresponds to the radiation through the cell walls.

When dealing with polymeric foams, the thermal conductivity properties are usually referred to the relative density ρ*/ρs, where ρ* is the foam density and ρs is the density of the not expanded polymer.

Solid conduction, λs, is due to two mechanisms: lattice vibrations, and translation of free conduction electrons. The free-electron contribution dominates in the energy transport in metals and the lattice vibration contribution is predominant in dielectric solids. The disordered dielectrics with no free electrons and considerable lattice imperfection are the poorest solid conductors of heat, and

consequently most porous insulations are made of materials such as glass or polymeric plastics. For a cellular polymeric material the conductivity through the solid phase λs is given by the product between the thermal conductivity of the monolithic bulk polymer, the relative density of the solid ρ*/ρs, and an efficiency factor that takes into account the shape of the cell walls [12]. Indeed the solid conduction takes place through the cell walls and membranes of the cells [14].

The contribution λs to the overall thermal conductivity is low (≈10% for polyurethane) for two reasons:

-the thermal conductivity of the plastic polymeric phase is intrinsically low (for the polyurethane it is 0.25 W/(m·K)) [12];

-the polymeric phase occupies a small fraction of the total volume of the foam.

The convection is relevant only when Grashof number is higher than about 1000. Grashof number describes the ratio between the convective force and the viscous force that is opposed to the convective flux:

$$Gr = \frac{g \cdot \beta \cdot \Delta T_c \cdot l^3 \cdot \rho^2}{\mu^2} \qquad (2.21)$$

Where *g* is the gravitational acceleration, β is the thermal expansion coefficient of the gas, ΔTc is the temperature difference in a cell, *l* is cell dimension, ρ is the gas density, μ is the dynamic viscosity of the gas.

Setting Gr =1000 and replacing the values of the other parameters of the cell gas define the minimum cell size for convection, *lmin*. For example, if it is considered air at pressure of 1 atm and room temperature (ρ=1 kg/m^3, μ=2x10-5 Ns/m^2, ΔTc=10°C, T=300 K) and ideal gas behavior (β=1/T) the value of *lmin* obtained is 10 mm. The result is not sensitive to the precise values of the variables. Most polyurethane foams have closed cells about one order of magnitude smaller than this, and therefore, heat transfer due to convection (λc) is negligible [12].

The radiation contribution, λr, depends on the cell dimensions and on the wall thickness; foams composed of many small cells transfer less heat by radiation than foams with few big cells. Valenzuela showed that published heat transfer models underestimated foam effective thermal conductivity if the contribution due to radiation was not considered. Cunningham et al. and Glicksman et al. indicated that the radiation contribution could account for approximately 30% of the measured effective conductivity at room temperature: it is a not negligible part of the thermal conductivity of the foam; λr increases exponentially with decreasing ρ*/ρs [2,12,13].

However conduction in the cell gas mixture, λg, stands for the main part of the thermal conductivity of a foam: this contribution is equal to the product between the gas conductivity and the relative density of the gas in the foam (1- ρ*/ρs) [12]. It is worth noting that conduction and radiation can be treated independently for this optically thick medium [14].

The thermal conductivity due to conduction in the cell gas mixture for low pressure can be calculated using the Wassiljeva equation:

$$\lambda_m = \sum_{i=1}^{n} \frac{y_i \lambda_i}{\sum_{j=1}^{n} y_j A_{ij}} \qquad (2.22)$$

where λm is the thermal conductivity of the mixture, λi is the thermal conductivity of pure component i, (yi,yj) are the mole fractions of components i and j and Aij is a function of the binary system that is equal to 1.

Maxon and Saxena suggested that Aij could be expressed as:

$$A_{ij} = \frac{\varepsilon\left[1+\left(\frac{\lambda_{tri}}{\lambda_{trj}}\right)^{1/2}\cdot\left(\frac{M_i}{M_j}\right)^{1/4}\right]^2}{\left[8\left(1+\frac{M_i}{M_j}\right)\right]^{1/2}} \qquad (2.23)$$

where Mi is the molecular weight (g/mol) of component i, λtr is the monatomic value of the thermal conductivity and ε is a numerical constant close to unit [16].

Table 1 reports the thermal conductivities of the gases obtained by physical or chemical expansion [17-21].

Table 1 Thermal conductivity of cell filling gases

Gas	λ ,W/(m K) a 25°C e 1 atm
CO_2	0.0166
CCl_3F (R11)	0.0078
CF_2Cl_2 (R12)	0.0097
Normal-pentane	0.0152
Air	0.0253
Cyclo pentane	0.0118
Isopentane	0.0141
CH_2FCF_3	0.0138

In addition, gas thermal conductivity increases as the temperature rises (Fig.4). This explains why the thermal conductivity of a specimen, for the same temperature gradient, increases with increasing average temperature between the two faces.

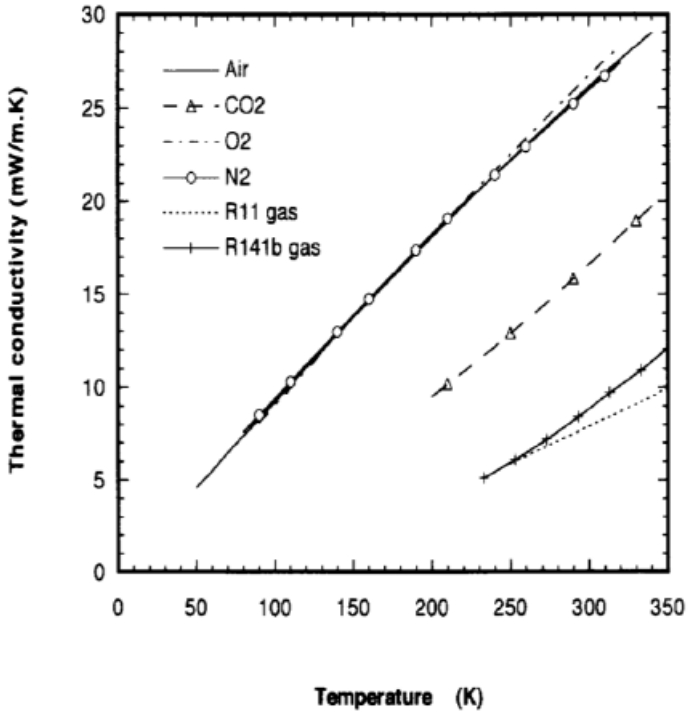

Fig.4. Variation of the thermal conductivity of some gases with the temperature

2.4.1. Knudsen effect and heat transfers

The gas conductivity can be decreased by decreasing the pore size of the material. The collisions between the gas molecules and the solid are elastic which transfer small amounts of energy compared to the collisions between gas molecules. Smaller pores/cells lead to a higher probability of collisions with pore walls instead of other gas molecules. This is called the Knudsen effect where the gas conductivity, λg, is governed by eq. (2.24) based on the Knudsen number, *Kn*, calculated by eq. (2.25) [22].

$$\lambda_g = \frac{\lambda_{g0}}{1 + 2\alpha K_n} \tag{2.24}$$

$$K_n = \frac{l_{mean}}{\delta} \tag{2.25}$$

where δ is the characteristic cell size, which can be interpreted as the distance between two parallel walls, l_{mean} is the mean free path, λg0 is the conductivity of the gas when moving freely and α is a constant for the effectiveness of the energy transfer between the gas molecules and the solid pore walls with a value commonly between 1.5 and 2 [22].

The gas conductivity is strongly dependent on the ratio between the pore size and the mean free path of the gas inside of the pores. The mean free path, l_{mean}, is the average distance a molecule travels before colliding with another molecule. The distance can be calculated by eq (2.26).

$$l_{mean} = \frac{k_B T}{\sqrt{2} \cdot \sigma \cdot P_g} \tag{2.26}$$

where T is the temperature, P_g is the gas pressure, σ is the molecular cross-sectional area and k_B is the Boltzmann constant. Therefore, from these equation is clear that both the reduction of cell

size and of gas pressure have increase the Knudsen number and thereby decrease the thermal conductivity of the gas.

2.5. Blowing agents for rigid polyurethane foams: focus box

The market of PURs has been impacted by, not only ozone depletion issues, but also by national or regional energy efficiency mandates, chemical restrictions (such as halogen free),'eco-label' requirements, etc. Energy efficiency requirements continue to play a significant role in blowing agent selection in the USA. Eco-label requirements, currently active in parts of Europe, encompass chemical restrictions and energy efficiency. Blowing agent emission levels within the appliance and their impact on food safety need to be considered too [5].

2.5.1. Low ODP blowing agent technologies

Many systems which replaced up to 50% of the total blowing from CFC-11 to CO_2 (water) with minimal impact on energy consumption were developed using new optimized components and λ-factor improvement technology in the late 1980s. Foams blown with low boiling blowing agents (LBBAs), such as HCFC as the sole PBAs have been evaluated and are being used in a few cases [5].

2.5.2. Zero ODP technologies

Environmental issues in play in the early 1990s, such as halogen-free foam and a push to use zero ODP blowing agent, led many European appliance manufacturers to use cyclopentane as early as 1993. Currently, cyclopentane alone or in mixtures with lower boiling hydrocarbons are widely used blowing agents in Europe, Japan, Australia and many other. Such wide use has been possible because foaming equipment manufacturers have developed features that can allow appliance moulders to use highly flammable hydrocarbon gas safely. This has involved the development and use of specific pre-blending stations, storage tanks, metering machines, foaming fixtures, ventilation equipment, gas monitoring networks, alarms, etc. Further studies, along the same line, have led to the development of formulations using *iso*-pentane and/or *n*-pentane. Even though hydrocarbons have been in wide use, they have not emerged as the preferred zero ODP option for the USA. Combinations of capital conversion cost and high insurance cost have made them less desirable. Through the various comparative studies, HFC has emerged as the leading zero ODP candidate for the USA [5]. An option

that has been evaluated in Western Europe, Japan and the USA has been the use of vacuum insulation panel (VIP). One route to make such panel is to encapsulate sheets of fully open celled rigid PU foam into gas tight film, under vacuum [23]. The vacuum panels require suitable getter systems to absorb various gas sources in the panel, such as residual blowing agent in foam, ingressed air, etc. Such vacuum panel is put in place in an appliance using all CO_2 (water) blown foam with superior flow performance, lower pressure and exotherm [23]. The relatively high cost of making VIPs, even when scaled up to mass production, coupled with the additional labor to install them, makes the use of VIPs an exception despite potential to get high energy efficiency.

2.6. References

[1] R. Herrington, K. Hock. Flexible polyurethane foams, Dow Chemical, 1997.

[2] D. Klempner, V. Sendijarevic. Polymeric Foams and Foam Technology. Hanser Publishers, 2004.

[3] J. H. Saunders, K. C. Frisch. Polyurethane: Chemistry and Technology; Vol. XVI, Part II Technology Interscience Publishers, 1964.

[4]D. Randall, S. Lee. The Polyurethanes Book, J. Wiley, 2002.

[5] S. N. Singh. Blowing Agents for Polyurethane Foams, Report 142, Volume 12, Number 10, Rapa Review Reports, 2002.

[6] A. Prins. Surface Rheology and Practical Behaviour of Foams and Thin Liquid Films. *Chem. Ing. Tech.* 64 (1992) 73.

[7] J.S. Colton, N.P. Suh. The nucleation of microcellular thermoplastic foam with additives: Part I: Theoretical considerations. *Polym. Eng*. 27 (1987) 485.

[8] H. Vehkamaki. Classical Nucleation Theory in Multicomponent Systems. Springer, 2006.

[9] C. Forest, P. Chaumont, P. Cassagnau, B. Swoboda, P. Sonntag. Polymer nano-foams for insulating applications prepared from CO2 foaming. *Prog. Polym. Sci.* 41 (2015) 122.

[10] N. K. Adam. The Physics and Chemistry of Surfaces; 3rd Edt. Oxford University Press, 1941.

[11] D. J. Shaw. Introduction to Colloid and Surface Chemistry. 4th Edt. Butterworth-Heinemann, 1992.

[12] L. J. Gibson, M. F. Ashby. Cellular Solids, Structure and Properties. 1st Edt. Pergamon Press, 1988.

[13] A. Demharter. Polyurethane rigid foam, a proven thermal insulating material for applications between +130°C and -196°C. *Cryogenics* 38 (1998) 113.

[14] C. Tseng, M. Yamaguchi, T. Ohmori. The Thermal Conductivity of Polyurethane Foams From Room Temperature to 20K. Cryogenics 37 (1997) 305.

[15] G. Venkatesan, G. P. Jin, M. C. Chyu, J. X. Zheng. T. Y. Chu. Measurement of thermophysical properties of polyurethane foam insulation during transient heating. *Int. J. Therm. Sci.* 40 (2001) 133.

[16] C. S. C. Louro. Thermal Conductivity of Gases-Transient Hot-Wire Method. Dissertation to obtain the Master Degree in Chemical Engineering, Istituto Superior Tecnico, Universidade Tècnica de Lisboa. Lisbon, 2008.

[17] R. H. Perry, D. W. Green. Chemical Engineers' Handbook, 8th Edt.. McGraw-Hill, 2007

[18] W. D Callister,. Scienza e ingegneria dei materiali- una introduzione. Edises, 2003.

[19] W. D. Callister, Jr. Materials Science and Engineering: An Introduction. Wiley, 2003

[20] 04, ASTM C518 – Standard Test Method for Steady-State Thermal Transmission Properties by Means of the Heat flow Apparatus. 2002.

[21] B. E. Yoldas, M. J. Annen, J. Bostaph. Chemical Engineering of Aerogel Morphology Formed under Nonsupercritical Conditions for Thermal Insulation. *Chem. Mater.* 12 (2000) 2475.

[22] R. Baetens, B. P. Jelle, A. Gustavsen. Aerogel insulation for building applications: A state-of-the-art review. *Energ. Buildings*. 43 (2011) 761.

[23] R. De Vos, D. Rosbotham, J. Deschaght. Open-Celled Polyurethane Foam Based Vacuum Panel Technology: A Fully Polyurethane Based Composite Technology for Vacuum Insulated Appliances. *Journal of Cellular Plastics* 32 (1996) 470.

Chapter 3: CO_2 solubility in polyol and isocyanate

In this chapter, measurements of solubility, mutual diffusivity, specific volume and interfacial tension of polyol/CO_2 and isocyanate/CO_2 solutions, by using an equipment based on the coupled gravimetry-Axisymmetric Drop Shape Analysis (ADSA), are reported. This fundamental study of the physical properties of the investigated polymer/CO_2 solutions have been performed at 35°C and at CO_2 pressures up to 8000 kPa for polyol and up to 6500kPa for isocyanate.

3.1. Introduction

Knowledge of the properties of polymer/gas solutions is of great importance both for the development of theories of polymer based mixtures and for several technological applications including, among others, polymer recycling, durability of polymers in gaseous environments and gas foaming of polymers [1]. With reference to this latter technology, it is of great importance to know how the gas gets into the polymer, to design the process and the equipment and to optimize the foaming reaction. For instance, gas solubility will determine the amount of gas available for blowing the polymer, in turn defining the final density of the foam, while diffusivity determines the minimal residence time of contact between the gas and the polymeric precursors at processing temperature and pressure to achieve the desired polymer/gas solution. In foaming, furthermore, it has been evidenced how low molecular weight penetrants (e.g. CO_2) extensively affect other properties of the polymer/penetrant solutions, which are involved in the foaming process, namely the interfacial tension of the polymer/penetrant solution in contact with the penetrant and, to a lesser extent, the specific volume of the polymer/penetrant solutions [2]. Accurate evaluation of these properties is often affected by assumptions that are needed for a proper re-elaboration of the experimental measurements. Moreover, measurement of different properties of the polymer-gas mixture of interest, for example solubility and interfacial tension, are frequently performed in different types of apparatus with the consequence that the working conditions of the measurements (actual pressure and actual temperature of the sample) could be not very close, thus affecting also reliable correlations between the measured properties. Regarding the experimental evaluation of solubility in polymers of gases at relatively high pressures, reliability of results often suffers from the unavailability of data on specific volume of the polymer/gas solutions, which are needed to correct sorption data for buoyancy effects [3] when measurement of gas sorption is performed by means of a microbalance operating in a controlled environment. A possible way to correct this effect is a trial and error analysis of

experimental data performed by combining the gravimetric measurements with the theoretical prediction of the equilibrium mixture density obtained from solution theories grounded on statistical thermodynamics (e.g. Sanchez and Lacombe [4-6] or Simha and Somcynsky [7] equations of state, to mention a few). However, the scarcity of experimental swelling data and, consequently, the actual validation of the effectiveness of the adopted models in correctly predicting the volume of the specific mixture under analysis, do suggest a certain caution in using these procedures [8]. As a consequence, a reliable evaluation of the amount of sorbed gas can only be obtained if a direct experimental evaluation of the specific volume of the molten polymer/gas mixture is available. The determination of the interfacial tension of the separation surface between the molten polymer/gas mixture and the surrounding gas can be performed by using the well established Axisymmetric Drop Shape Analysis (ADSA), which is based on the evaluation of the shape of an axisymmetric pendant drop [9]. This technique consists of fitting the shape of an experimental drop to the theoretical drop profile according to the Laplace equation [10,11], properly modified to account for the action of the gravitational field [12-14]. The ADSA procedure provides the interfacial tension between the polymer/gas solutions and the gaseous bulk phase once the specific volume of the gas saturated polymer drop, the specific volume of the fluid surrounding it and the coordinates of several points of the drop profile are available. In order to evaluate the specific volume of the mixture, both reliable gas solubility data and total volume of the polymer-gas mixture are needed [15,16]. To this aim, the volume of the drop can be first obtained from image analysis of the drop itself by integrating the drop profile. Since the starting weight of the drop of neat polymer is known, this measured volume can be used to evaluate also the corresponding volume of the polymer/gas mixture contained in the weighing crucible, thus allowing the calculation of the related buoyancy lift. As will be discussed in detail in the following, the quantitative evaluation of this buoyancy effect allows for the reliable calculation of the actual amount of gas sorbed (from gravimetric measurements). At this stage, both the volume and the weight of the drop can then be estimated, thus allowing the evaluation of the requested equilibrium specific volume of the polymer-gas mixture at the pressure of interest. The specific volume of the surrounding fluid, which is also needed for ADSA, can be calculated either on the basis of reported data for the density of the fluid as a function of temperature and pressure or by concurrent direct measurement, with the microbalance assembly, of the weight of a non adsorbing metal piece of known-volume. Finally, the calculation of interfacial tension can be performed by ADSA, by coupling the information on specific volumes with the acquired drop profile.

From this brief description, it is evident how the interfacial tension and sorption measurements are strongly interconnected, and how a reliable evaluation of solubility and interfacial tension would certainly benefit from a concurrent volume and weight evaluation in a single experiment under

identical experimental conditions without relying on any theoretical assumption or equation of state at any stage of the properties evaluation. In fact, the proposed approach is based on a coupling of sorption and ADSA measurements, allowing for the simultaneous measure of those properties in a single experiment.

For what concerns the physical properties of polyol/CO_2 solutions, in the literature only two papers addressed sorption of CO_2 in polyols. Kazarian et al. [17] simultaneously measured CO_2 sorption and swelling in polyether polyols such as polyethylene glycol (PEG) and polypropylene glycol (PPG) by using in-situ near-infrared spectroscopy. Authors reported data on CO_2 sorption in PEG and corresponding volume increase (swelling) at 40°C and up to 11600 kPa, evidencing a solubility of CO_2 of 22.6% by weight and a swelling of 35%; for PPG, measurement have been conducted at 25°C and 35°C and at pressures up-to 6000 kPa. In particular, at 35°C and 6000 kPa authors observed a solubility of 11.8% by weight and a swelling of 24.5%. Fieback et al. [18] measured the sorption of CO_2 and N_2 in a formulation of polyol (without any further details on its chemistry) and the correspondent swelling by using a magnetic suspension balance equipped with a view cell. Sorption experiments were conducted at temperatures ranging from 20°C to 40°C and at pressures up to 6000 kPa, and revealed a maximum in solubility of 38.2% by weight and a swelling as high as 47% at 20 °C and at 5400 kPa. No data have been reported so far on polyol/CO_2 mutual diffusivity and interfacial tension. Furthermore, in the literature no papers addressed physical properties of isocyanate/CO_2 solutions to date.

3.2. Materials

A formulated polyether polyol (Table 1) and polymeric methylene diphenyl diisocyanate (PMDI) (Table 2) were supplied by DOW Chemical Italy S.r.l. (Correggio, RE, Italy) and used “as received”. High purity grade CO_2 was supplied by SOL (Naples, Italy). The polyol and the PMDI were mixed in a quantity related to the isocyanate Index equal to 115. This formulation has been the object of the overall studies following reported in this thesis.

Table 1 Composition of the "as received" formulated polyether polyol propylene oxide based.

Components	Molecular weight (Mw) (Da)	Parts (%)
Glycerin initiated polyether polyol	1000	95
Amine initiated polyether polyol	500	
Sorbitol initiated polyether polyol	700	
Sucrose/glycerin initiated polyether polyol	500	
Catalysts	/	3
Surfactant	/	2

formulated polyol is not anhydrous (0.2% water); viscosity 15150 mPa.s (25°C)

Table 2 Properties of the "as received" PMDI.

Component	Equivalent weight	NCO content (%)	Functionality	Viscosity mPa.s (25°C)	Acidity as %HCl
PMDI	135	31.1	2.7	190	0.02

3.3. Experimental set-up for solubility study

The direct and simultaneous determination of solubility, diffusivity, interfacial tension and specific volume of polymer/CO_2 solutions is based on the coupling of gravimetric measurement with ADSA. In detail, it consists in the combination of the gravimetric determination of mass transfer from the CO_2 phase to the polymer contained in a crucible, and the simultaneous optical observation of volume and shape changes of a pendant drop (see Fig. 1). The adopted experimental set-up, schematized in Fig. 2, consists of a magnetic suspension balance (MSB) (Rubotherm Prazisionsmesstechnik GmbH, Germany) equipped with a high pressure and temperature (HT-HP, up to 250°C and 13500 kPa) view cell, where a custom-designed cylindrical crucible containing 0.5 g ca. of polymer hangs from the hook of the balance weight measuring assembly, and a rod is fixed inside the cell to which the polymer pendant drop is attached. In this experimental configuration, the balance is continuously measuring the weight change of the polymer contained in the crucible and, at the same time, a high-resolution digital camera acquires the profile of the pendant drop. The relative position of the crucible and of the rod is such to avoid any interference with the gravimetric

measurement and to allow the reliable continuous acquisition of the drop shape. Drop changes in volume and shape were observed through two optical quality windows, by using an adjustable high resolution CCD camera (BV-7105H, Appro), equipped with a modular zoom lens system (Zoom6000, Navitar). The CCD camera is connected to a computer, and a commercial software (FTA32 Video 2.0, First Ten Angstroms) is used to analyse drop profile [19,20]. Furthermore, in order to achieving the optimal threshold background for digitizing the drop image, a uniform bright background was provided by light emitting diodes.

In this type of balance, the electronics and weight measuring unit work at room conditions since they are fully separated from the measuring chamber where high pressure/temperature conditions can be safely used. The coupling between the sample weighing equipment and the microbalance itself is operated via a magnetic system. Computer control ensures the correct positioning of the weighing assembly to allow the best magnetic coupling with the microbalance. The temperature inside the cell is controlled by a heating bath circulator and a temperature controller to an accuracy of ±0.05 °C.

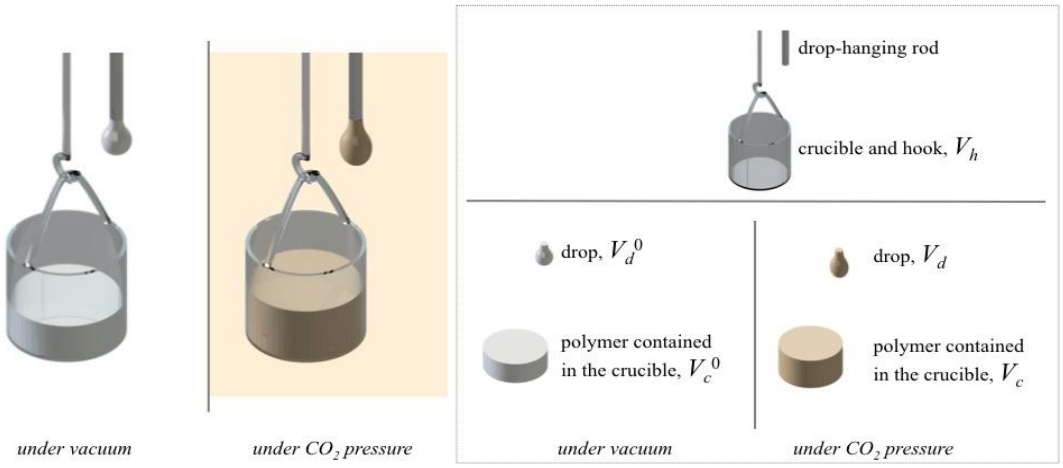

Fig. 1. Schematization of the samples and sample holders and definitions of the volumes addressed to in the text, under vacuum or under any CO_2 pressure.

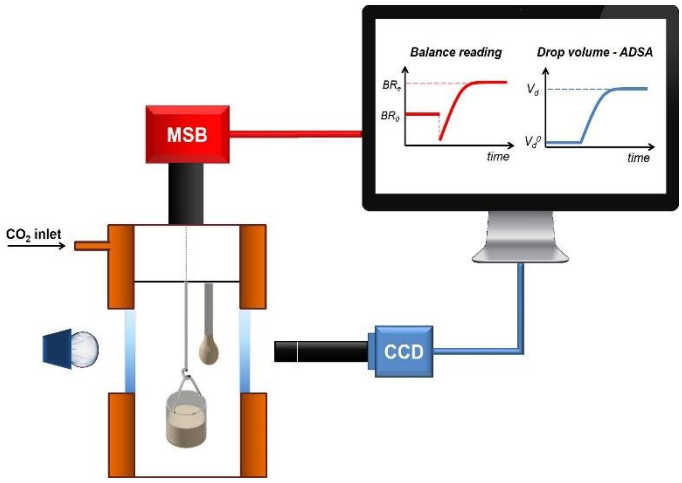

Fig. 2. Schematic illustration of the experiment and a typical step-pressure data chart.

The data flow adopted for the elaboration of the data acquired during the coupled sorption-ADSA measurement is illustrated in Fig. 3. First, from the gravimetric experiment, apparent solubility (i.e. not yet corrected to account for the effect of change of sample buoyancy due to sorption and compressive action of pressure) was measured as a function of gas pressure (A). Concurrently, data from ADSA were used to evaluate the volume of the polymer/CO_2 solution contained in the crucible (B), thus allowing for the correction of sorption data with the proper buoyancy force and, consequently, for the calculation of actual solubility and diffusivity of the polymer/CO_2 solution at each gas pressure (C). Then, the specific volume of the polymer/gas solution was calculated from CO_2 sorption amount and solution volume per unit mass of polymer (D). As a final step, this value was fed to the ADSA software to calculate (properly, by correcting gravitational forces with actual drop mass) the interfacial tension (E) [19,20].

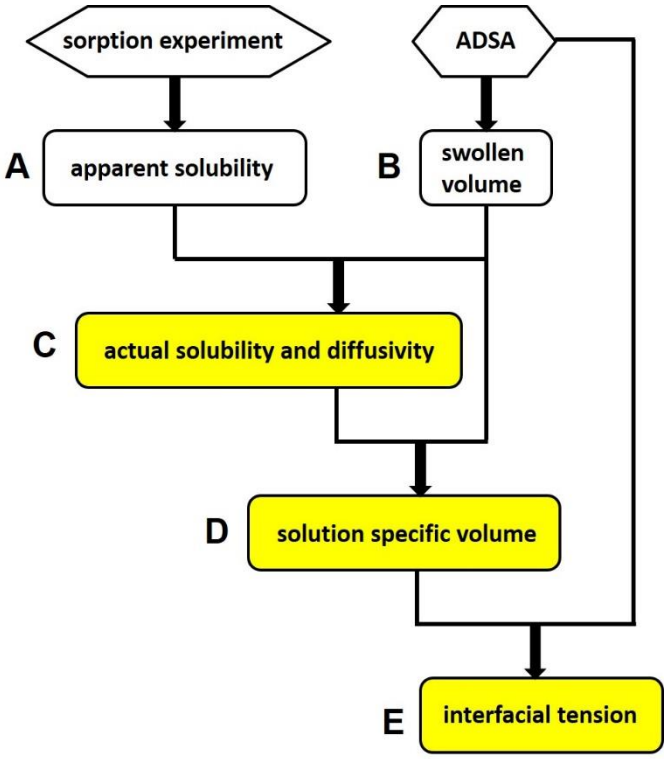

Fig. 3. Data flow used in the coupled sorption–ADSA measurement (in yellow properties measured).

A Teflon rod with a diameter of 2.03 mm was chosen as drop holder. The pendant drop was created by disposing a small amount of polymer on the top of the rod, using a pipette. Care was taken in order not to wet the lateral surface of the rod itself.

After having placed both the crucible containing the polymer and the rod with the polymer drop in the HT–HP view cell, sorption and ADSA experiments were carried out by isothermal pressure increments, at 35°C which is the typical temperature utilized in the industry to conduct polyurethane foam synthesis in presence of CO_2 at high pressure. In detail, sorption measurements were performed by step-wise increments of the gas pressure (500 kPa steps ca.), after the attainment of equilibrium sorption in the previous step. Concurrently, during each pressure step, image acquisition of the pendant drop was performed every 10 min.

Drop preparation is a fundamental step in ADSA technique, in particular in the selection of the drop size. It has been found that, if the drop is too small (Bond number << 1) and, correspondingly, its shape is close to a hemisphere, numerical problems arise in the fitting procedure; furthermore, if the drop is bigger than a critical volume (Bond number >> 1), it necks and detaches from the rod [19,21,22]. Here, small or big depends on drop volume, drop mass, interfacial tension and density of outer phase (CO_2). Since all of these conditions change dramatically at the different CO_2 pressures,

it is not possible, in the experimental range of interest in this work, to use a single drop size. As the CO_2 pressure increases, the drop swells until it detaches from the rod.

In the case of the polyol, due to conditions of CO_2 at high pressure, three different initial drop sizes were used (V_d^0 is the volume of the drop under vacuum), each suitable for a different pressure range. Fig. 4 reports the optical images of different polyol drops for the different conditions of measure. The partial overlap of the pressure ranges (see Fig. 4) is then a good check for the reliability of the volume and interfacial tension data and for the whole data evaluation chain. ADSA experiments were performed up to 6800 kPa, while gravimetric experiments were extended up to 8000 kPa.

In the case of isocyanate, it was used only one drop because the CO_2 pressure reached was not so high and the drop did not detach.

Before starting an experiment, image quality was enhanced by optimizing CCD parameters (such as working distance, zoom and contrast) and the optimal magnification was selected in order to achieve good drop profile edge detection. The pixel/mm calibration was then performed by evaluating the number of pixels corresponding to the rod diameter (actual diameter known to be 2.03 mm from digital micrometer measurement). Also, a preliminary validation with a calibrated steel sphere was performed to verify any presence of image distortion due to the CCD lens and optical windows.

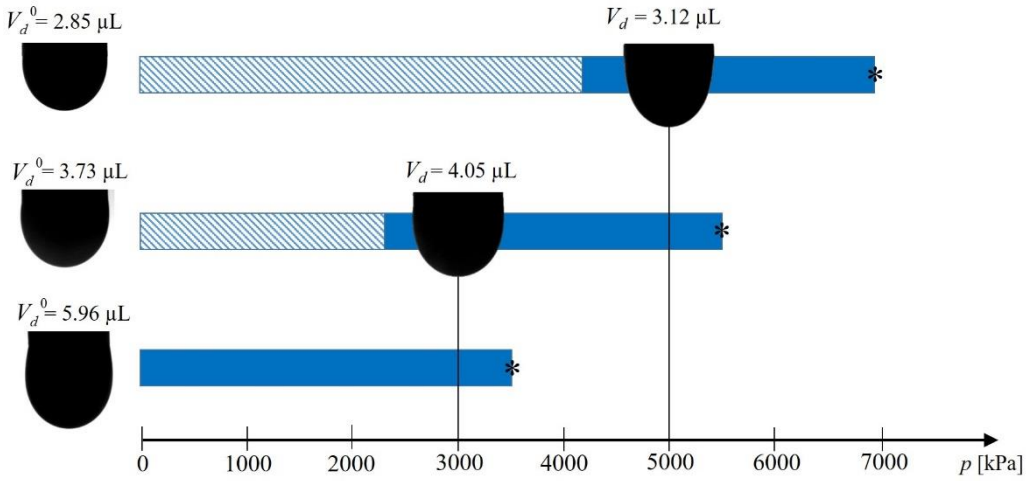

Fig. 4. Digitalized images of the different polyol drops utilized in the different pressure ranges (blue bar), under vacuum and at measuring pressure. Asterisk indicate drop detach event; dashed line indicate pressure range where numerical ADSA procedure gives inaccurate interfacial tension calculation.

3.4. Data treatment

Data treatment is described in the following according to the measurement flow chart reported in Fig. 3.

A. *Apparent solubility*, ω_{APP}

Sorption measurements were conducted by performing step-wise increments of the gas pressure (about 0.5 MPa steps) with pre-heated gas, after the attainment of equilibrium sorption in the previous step. Sample weight data were collected by the balance software and apparent gas weight fraction, ω_{APP}, at the end of the transient sorption, at each pressure, was computed according to the following expression:

$$\omega_{APP} = \frac{W_{APP}^{gas}(p)}{W_c^0 + W_{APP}^{gas}(p)} \tag{3.1}$$

where the apparent gas weight gain, W_{APP}^{gas} is calculated as by eq. (3.2):

$$W_{APP}^{gas}(p) = BR_e - BR_e^0 + \rho_{gas}(p)[V_c^0 + V_h] \tag{3.2}$$

Buoyancy correction was performed on the basis of CO_2 density (ρ_{gas}) [23], volumes of crucible and hook (V_h) (see Fig. 1) and volume of the polymer contained in the crucible at initial conditions (under vacuum) (V_c^0). BR_e is the Rubotherm balance reading at equilibrium at each pressure (attainment of homogeneous CO_2 concentration), BR_e^0 is the initial balance reading at equilibrium (under vacuum) and W_c^0 is the initial weight of the sample contained in the crucible (neat polymer) as measured by an analytical balance with a sensitivity of 10^{-5} g (Mettler AE240). The overall volume of crucible and hook and of the initial volume of the sample was previously determined by evaluating the buoyancy effect in a blank test with helium. As already mentioned, the proper correction of buoyancy to account also for the volume change associated with solubilized gas and compression due to pressure isotropic stress was possible only after having performed the measurement of the volume of the molten polymer/gas mixture, as described below.

B. *Evaluation of the swelling of the polymer/gas solution*.

Firstly, the optical observation of volume changes of the polymer drop exposed to CO_2 atmosphere was used for the analysis of the swelling of the polymer/CO_2 solution. In particular, for each pressure step, the volume of the CO_2-saturated polymer drop, $V_d(p)$, was computed by integrating the drop profile, as performed by the ADSA software. The volume of the sample contained in the crucible, $V_c(p)$, at equilibrium, can then be calculated as by eq.(3.3):

$$V_c(p) = \frac{V_d(p) - V_d^{\,0}}{V_d^{\,0}} V_c^{\,0} + V_c^{\,0} \tag{3.3}$$

where V_d^0 is the initial volume of the drop. It was assumed that, at equilibrium, drop curvature has negligible effects on specific volume and local gas concentration [24] and, consequently, that the drop and the sample in the crucible reach the same volume per unit mass of starting polymer.

C. *Actual solubility and diffusivity*

Data obtained from the gravimetric determination of mass transfer from the CO_2 phase to the polymer contained in a crucible suffer from buoyancy effect due to change in gas density at several pressures and to sample swelling upon sorption. The apparent solubility needs to be corrected with the proper buoyancy force. Having calculated in section B, for each pressure, the volume at equilibrium of the sample contained in the crucible, $V_c(p)$, it was used for proper evaluation of buoyance, to correct gravimetric data thus giving the actual gas weight fraction in the polymer/CO_2 solution (ω_{ACT}), as calculated as by eq. (3.4).

$$\omega_{ACT}(p) = \frac{W_{ACT}^{gas}(p)}{W_c^0 + W_{ACT}^{gas}(p)} \tag{3.4}$$

where W_{ACT}^{gas} is the actual gas weight gain, as calculated as by eq. (3.5):

$$W_{ACT}^{gas}(p) = BR_e - BR_e^0 + \rho_{gas}(p)[V_c(p) + V_h] \tag{3.5}$$

The kinetics of sample weight increase in step-wise sorption experiments was analysed to gather information on the value of the average mutual diffusivity as a function of CO_2 concentration in the polymer. The average mutual diffusivity ($\overline{D}$) in each step-wise sorption experiment was calculated as follows [25]:

$$\overline{D} = \frac{\pi L^2}{4}\left(\frac{d(M_t / M_\infty)}{d(\sqrt{t})}\right)^2 \tag{3.6}$$

where M_t is the mass of the CO_2 sorbed at time t and M_∞ is the mass of the CO_2 sorbed at equilibrium and L is the actual sample thickness (sample is exposed to the gas phase on one side only). M_t has been calculated as $BR_{(t)} - BR_{(o)}$ and M_∞ has been calculated as $BR_{(\infty)} - BR_{(o)}$, where $BR_{(o)}$ is the balance reading just after the pressurization, $BR_{(t)}$ is the balance reading at time t, $BR_{(\infty)}$ is the balance reading at equilibrium.

The value of $\overline{D}$ calculated through eq. (3.6) corresponds to the value of the CO_2 mutual diffusivity, *D(C)* at an intermediate concentration, *C*, the value of which can be calculated according to the procedures proposed by Vrentas and Duda [26]. Since *L* increases as the CO_2 sorbed amount increases, the actual sample thickness used in this analysis was evaluated on the basis of the arithmetic average of initial and final measured equilibrium volume of the polymer-gas solution. It is worth noting that the evaluation of diffusivity was based on balance reading, and the buoyancy correction was applied only to correct for the initial lift promoted by the additive gas entering the measuring cell during the step pressure increase. Actually, the lift changes also during sorption due to the weight and, in turn, volume increase of the polymer-CO_2 mixture. However, in view of the slight weight increase during a step sorption, this correction was not applied.

D. *Evaluation of specific volume of the polymer/CO_2 solution*.

Having determined gas sorption amount and solution volume per unit mass of polymer, these results were then used to calculate the specific volume of the polymer/gas solution. In detail, combining the volume (V_c) and the actual weight of the sample contained in the crucible (W_c) thus allowed for the calculation of the specific volume of the polymer/CO_2 solution, $v_{s(p)}$, as by eq. (3.7).

$$v_s(p) = \frac{V_c(p)}{W_c(p)} = \frac{V_c(p)}{\left(\frac{W_c^0}{1-\omega_{ACT}(p)}\right)} \tag{3.7}$$

E. *Evaluation of interfacial tension of the polymer/gas solution.*

Finally, the determination of the interfacial tension of the separation surface between the polymer/CO_2 solution and the surrounding CO_2, γ, was performed by using the well-established ADSA, which consists in fitting the shape of the experimental drop (that was continuously monitored during the simultaneous measurement) to the theoretical drop profile according to the Laplace equation, properly modified to account for the action of the gravitational field [12-14]. Therefore, the specific volume of the solution at different pressures, $v_{s(p)}$, as determined according to section C, was used as input to the ADSA software to perform the calculation of the equilibrium value of interfacial tension at each pressure.

3.5. Gel Permeation Chromatography and Transmission Fourier Transform Infrared analysis

Gel Permeation Chromatography (GPC) analysis was conducted on the "as received" samples, on the samples recovered from the crucible after the sorption campaign (addressed to, in the following, as "treated") and on the extracted fluid contained in the CO_2-rich phase spilled from the pressure vessel, after CO_2 volatilization (addressed to, in the following, as "extracted") in order to verify any effect of the treatment on molecular weight and on chemical features.

The samples were completely dissolved in THF in concentration of ≈ 0.5% w/v and passed through a 0.22µm PTFE membrane filter. Measurements were performed on an injected volume of 100 µL by using a Malvern - Viscotek GPC MAX/TDA 305 quadruple detector array equipped with a precolumn and two columns Phenogel Phenomenex with exclusion limits 106 and 103 respectively. The GPC instrument was used at flow rate of 0.8 mL/min and at column and system temperature of 35°C. Universal calibration was based on a series of polystyrene standards ranging in molecular weight from 150000 to 1500.

FT-IR spectra were collected at room temperature by using a Nexus-Nicolet apparatus with a wavenumber resolution of 4 cm^{-1}, from 4000 to 400 cm^{-1}, for 64 scans.

3.6. Results and discussion for polyol

3.6.1. Sorption isotherm

Fig. 5 reports the sorption isotherm for the polyol/CO_2 solution (calculated as by eq. (3.4)), up to 8000 kPa and at a temperature of 35°C, showing a rather linear dependence, with a maximum ω_{ACT} of 17% at a pressure of 8000 kPa. Data are also reported in Table 3.

Since polyol drop detaches at 6800 kPa (see Fig. 4), the last two data, at pressure of 7405 kPa and 7989 kPa, were estimated by extrapolating $V_d(p)$, as reported in the inset of Fig. 5.

It is worth of note, furthermore, that above 8000 kPa (at a pressure of 8270 kPa) we observed a sharp reduction of the final equilibrium weight of the sample contained in the crucible (data not reported). This, as it will be described in the FT-IR section, was attributed to the partial solubilization of polyol in sc-CO_2 (extraction).

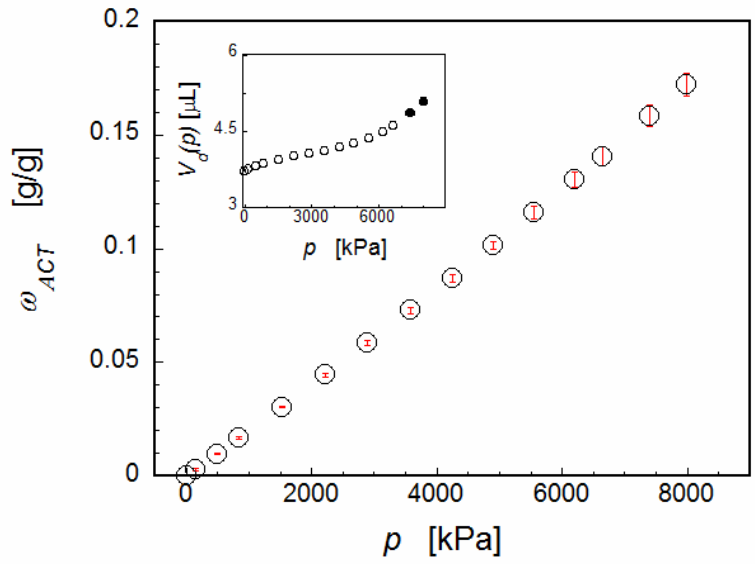

Fig. 5. Sorption isotherm of CO_2 in polyol at 35°C (in red, the error bars). Inset: $V_d(p)$ vs. pressure. $V_d(p)$ data above 6800 kPa (closed symbols in the inset) have been extrapolated because of the occurrence of drop detachment event, to evaluate buoyancy corrected sorption data.

Table 3 CO_2 sorption at different pressure and at T=35°C.

p (kPa)	ω_{ACT} (g/g)	*uncertainty for* ω_{ACT}
0	0	
153.1	0.0029	5e-04
500.0	0.0097	2e-04
845.4	0.0166	4e-04
1531.7	0.03041	2e-05
2215.9	0.0443	7e-04
2898.0	0.058	1e-03
3575.8	0.072	1e-03
4240.9	0.087	1e-03
4892.6	0.101	1e-03
5549.3	0.116	2e-03
6190.7	0.130	3e-03
6635.2	0.140	4e-03
7405.3	0.158	4e-03
7989.4	0.172	5e-03

3.6.1.1. GPC characterization

In Figs. 6a and 6b, the GPC refractive index and viscosity chromatograms, for the "as received" and the "treated" polyol, are reported. Both detection responses revealed that the "treated" polyol is missing some lower molecular weight fraction with respect to the "as received" one, possibly proving the extraction by the CO_2 of the polyol contained in the crucible.

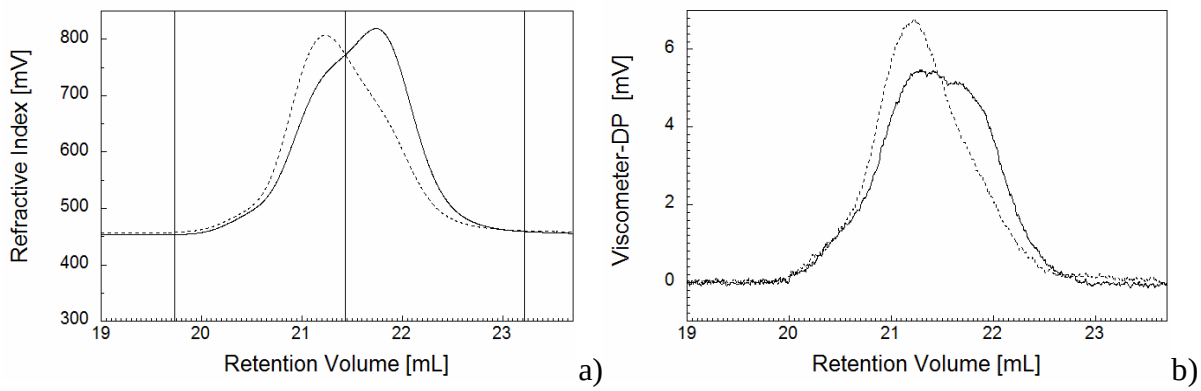

Fig. 6. GPC refractive index chromatograms (a) and GPC viscosity chromatograms (b) of "as received" polyol (solid line) and the "treated" polyol (dashed line).

Data reveal the presence of two main molecular weight distributions, as also shown in Fig. 7 reporting the fitting of the refractive index chromatograms by two Gaussian functions (indicated as peak 1 and peak 2). For a quantitative estimation of the relative concentration of the "as received" and the "treated" polyol, Table 6 reports the variation of the relative composition, above and below 600 Da (corresponding to the formulated polyol Mw average), which can be explained assuming that 56% of the fraction below 600 Da is extracted by CO_2. To further verify this, FT-IR was conducted on the "as received" and the "extracted" polyols, as follows.

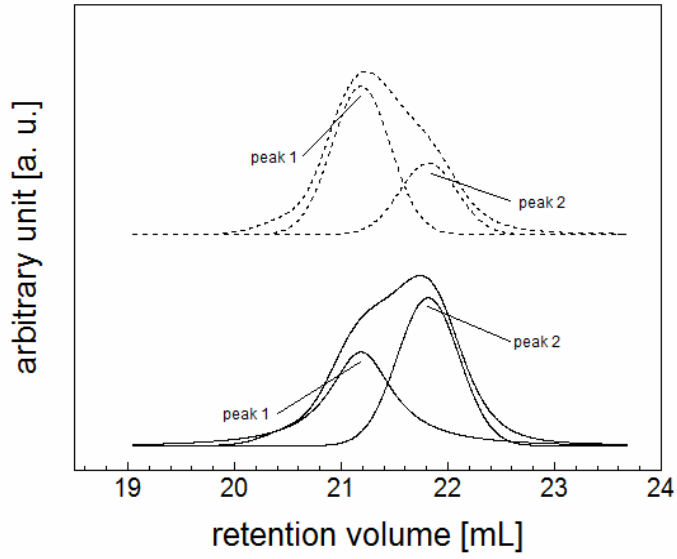

Fig. 7. GPC refractive index chromatograms of "as received" polyol (solid line) and the "treated" polyol (dashed line) fitted by two Gaussian functions.

Table 6 Sample concentrations, average Mws and relative composition of "as received" and "treated" polyols.

	sample concentration mg/mL	average Mw peak 1	average Mw peak 2	% above 600Da (peak 1)	% below 600Da (peak 1)
"as received" polyol	5.656	738	302	68.7	31.3
"treated" polyol	5.572	877	298	83.3	16.7

3.6.1.2. FT-IR characterization

Fig. 8 shows the FT-IR spectra of the "as received" polyol and of the "extracted" fluid contained in the CO_2-rich phase spilled from the pressure vessel, after CO_2 volatilization. It can be observed that curves present the same spectral features with the main characteristic absorption bands of a polyether polyol at 1100 cm^{-1} (C-O-C ether stretch), 2840 cm^{-1} (C-H stretch) and at 3100-3600 cm^{-1} (O-H stretch) [27,28]. This may confirm that part of polyol was solubilized in CO_2 at high pressures, thereby justifying the weight reduction observed at 8270 kPa.

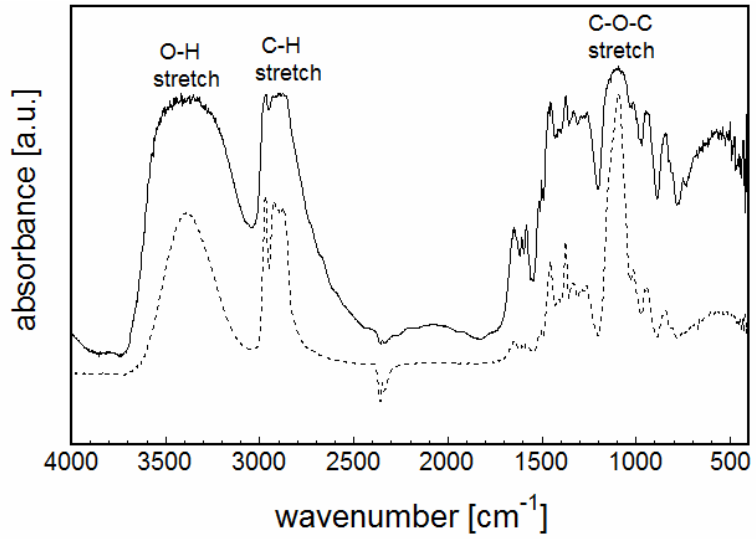

Fig. 8. FT-IR spectra of the "as received" polyol (solid line) and the "extracted" polyol (dashed line).

3.6.2. CO_2/polyol mutual diffusivity

The values of $\overline{D}$ for the polyol/CO_2 system, as obtained from eq. (3.6), are reported in Fig. 9 and in Table 5, as a function of average CO_2 mass fraction ($\overline{\omega}_{ACT}$). Again, sample volume swelling was used to correct the initial sample thickness L through which sorption occurs and actual sample thickness used in this analysis was evaluated on the basis of the arithmetic average of initial and final measured equilibrium volume of the polyol/CO_2 solution. Within the investigated pressure range, it was found that $\overline{D}$ changes with CO_2 concentration, varying from 1e-6 to 1e-5 cm^2/s with CO_2 pressure changing from 0 to 6800 kPa. No other data on similar (polyol/CO_2) systems were found in the literature for proper comparison. As a general comment, measured polyol/CO_2 mutual diffusivities are rather low, with respect to typical molten polymer/penetrant systems utilized for

foaming [20] and indicate that long residence times are needed in industrial applications to attain equilibrium.

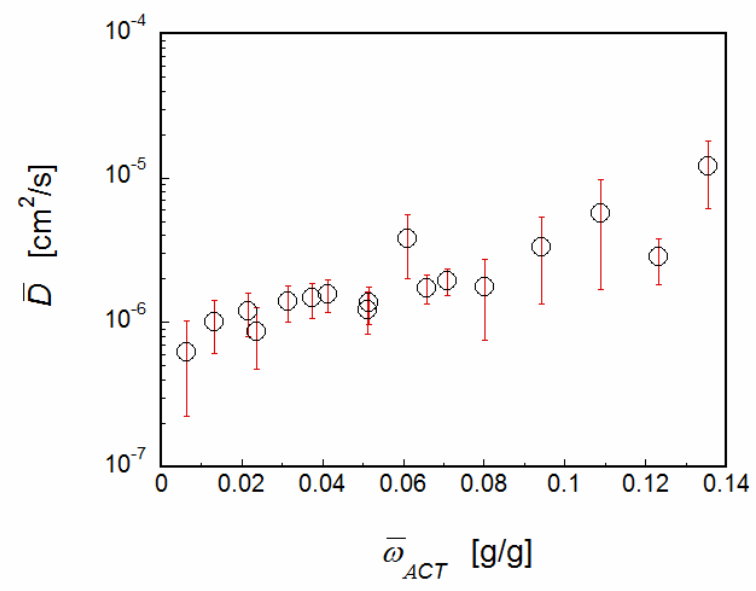

Fig. 9. Mutual diffusivity of CO_2 and polyol at 35°C (in red, the error bars).

Table 5 Mutual diffusivity at different average CO_2 mass fraction and at T=35°C.

$\bar{\omega}_{ACT}$ (g/g)	$\bar{D}$ (cm^2/s)
0.0064	6e-07
0.0132	1.0e-06
0.0216	1.1e-06
0.0235	8e-07
0.03147	1.4e-06
0.0374	1.5e-06
0.0414	1.6e-06
0.051	1.2e-06
0.052	1.3e-06
0.061	3.8e-06
0.066	1.7e-06
0.071	1.9e-06
0.080	1.7e-06
0.094	3.3e-06
0.109	5.7e-06
0.123	2.8e-06
0.135	1.21e-05

Uncertainty is ±5e-07 for $\bar{D}$

3.6.3. Specific volume of polyol/CO_2 solution

Fig. 10 shows the specific volume of the polyol/CO_2 solutions in the investigated experimental range, calculated as by eq. (3.7). v_s data, reported in Table 6, evidence a non-monotonic dependence. In fact, when a polymer is exposed to a high-pressure gas, two mechanisms compete in affecting the specific volume: (i) compression of the gas-saturated polymer by the mechanical action of pressure exerted by the external gas; (ii) gas-solubilization. With the increase of external gas pressure, the latter mechanism is responsible for an increase of the volume, while the first is responsible for a reduction of the volume. In our case, $V_d(p)$ is monotonically increasing with gas pressure, proving a prevailing effect of the gas solubilization. However, mass increase of the gas saturated polymer drop is occurring. As a final balance, in our case, at low gas concentration, the mass increase is the dominant effect, and a reduction of v_s is observed. At higher gas concentration, conversely, the volume increase becomes the predominant effect. This non monotonic dependence has been already observed on PCL/CO_2 [19,20] and has been justified (and also verified by Raman spectroscopy) in view of the presence, in the PCL/CO_2 solution, of two populations of CO_2 molecules, one polymer-associated and one non-associated, with associated molecules contributing a lower volume of mixing as compared to non-associated ones and a prevalence of associated molecules at low CO_2 pressure [29]. As in the cited work, spectroscopic experiments on our system could reveal the existence of molecular interactions between the polyol and CO_2, which would help explaining the non-monotonic dependence of specific volume of polyol/CO_2 solution.

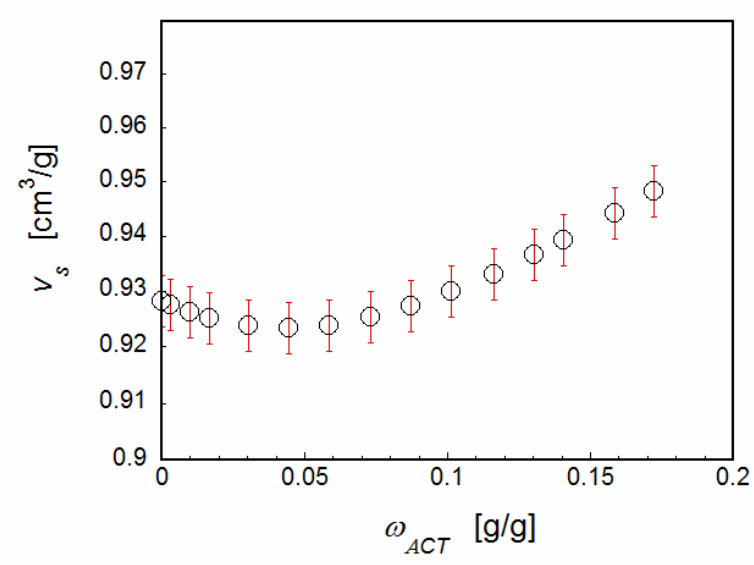

Fig. 10. Specific volume of polyol/CO_2 solutions at 35°C (in red, the error bars).

Table 6 Specific volumes at different CO_2 mass fraction and at T=35°C.

ω_{ACT} (g/g)	v_s (cm^3/g)
0	0.928
0.0029	0.927
0.0097	0.926
0.0166	0.925
0.03041	0.924
0.0443	0.923
0.058	0.924
0.072	0.925
0.087	0.927
0.101	0.929
0.116	0.933
0.130	0.936
0.140	0.939
0.158	0.944
0.172	0.948

Uncertainty is ±0.5% for v_s

3.6.4. Interfacial tension of the polyol/CO_2 solution

Fig. 11 reports the effect of CO_2 concentration on γ. In the selected experimental range, interfacial tension of the polyol/CO_2 solution was found to be nearly linear decreasing function of the CO_2 pressure (data are reported in Table 7). Such a decrease in the interfacial tension with the gas pressure has already reported elsewhere [15,30-33] and is generally attributed to two concurrent phenomena [32,33]: (i) as pressure increases, the free energy density of CO_2 becomes closer to that of the polymer phase and the interfacial tension decreases; (ii) as gas pressure increases, the concentration of CO_2 in the polymer phase increases thus further promoting a decrease of interfacial tension since the two phases in contact become more similar.

It is important to note that at the highest CO_2 pressure of the investigated experimental range, these data reveal that the interfacial tension of the polyol/CO_2 solution is vanishing, which, by observing that the densities of the two phases are approaching, could justify the solubilization of the polyol in the CO_2-rich phase [34]. To verify this significant phenomenon, at the end of the coupled sorption-ADSA experimental campaign, when the pressure vessel was at highest pressure and it was observed the sharp reduction of the weight of the polymer contained in the crucible, both the CO_2-

rich phase and the “treated” polyol were spilled out for further characterization, as it is reported in the following.

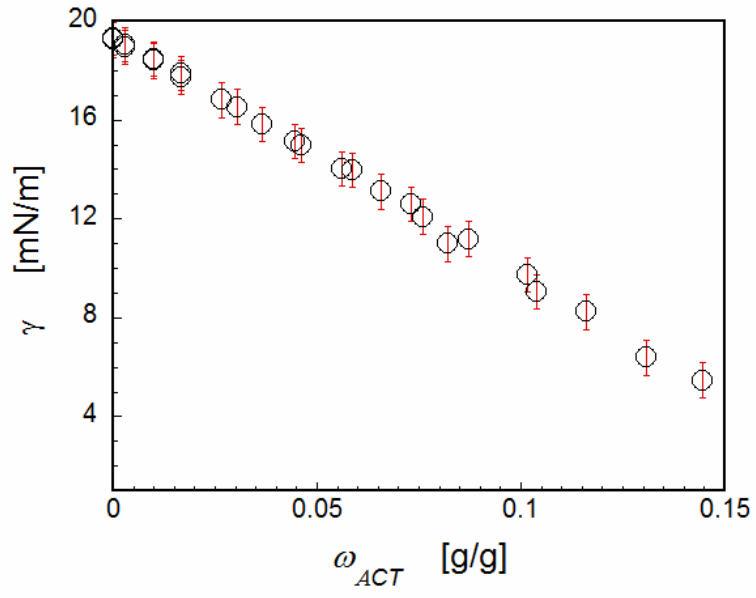

Fig. 11. Interfacial tension between polyol/CO_2 solutions and CO_2 at 35°C (in red, the error bars).

Table 7 Interfacial tension at different CO2 mass fraction and at T=35°C.

ω_{ACT} (g/g)	γ (mN/m)
0	19.3
0.0029	19.0
0.0097	18.4
0.0166	17.8
0.0265	16.8
0.03041	16.5
0.0364	15.8
0.0443	15.1
0.0462	14.9
0.056	14.0
0.058	13.9
0.065	13.1
0.072	12.5
0.075	12.0
0.087	11.1
0.082	10.9
0.101	9.7
0.103	9.0
0.116	8.2
0.130	6.3
0.144	5.4

Uncertainty is ±0.7 for γ

A common treatment of interfacial tension data is based on Macleod's relation (eq.3.8), in which γ is reported as function of the density difference between the dense and the light phases (in our case the polyol/CO_2 solution and the CO_2, respectively):

$$\gamma = k(\rho_s - \rho_{gas})^n \tag{3.8}$$

where *k* is a characteristic constant for a given liquid, $\rho_s = 1/v_s$ is the density of the polyol/CO_2 solution, and *n* is the Macleod's exponent. The exponent *n* is close to 4 for many unassociated liquids of low-molecular-weight substances [35]. In this case ln *k* is equal to 2.5 (*k* =12.2) while *n* is equal to 5.8 (see Fig. 12).

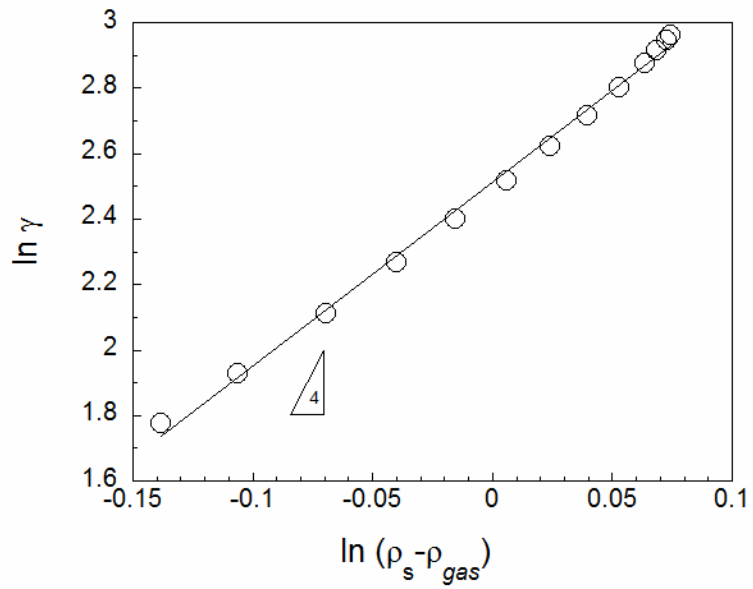

Fig. 12. Macleod plot for the polyol/CO_2 solution (fitting with eq.3.8).

According to Sugden's equation (eq.3.9) [36], from *k* it is possible to calculate the parachor (*P)*, an empirical constant that relates γ to the molecular volume:

$$P = k^{1/n} M = \frac{M}{\rho_s - \rho_{gas}} \gamma^{1/n} \qquad (3.9)$$

where *M* is the molecular weight of the liquid. The quantity $M/(\rho_s - \rho_{gas})$ has the dimensions of a volume and, at low temperatures, where ρ_{gas} becomes very small, is the molecular volume of the polyol. In this case, *Mw*=600 and *n*=5.8 giving *P* = 925 $(cm^3/mol)*(mN/m)^{1/5.8}$ (use of *n*=4 gives an estimate for *P* = 1124 $(cm^3/mol)*(mN/m)^{1/4}$).

The values of γ can be also correlated to CO_2 concentration by using the following empirical equation [37]:

$$\gamma = (1 - \omega_{ACT}) \gamma_{polyol}^{1/r} \qquad (3.10)$$

where γ_{polyol} is the surface tension of the "as received" polyol at 0 kPa.

From the fitting of the experimental data (not shown), the parameter *r* was estimated to be equal to 0.979.

3.7. Results and discussion for PMDI

3.7.1. Sorption isotherm

Fig. 13 reports the sorption isotherm for the PMDI/CO_2 solution (calculated as by eq. (3.4)), up to 6500 kPa and at a temperature of 35°C, showing a monotonic increase of the ω_{ACT} as a function of pressure, up to 6% ca. at a pressure of 5000 kPa (data are also reported in Table 8). It is worth of note that around 5000 kPa a change in the trend of sorption isotherm was observed and above 6500 kPa a sharp ω_{ACT} drop is evident. These outcomes point to the possible partial solubilization of PMDI in CO_2 at high pressures (PMDI "extraction"), likely involving the low-molecular weight "tail" of the molecular weight distribution. A similar behavior was already observed in the case of polyol-CO_2 system. To verify this hypothesis, further tests were conducted.

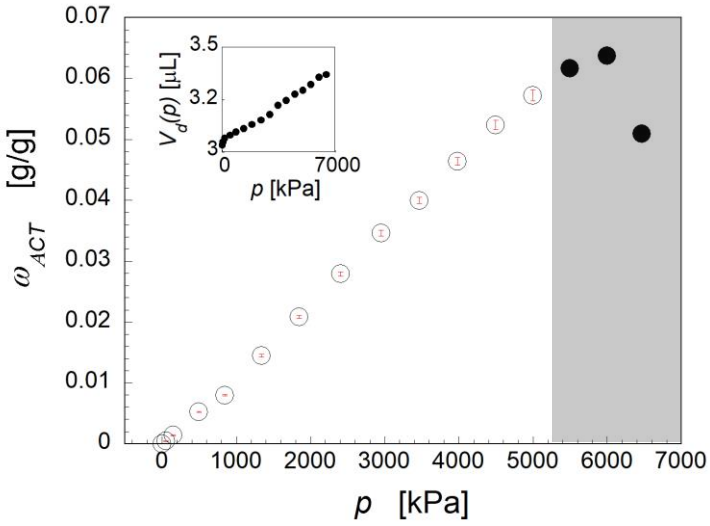

Fig. 13. Sorption isotherm of CO_2 in PMDI at 35°C (in red, the error bars). In the gray zone, closed symbols indicate erroneous solubility data, due to the partial extraction of PMDI by CO_2 at high pressures. Inset: $V_d(p)$ vs. pressure.

Table 8 CO_2 sorption at different pressure and at T=35°C.

p (kPa)	ω_{ACT} (g/g)	*uncertainty for* ω_{ACT}
0	0	
51.7	0.00042	3e-05
150.2	0.00139	4e-05
497.5	0.00522	9e-05
842.3	0.0080	1e-04
1339.3	0.0145	2e-04
1845.9	0.0209	3e-04
2406.9	0.0279	4e-04
2950.0	0.0346	4e-04
3466.8	0.0400	5e-04
3978.9	0.0464	6e-04
4496.9	0.0524	8e-04
4998.0	0.0573	9e-04

In particular, gravimetric tests were conducted by using a thermoregulated pressure vessel, having a volume of 0.3 L, in which 2 g of the "as received" PMDI, contained in a petri dish, were placed, pressurized with CO_2 at 4500 or 5500 kPa and 35°C for a day and then the pressure was released slowly enough to prevent foaming. PMDI was weighed before and after the treatment (also, after CO_2 de-sorption) in order to evaluate a possible loss in weight. It was found no weight loss at 4500 kPa (<0.01%wt), while at 5500 kPa (the first point that shows a deflection in the sorption isotherm in Fig. 13) a loss of 0.3%wt was observed. GPC and FT-IR were utilized to better analyze the extraction process by CO_2, on the "as received" PMDI, on the PMDI held in contact with CO_2 for one day at said conditions, addressed to as "treated", and on the small amount (<1mg) of the material "extracted" (collected by filtering the evacuated CO_2).

3.7.1.1. GPC characterization

PMDI is a complex mixture of molecules. It contains both 4,4'-MDI and 2,4'-MDI and different grades may have different ratio of these two. In addition, there are three functional and higher oligomers, each of which has multiples of isomers. Some of the molecules contain randomly distribuited N-methyl carbamoyl chloride groups and other acidic impurity groups. Uretonimine, biuret or isocyanurate species are also present (see the main peak assignment in Fig. 14). All of these chemicals are difficult to be analytically separated and individually characterized. GPC is, however,

capable of qualitatively characterizing PMDI, and base-line separation of di, tri and tetra oligomers is also possible [19]. By comparing the GPC refractive index chromatograms of the "as received" and the "treated" PMDI (see Fig. 14, solid line and dashed line, respectively), it is possible to observe that the "treated" PMDI is missing some lower molecular weight fraction with respect to the "as received" one, thus indicating that solubilization of part of the material contained in the crucible by the CO_2 (extraction) likely occurs, consistently with the sharp decrease in sorption evident in the isotherm reported in Fig.13. In particular, we may speculate that the diisocyanate isomers, the lowest molecular weight components in the mixture, are prevalently extracted.

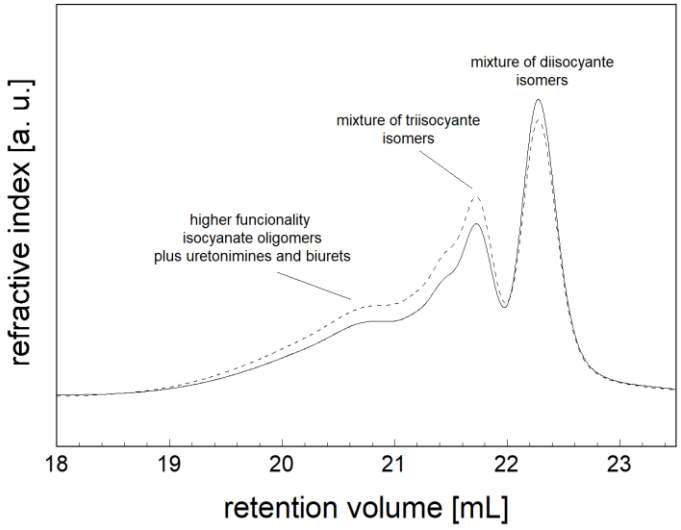

Fig. 14. GPC refractive index chromatograms of "as received" PMDI (solid line) and "treated" PMDI (dashed line).

3.7.1.2. Spectroscopic characterization

Fig. 15 shows the FT-IR spectra of the "as received" PMDI (solid line) and of the "extracted" fluid (dotted line) contained in the CO_2-rich phase spilled from the pressure vessel, after CO_2 volatilization. It can be observed that curves present the main characteristic absorption band of PMDI at 2280 cm^{-1} (NCO stretch) [38], confirming that part of PMDI was solubilized in CO_2 at high pressures.

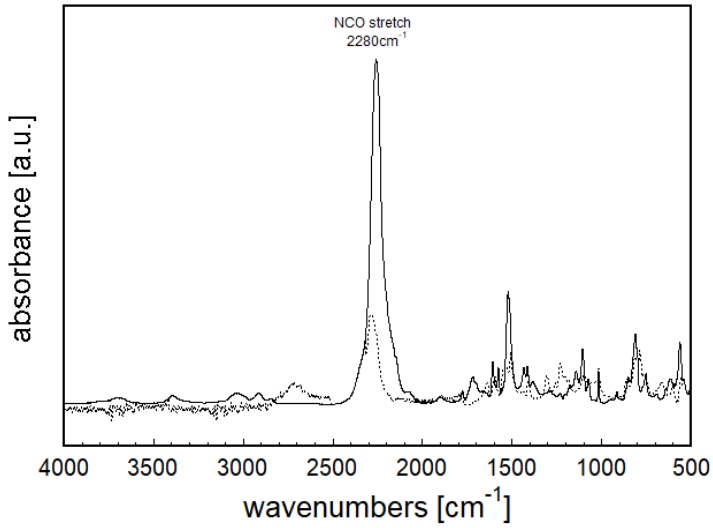

Fig. 15. FT-IR spectra of the "as received" (solid line) and the "extracted" PMDI (dotted line).

In view of the observed extraction, data at pressures above 5000 kPa will not be considered in the following of the thesis, and the data will be reported in the range 0-5000 kPa. In interpreting these data, it will be assumed that PMDI is not solubilized within the external CO_2 gaseous phase.

3.7.2. CO_2/PMDI mutual diffusivity

The values of $\overline{D}$ for the PMDI/CO_2 system, as obtained from eq. (3.6), are reported in Fig. 16 and in Table 9, as a function of average CO_2 mass fraction ($\overline{\omega}_{ACT}$). Within the investigated pressure range, it was found that $\overline{D}$ exhibits a slightly increasing trend as a function of CO_2 concentration. This effect is related to the increase of free volume of the solution that promotes, in turn, an increase of the average mobility of the system and, hence, of the mutual diffusivity. No other data on similar (PMDI/CO_2) systems are available in the literature to perform a comparison.

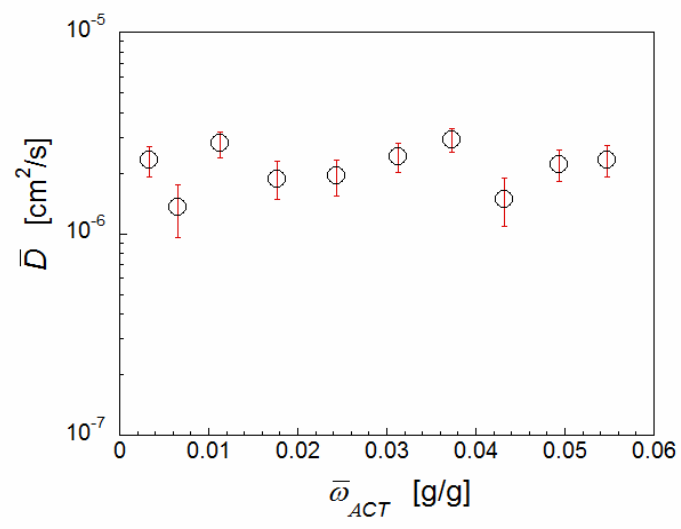

Fig. 16 Mutual diffusivity of CO_2 and PMDI at 35°C (in red, the error bars).

Table 9 Mutual diffusivity at different average CO_2 mass fraction and at T=35°C.

$\bar{\omega}_{ACT}$ (g/g)	$\bar{D}$ (cm^2/s)
0.00330	2.4e-06
0.0066	1.4e-06
0.0112	2.8e-06
0.0177	1.9e-06
0.0244	1.9e-06
0.0313	2.4e-06
0.0373	2.9e-06
0.0432	1.5e-06
0.0494	2.2e-06
0.055	2.3e-06

Uncertainty is ±5e-07 cm^2/s for $\bar{D}$

3.7.3. Specific volume

Fig. 17 shows the specific volume of the PMDI/CO_2 solutions in the investigated experimental range, calculated as by eq. (3.7). v_s data, reported in Table 10, show an increase with the increase of the gas pressure. In this case, v_s is monotonically increasing with gas pressure, proving a prevailing effect of the gas solubilization.

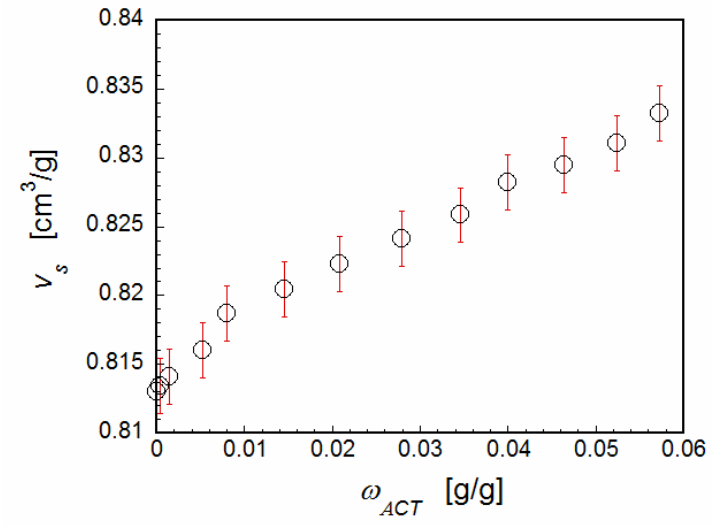

Fig. 17. Specific volume of PMDI/CO_2 solutions at 35°C (in red, the error bars).

Table 10 Specific volumes at different CO_2 mass fraction and at T=35°C.

ω_{ACT} (g/g)	v_s (cm^3/g)
0	0.813
0.00042	0.813
0.00139	0.814
0.00522	0.816
0.0080	0.819
0.0145	0.820
0.0209	0.822
0.0279	0.824
0.0346	0.826
0.0400	0.828
0.0464	0.829
0.0524	0.831
0.0573	0.833

Uncertainty is ±0.2% for v_s

3.7.4. Interfacial tension of the PMDI/CO_2 solution in contact with CO_2

Fig. 18 reports the effect of CO_2 concentration on γ. In the selected experimental range, interfacial tension of the PMDI decreases with the CO_2 pressure (data are reported in Table 11). The minimum measured value for γ is 15 mN/m ca. at 5000 kPa.

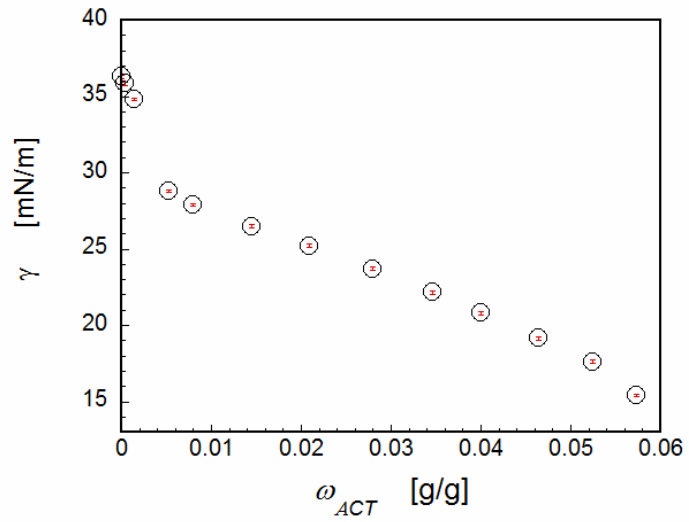

Fig. 18. Interfacial tension between PMDI/CO_2 solutions and CO_2 at 35°C (in red, the error bars).

Table 11 Interfacial tension at different CO_2 mass fraction and at T=35°C.

ω_{ACT} (g/g)	γ (mN/m)
0	36.3
0.00042	35.9
0.00139	34.8
0.00522	28.8
0.0080	27.9
0.0145	26.5
0.0209	25.2
0.0279	23.7
0.0346	22.2
0.0400	20.8
0.0464	19.1
0.0524	17.6
0.0573	15.4

Uncertainty is ±0.1mN/m for γ

According to Macleod's relation (eq. 3.8), values of 10 and 5.2 were respectively estimated for *k* and *n* (see Fig. 19) for PMDI/CO_2 solution. In this case values of 10 and 5.2 were respectively estimated for *k* and *n* (see Fig. 19).

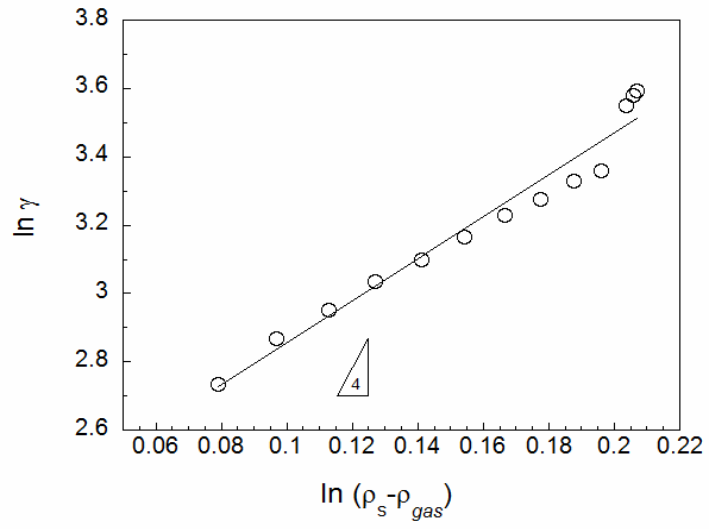

Fig. 19. Macleod plot for the PMDI/CO_2 solution (fitting with eq. (3.8)).

Furthermore, according to Sugden's equation (eq.3.9) and considering the theoretical value for M equal to 365 Da, parachor value is P=565 (cm^3/mol)*(mN/m)$^{1/5.2}$ (use, instead, of n=4 gives as estimate for P=649 (cm^3/mol)*(mN/m)$^{1/4}$).

Correlating the values of γ to CO_2 concentration by the empirical equation (10), the parameter r was estimated to be equal to 1.02.

3.8. Overview of the CO_2 solubility results

In the investigated experimental range, the sorption isotherm for the polyol/CO_2 solution shows a rather linear CO_2 pressure dependence, with a maximum ω_{ACT} of 17% at 8000 kPa. Mutual diffusivity goes from 1e-6 to 1e-5 cm^2/s in the whole experimental range, while the specific volume data evidence a non-monotonic dependence on CO_2 mass fraction. Furthermore interfacial tension was found to be a nearly linear decreasing function of the CO_2 pressure. Finally, it has been found that, at pressures higher than 8000 kPa, low molecular weight components of polyol are solubilized in sc-CO_2, as confirmed by GPC and FT-IR analysis.

The sorption isotherm for the PMDI/CO_2 solution shows a monotonic increase of the ω_{ACT} as a function of pressure, up to 6% ca. at a pressure of 5000 kPa, while mutual diffusivity slightly increases with CO_2 concentration. Furthermore, interfacial tension decreases with the CO_2 pressure, reaching the value of 15 mN/m ca. at 5000kPa, while specific volume increase with increasing of CO_2 concentration. Finally, GPC and FT-IR characterizations reveal that some lower molecular weight fractions of PMDI, possibly diisocyanate isomers, are extracted by CO_2 at pressures.

In particular, in the case of PMDI from sorption data was observed extraction of some lower molecular weight fractions at CO_2 pressure above 5000 KPa. For this reason in order to avoid extraction foaming experiments, described in Chapter 4, were conducted at 4000 KPa.

3.9. References

[1] D. L. Tomasko, H. Li, D. Liu, X. Han, M. J. Wingert, L .J. Lee, K. W. Koelling, A Review of CO2 Applications in the Processing of Polymers. *Ind. Eng. Chem. Res.* 42 (2003) 6431.

[2] E. Di Maio, G. Mensitieri, S. Iannace, L. Nicolais, W. Li, R.W. Flumerfelt, Structure optimization of polycaprolactone foams by using mixtures of CO_2 and N_2 as blowing agents, *Polym. Eng. Sci*. 45 (2005) 432.

[3] G. Li, J. Wang, C. B. Park, R. Simha, Measurement of gas solubility in linear/branched PP melts. *J. Polym. Sci. Part B. Polym. Phys*. 45 (2007) 2497.

[4] I. C. Sanchez, R. H. Lacombe. An elementary molecular theory of classical fluids. Pure fluids. *J. Phys. Chem*. 80 (1976) 2352.

[5] I. C. Sanchez, R. H. Lacombe. An elementary equation of state for polymer liquids. *Polym. Lett.* 15 (1977) 71.

[6] I. C. Sanchez, R. H. Lacombe, Statistical thermodynamics of polymer solutions. *Macromolecules* 11 (1978) 1145.

[7] R. Simha, T. Somcynsky. On the statistical thermodynamics of spherical and chain molecule fluids. *Macromolecules* 2 (1969) 342.

[8] G. Li, J. Wang, C. B. Park. Investigating the solubility of CO_2 in polypropylene using various EOS models. *Cell Polym*. 25 (2006) 237.

[9] S. Wu. Polymer Interface and Adhesion. CRC Press, 1982.

[10] T. Young. III. An essay on the cohesion of fluids. *Phil. Trans. R. Soc. Lond.* 95 (1805) 65.

[11] P.S. Laplace. Traitè de Mécanique Céleste, Supplement to Book 10. Gauthier-Villars, 1805.

[12] S. Bashforth, J.C. Adams, An Attempt to Test Capillary Action. Cambridge University Press and Deighton, Bell and Co, 1882.

[13] O. I. del Rio, A. W. Neumann. Axisymmetric Drop Shape Analysis: Computational Methods for the Measurement of Interfacial Properties from the Shape and Dimensions of Pendant and Sessile Drops. *J. Colloid Interface Sci*. 196 (1997) 136.

[14] P. Cheng, D. Li, L. Boruvka, Y. Rotenberg, A.W. Neumann, Automation of axisymmetric drop shape analysis for measurements of interfacial tensions and contact angles. *Colloid Surf*. 43 (1990) 151.

[15] D. Liu, D. L. Tomasko. Carbon dioxide sorption and dilation of poly(lactide-co-glycolide). *J. Supercrit. Fluids* 39 (2007) 416.

[16] Y. G. Li, C. B. Park, H. B. Li, J. Wang, Measurement of the PVT property of PP/CO_2 solution. Fluid Phase Equilib. 279 (2008) 15.

[17] T. Guadagno, S.G. Kazarian, High-pressure CO_2-expanded solvents: simultaneous measurement of CO_2 sorption and swelling of liquid polymers with in situ near-IR spectroscopy, *J. Phys. Chem. B* 108 (2004) 13995.

[18] T. Fieback, W. Michaeli, S. Latz, M.E. Mondejar, Sorption and Swelling Measurements of CO_2 and N_2 on polyol for their use as blowing agents in a new pu foaming process device. *Ind. Eng. Chem. Res.* 50 (2011) 7631.

[19] M. G. Pastore Carbone, E. Di Maio, S. Iannace, G. Mensitieri. Simultaneous experimental evaluation of solubility, diffusivity, interfacial tension and specific volume of polymer/gas solutions. *Polym. Test.* 30 (2011) 303.

[20] M. G. Pastore Carbone, E. Di Maio, G. Scherillo, G. Mensitieri, S. Iannace. Solubility, mutual diffusivity, specific volume and interfacial tension of molten PCL/CO_2 solutions by a fully experimental procedure: effect of pressure and temperature. *J. Supercrit. Fluids*. 67, (2012) 131–138.

[21] M. Hoorfar, A.W. Neumann. Recent progress in Axisymmetric Drop Shape Analysis (ADSA). *Adv. Colloid Interface Sci*. 121 (2006) 25.

[22] S. M. I Saad, Z.Policova, E. J. Acosta, A.W. Neumann. Range of Validity of Drop Shape Techniques for Surface Tension Measurement. *Langmuir* 26 (2010) 14004.

[23] R. Span, W. Wagner. A New Equation of State for Carbon Dioxide Covering the Fluid Region from the Triple-Point Temperature to 1100 K at Pressures up to 800 MPa. *J. Phys. Chem. Ref. Data*. 25 (1996) 1509.

[24] R. T. Dehoff, Thermodynamics in Materials Science; McGraw-Hill, 1993.

[25] J. Crank. The Mathematics of Diffusion. 2nd Edt. Oxford University Press, 1975.

[26] J. S. Vrentas. J. L. Duda, Y. C. Ni. Analysis of step-change sorption experiments. *J. Polym. Sci., Part B: Polym. Phys.* 15 (1977) 2039.

[27] G. Lligadas, J. C. Ronda, M. Galia`, U. Biermann, J. O. Metzger. Synthesis and Characterization of Polyurethanes from Epoxidized Methyl Oleate Based Polyether Polyols as Renewable Resources. *J. Polym. Sci., Part A: Polym. Chem.* 44 (2006) 634.

[28] P. Larkin, Infrared and Raman Spectroscopy, Principles and Spectral Interpretation; 1st Edition; Elsevier, 2011.

[29] M. G. Pastore Carbone, E. Di Maio, P. Musto, A. Braeuer, G. Mensitieri, On the unexpected non-monotonic profile of specific volume observed in PCL/CO_2 solutions. *Polymer* 56 (2015) 252.

[30] S. P. Nalawade, F. Picchioni, L. P. B. M. Janssen, D. W. Grijpma, J. Feijen, Investigation of the interaction of CO_2 with poly(L-lactide), poly(DL-lactide) and poly(ε-caprolactone) using FTIR spectroscopy. *J. Appl. Polym. Sci.* 109 (2008) 3376.

[31] H. Li, L. J. Lee, D. L. Tomasko. Effect of carbon dioxide on the interfacial tension of polymer melts. *Ind. Eng. Chem. Res.* 43 (2004) 509.

[32] K. L. Harrison, S. R. P. da Rocha, M. Z. Yates, K. P. Johnston, D. Canelas, J. M. De Simone. Interfacial activity of polymeric surfactants at the polystyrene–carbon dioxide interface. *Langmuir* 14 (1998) 6855.

[33] K. L. Harrison, K. P. Johnston, I. C. Sanchez. Effect of surfactants on the interfacial tension between supercritical carbon dioxide and polyethylene glycol. *Langmuir* 12 (1996) 2637.

[34] E. Kiran, J. F Brennecke. Supercritical Fluid Engineering Science: Fundamentals and Applications. ACS Symposium Series 514; American Chemical Society: Washington, DC, 1993.

[35] D. B. Macleod. On a relation between surface tension and density. *Trans. Faraday So.* 19 (1923) 38.

[36] S. Sudgen. Relation between Surface Tension, Density, and Chemical Composition. *J. Chem. Soc., Trans.* 125 (1924) 1177.

[37] R. Reid, J. M. Prausnitz, B. E. Poling, The Properties of Gases and Liquids, 4th Edt. McGraw-Hill International Editions, 1988.

[38] F. Fug, K. Rohe, J. Vargas, C. Nies, M. Springborg, W. Possart, 4,4'-methylene diphenyl diisocyanate e Conformational space, normal vibrations and infrared spectra. *Polymer* 99 (2016) 671.

Chapter 4: Development of a novel lab-scale batch equipment for studying CO_2 sorption and synthesis of rigid polyurethane foams

In this Chapter, the design of a novel batch foaming apparatus to obtain PURs by using CO_2 as PBA, is described. In particular, the aim of the present contribution is to report the criteria that led to the design of this single piece of equipment capable of allowing a throughout study of CO_2 sorption, polyurethane curing reaction and CO_2 foaming of rigid polyurethane. Furthermore, the interesting results obtained by using this apparatus are reported.

4.1. Introduction

Use of sensors to control gas sorption and curing processes has rapidly grown in the last decades in chemical industry in order to control the actual state of the process and the quality of the products [1]. More recently, some monitoring techniques were greatly improved by the combination of spectroscopic methods and fiber optics technology, which allow for the in situ and in-line acquisition of process data, consequently allowing for reduction of time delays normally involved with sample preparation. Among them, techniques based on the near infrared (NIR) spectroscopy have certainly become the most important ones [2]. In this contest, in-situ NIR spectroscopy has been used to simultaneously measure the gas sorption and the swelling of polymers [3]. Furthermore, several studies report the use of NIR spectroscopy for curing process monitoring, by controlling in situ and on-line monomers conversion during chemical reactions. In particular, NIR spectroscopy was used to monitor and control the curing reaction, in real time, of thermosetting polymers, e.g. polyisocyanurate resin system, epoxy resin and polyurethanes [4-8].

The design of an apparatus, developed during the Ph.D., for studying the concurrent chemo-physical processes occurring during gas foaming of thermosetting polymers is reported. In particular, to address the recent interest in combining the gas (physical) foaming with the classical (chemical) polyurethane foaming, this novel instrumented pressure vessel was designed for investigating: i) gas sorption under high pressure on the different reactants, kept separate; ii) synthesis under high gas pressure, upon mixing and iii) foaming upon release of the pressure. The design of the new pressure vessel relies on two key features. From the processing side, a rubber impeller was used to keep the two reactants separate during gas sorption and to allow for an efficient mixing at the end of the

sorption stage. From the analytic side, a sapphire window beneath the sample holder was utilized to use diffuse reflectance near-infrared spectroscopy to measure both the amount of sorbed gas and the reaction kinetics under gas pressure. Preliminary results are reported for the polyol-isocyanate/CO_2 system.

4.2. Design criteria

The proposed apparatus is designed to meet the requirements for:

1. allowing PBA sorption at high-pressure and moderate temperature for long time (tens of hours);
2. keeping separate the two reactants for same long time during sorption;
3. mixing the two PBA-laden reactants (tens of seconds);
4. allowing partial curing (minutes);
5. allowing fast and controlled PBA release for foaming (milli- to deci-seconds);
6. allowing curing to go to completion;
7. NIR-monitoring all (but No. 5) of the above stages.

To do so, two main features are herein proposed for the novel instrumented pressure vessel: i) the use of a rubbery impeller for the reactant sealing (and successive mixing), ii) a high-pressure-tight sapphire window mounted beneath an IR-transparent sample holder for remote NIR monitoring. Fig. 1 reports 3D renderings of the proposed pressure vessel and of some details of the sapphire window for NIR monitoring, and the sample holder with the two reactants, before and after mixing.

4.3. Experimental set-up

The pressure vessel is 1L, 150mm in height, from Avantes BV (Eerbeek, The Netherlands). It has several ports for control and accessing: 1. for temperature measurement inside the pressure vessel (Pt 100); 2. for the pressure sensor (IMP-G300, Impress, Kingsclere, UK); 3. for the gas-dosing, achieved via a 500D syringe pump (Teledyne Isco, Lincoln, NE, USA); 4. for gas evacuation, achieved in a controller manner via a 10-80NFH ball valve equipped with a TSR-20 actuator (High Pressure Equipment Company, Erie CO, USA); for the sapphire window (5) (custom made, Precision Sapphire, Vilnius, Lituania); for the mixing shaft (6), connected to the pressure vessel with a Single

Lip V-spring-loaded rotary shaft seal (7) (RS19B, American High Performance Seals, Inc., Oakdale, PA, USA). In the pressure vessel, a sample holder (8) made of Pyrex glass (internal diameter 29mm), with an optical bottom disc is placed on to the sapphire window. Finally, a rubbery impeller (9) (mod. BG 06, Ancor S.r.l., Caronno Pertusella, Va, Italy) connected to the mixing shaft, is placed in the sample holder. A standard lab mixer (mod. Euro-ST P CV, IKA-WERKE GmbH & Co. KG, Staufen, Germany) is utilized for mixing, connected to the mixing shaft. The lab mixer also provides the torque exerted to rotate the shaft. Torque evolution could be in principle utilized to monitor the curing reaction, which has a large effect on the rheological properties of the mixture. At the present state of the development, however, due to the geometry of the sample holder and the friction at the rotary shaft seal, the lab-scale mixer is not sensible enough to allow such measurement. NIR spectroscopy was conducted by using Frontier™ NIR spectrometer (Perkin Elmer Inc., Waltham, MA, USA) equipped with a FlexIR™ NIR Fiber Optic diffuse reflectance probe (PIKE Technologies, Inc., Madison, WI, USA). Fig. 2 reports images of the pressure vessel, the gas evacuation system and the mixer, assembled, together with some details of the sample holder and the impeller. Fig. 3 reports the inner of the pressure vessel with the NIR probe. In this configuration, the equipment can operate at maximum 200°C and 20000 kPa.

A typical test, with the aim of measuring sorption and curing under high blowing agent pressure, is conducted as follows. First, the samples in the form of the two viscous liquids (namely, the polyol and the isocyanate), are gently cast in the sections of the cylindrical sample holder formed by the blades of the impeller. Being made of rubber, the blades leak-seal (not high-pressure seal, not needed here) the sections, avoiding premature mixing of the two reactants (see Fig. 2c), which will get in contact and react only when the impeller is actuated by operating the lab mixer. Next, the sample holder is placed in the pressure vessel on the sapphire window by a Teflon coupling (see Fig. 3c) and then the pressure vessel is closed. After reaching the testing temperature, in this case 35°C, pressure is increased up to the saturation pressure (here 4000 kPa) and kept for a sufficient amount of time. During the sorption stage, the probe can alternatively monitor sorption in both the polyol and the isocyanate (*slow NIR monitoring*, see paragraph 4.4. for details).

It is worth of note, here, that sorption monitoring by spectroscopy has been already reported [3] and it is semi-quantitative, as it necessitate for calibration by other sorption techniques. Sorption was measured by a coupled gravimetry-axysimmetric drop shape analysis (see [9] for the details) on the two reactants, as reported in [10,11]. When a suitable amount of gas has been sorbed in the two reactants, the curing stage can be initiated (in case, at a different temperature). In order to monitor the reaction (here, in particular, the effect of the sorbed gas on the reaction kinetics), the NIR probe is positioned under the isocyanate, and *fast NIR monitoring* starts (see paragraph 4.4. for details). Then,

the mixer is activated at a certain speed of rotation for a suitable amount of time (mixing time). The curing reaction is conducted, still under pressure, for a suitable amount of time (curing time) and finally the pressure is released for gas foaming in a controlled manner [12,13]. Finally, when the curing reaction has gone to completion, the pressure vessel is opened and the foam can be extracted for characterization.

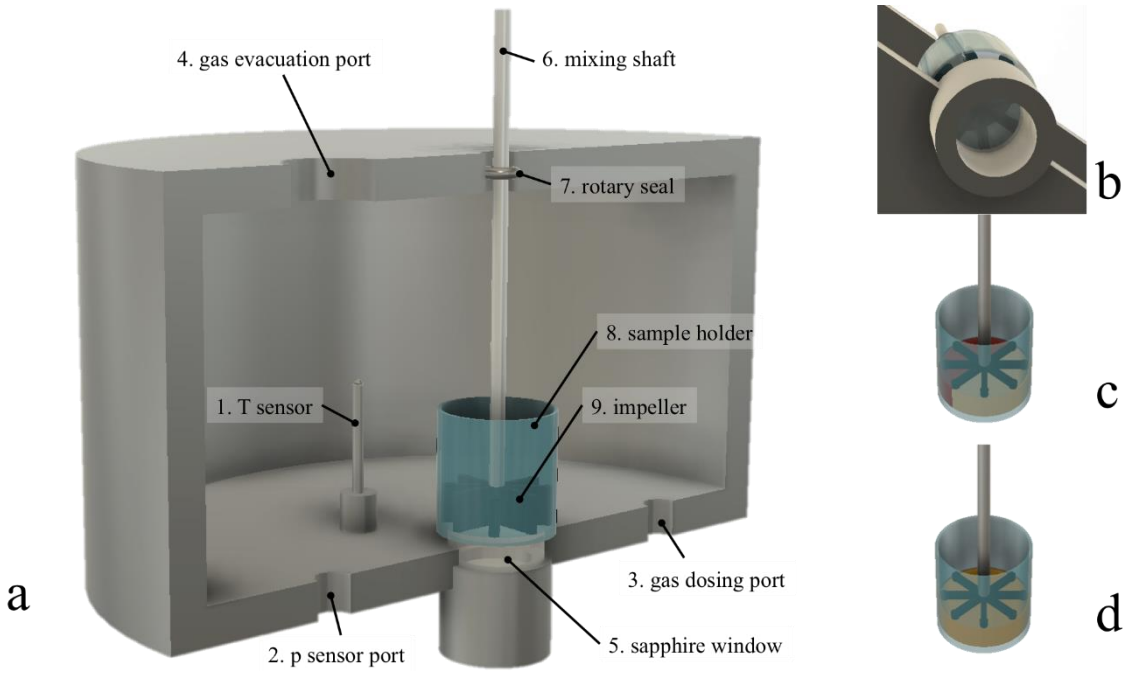

Fig. 1. 3D rendering of the pressure vessel. a) Cross section of the pressure vessel and the sample holder and impeller; b) details of the sapphire window and the impeller (bottom view); schematic of the sample holder and the two reactants before (c) and after (d) mixing.

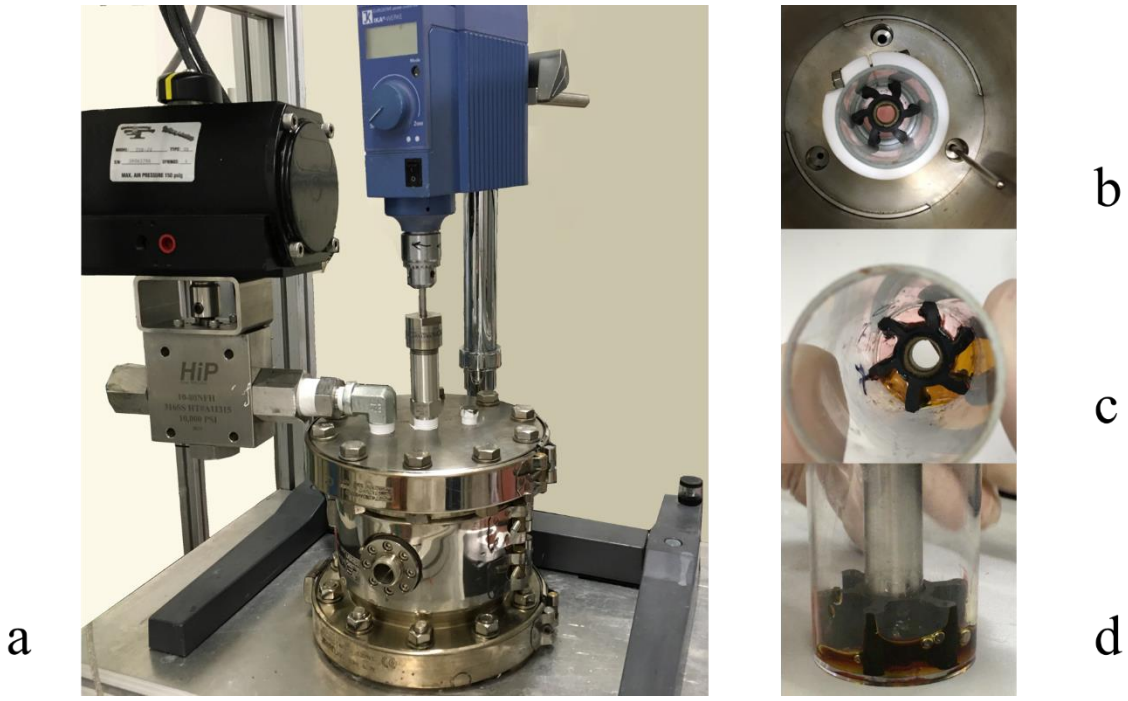

Fig. 2. Images of the apparatus. a) Assembly, with the mixing head and the gas evacuation system; b) details of the sapphire window and the impeller (top view); c) and d) sample holder with the rubbery impeller, top view (c) and side view (d).

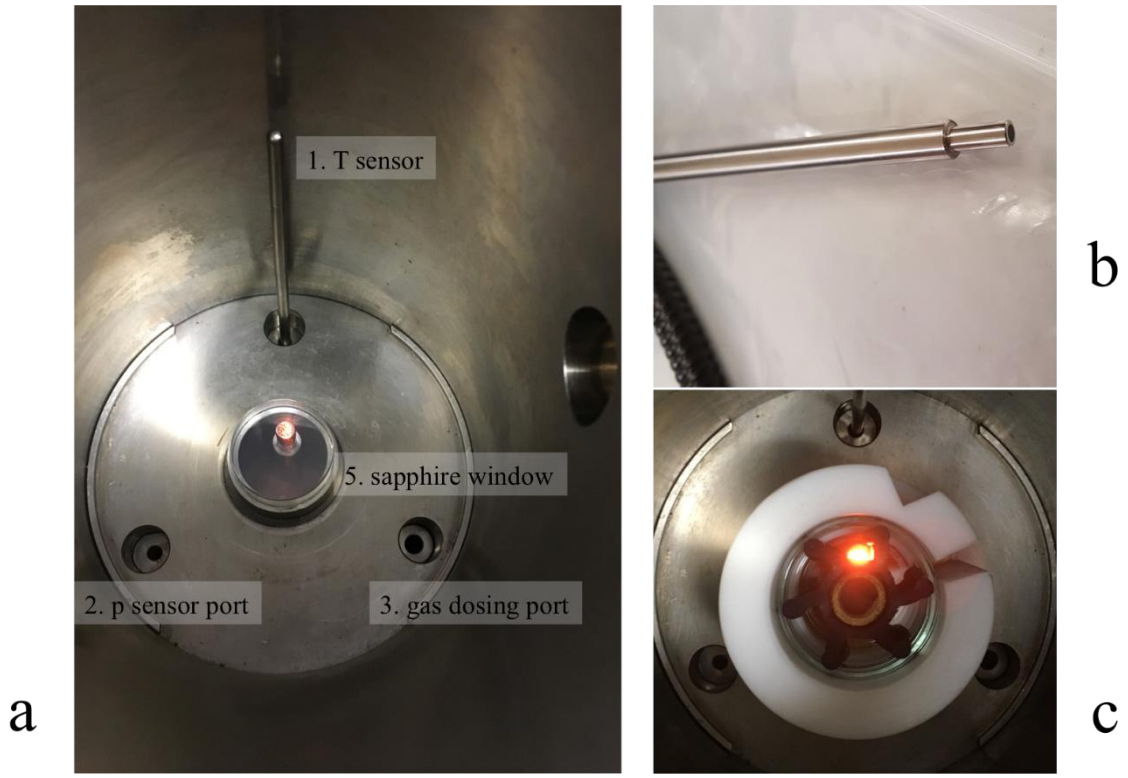

Fig. 3. Images of the apparatus with the NIR probe. a) Inner of the pressure vessel, showing the NIR probe facing inside through the sapphire window (see paragraph 4.3. for details); b) the NIR probe; c) details of the sample holder fixed by a Teflon coupling to the sapphire window, with the rubber impeller and the light from the NIR probe.

4.4. Spectroscopic measurements

FT-NIR spectroscopy measurements, during CO_2 gas sorption in polyol and PMDI at 4000 kPa and 35°C and curing reaction without CO_2 pressure, were conducted by using Frontier™ NIR spectrometer equipped with a tungsten halogen source, a CaF_2 beam splitter and a fiber optic diffuse reflectance probe equipped with an InGaAs detector (see paragraph 4.3. for details).

During CO_2 sorption, spectra were recorded automatically at regular time interval of 30 min (*slow NIR monitoring)* for 2 days using Perkin Elmer TimeBase software, in the spectral range 4000-10000 cm^{-1} with a resolution of 4 cm^{-1} and 32 scans. Polyol and isocyanate used in this dissertation are colored transparent viscous liquids and a reflective mirror aid in returning the near-infrared light to the collecting part of the fiber (transflectance sampling). Therefore, a metal reflector (with a

pathlength of approximately 0.5 mm) was placed on the top of the sample and carefully pushed against the bottom of the glass sample holder before monitor sorption in both the polyol and the isocyanate.

The curing reaction was followed by collecting spectra at regular time interval of 30s (*fast NIR monitoring)* for 15 min, in the spectral range 4000-10000 cm^{-1} with a resolution of 16 cm^{-1} and 4 scans.

4.5. Results and discussion

4.5.1. Sorption

NIR spectra of polyol and PMDI before and after exposure for 2 days at 4000 kPa of CO_2 pressure and 35°C are reported in Figs. 4a and b, respectively. Such a long sorption time was selected, based on diffusivity data (gathered on both the polyol and the PMDI [10,11]) and on the sample amount, to attain equilibrium (uniform CO_2 concentrations in both the polyol and the PMDI). Spectra of the samples exposed to CO_2 reveal the CO_2-combination band at 4950 cm^{-1}(arrow highlight the position of this band) [14]. The quantitative analysis of the sorbed CO_2 can be performed by multivariate chemometric Partial Least Squares (PLS) models, typically used in the literature [15]. PLS has to be calibrated, however, with a known concentration. In this case, data gathered by a coupled gravimetric/ADSA technique may be used [10,11]. For the case at hand, when equilibrium is attained, CO_2 weight fractions of 8.4% and 4.6% were reported for the polyol and PMDI, respectively [10,11]. The analysis by PLS models will be developed and reported in a future work. Finally, in general, other spectroscopic techniques could be used in combination with or in place of NIR. For example, in case N_2 is used as the blowing agent [16], Raman spectroscopy may be used [17,18], as N_2 vibrations are not NIR-active.

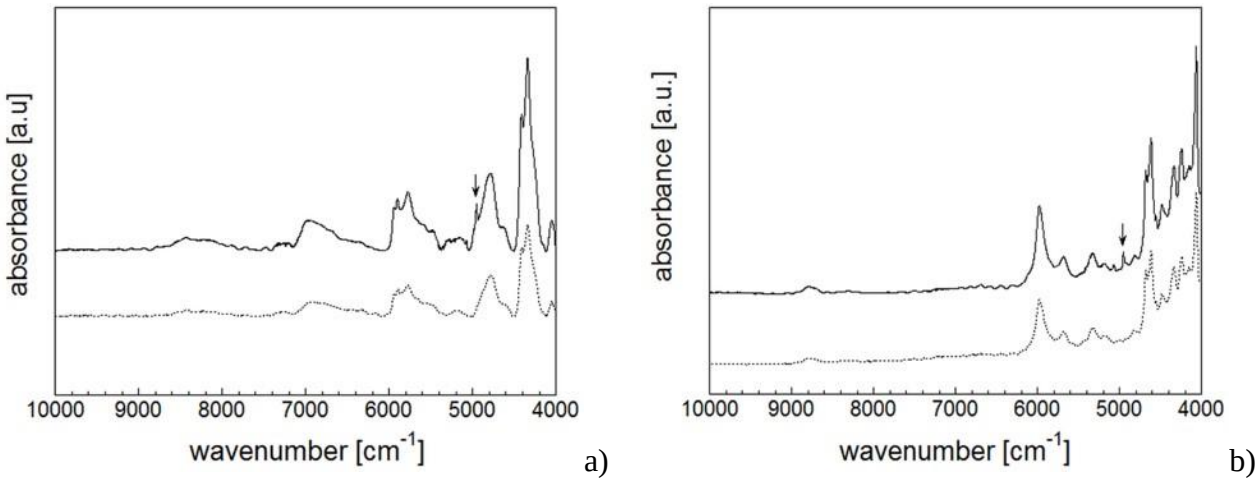

Fig. 4. NIR spectra of polyol (a) and PMDI (b) at 35°C before (dashed line) and after exposure for 2 days at CO_2 at 4000 kPa and 35°C (solid line). The arrow indicate the combination band of the CO_2 dissolved in the two reactants.

4.5.2. Curing

To prove the effectiveness of the proposed technique to monitor the curing reaction, Fig. 5 reports spectra collected after mixing the two components at 250 rpm for 10s, right after mixing and at the end of the curing reaction, at 35°C and atmospheric pressure. The effect of CO_2 pressure on the curing reaction will be discussed in detail in a separate section in Chapter 5. Here, it is noteworthy that from evaluation of these spectra it is possible to detect the NCO band decrease and the NH band (of urethane group) formation and increase, which allows for a quantitative analysis of the curing process in combination with chemometric methods [6,7]. Spectra reported in Fig. 5 show that the NCO band at 4680 cm^{-1}, characteristic of the PMDI, does not completely disappear at the end of the cure, proving it is in excess with respect to the polyol in the adopted formulation. Data are, in this case, limited to wavenumbers from 4000 to 8000 cm^{-1} of interest in this specific system. The possible NIR range of the present set-up extends to 10000 cm^{-1}. As already mentioned, the sapphire window and the equipment as the whole could also work with other spectroscopic techniques, such as Middle Infrared as well as Raman. However, the former technique poses some assembly problems, for the limited penetration depth of the radiation and the impossibility to use long (remote) probes, while the latter could give some fluorescence effect covering the colored materials signal. In fact, in our case, Raman spectra were acquired on the two formulated reactants and the signal was covered by fluorescence to a large extent (data not reported). For these reasons, NIR has been selected in the present work, specifically for the polyol/PMDI/CO_2 system under investigation.

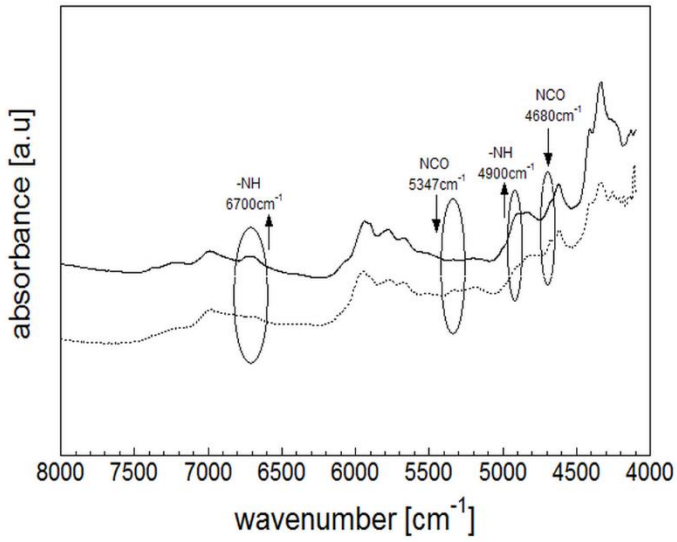

Fig. 5. NIR spectra collected at the beginning (dashed line) and the end (solid line) of the cure. The absorption bands are assigned according to the literature results [6,7]. Arrows pointing upward or downward indicate, respectively, bands that increase or decrease with proceeding of the curing reaction.

4.5.3. Processing (foaming)

In Fig. 6, images of the PURs foams achieved via the new pressure vessel are reported. Fig. 6a) shows a foam achieved at 35°C and ambient pressure (without physical CO_2). In this case, the small amount (0.2% wt. ca.) of water in the as-received polyol is responsible for the expansion. Fig. 6b) shows a foam achieved (with a depressurization rate of 20000 kPa/s) after CO_2 sorption at 4000 kPa until equilibrium, which corresponds to an average CO_2 content of 7%wt ca. [10**,**11]. These preliminary results show the effect of the PBA on the expansion of the PUR, responsible for a density decrease from 0.5 to 0.2 g/cm^3 (according to ASTM-D792) when using CO_2 as an additional blowing agent.

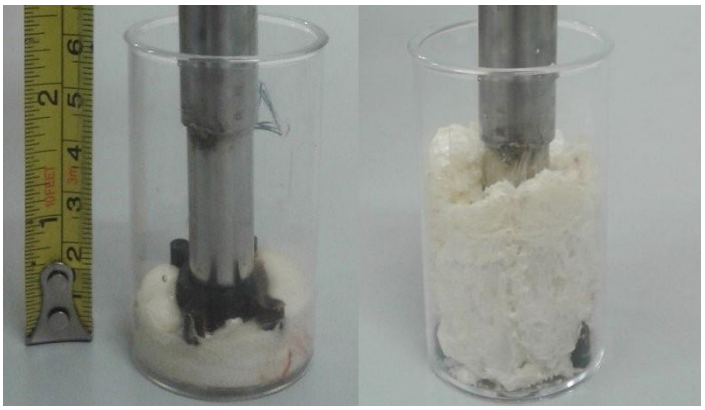

a) b)

Fig. 6. PURs obtained at 35°C and a) ambient pressure and b) 4000 kPa of CO_2 pressure.

4.6. Foaming experiments

According to CO_2 solubility data in polyol and in PMDI, shown in Chapter 3, foaming experiments were conducted at 35°C e 4000 kPa in order to avoid CO_2 extraction of low molecular weight fractions of the two reactants. The mixing mode was fixed at 250 rpm for 10s (this mode was considered the best after many mixing tests conducted on the formulated under hood at ambient pressure and room temperature), pressure drop rate at 20 MPa/s and temperature at 35°C. In addition, the quantitative of the reactants was fixed. In Fig. 7, the steps of batch foaming experiment are shown. In the pressure vessel, the polymeric precursors (polyol and isocyanate), separated by the flexible impeller, are loaded (1), pressurized CO_2 until saturation (2) and mixed (3). Finally, at any stage of the curing reaction physical foaming may occur due to pressure release (4).

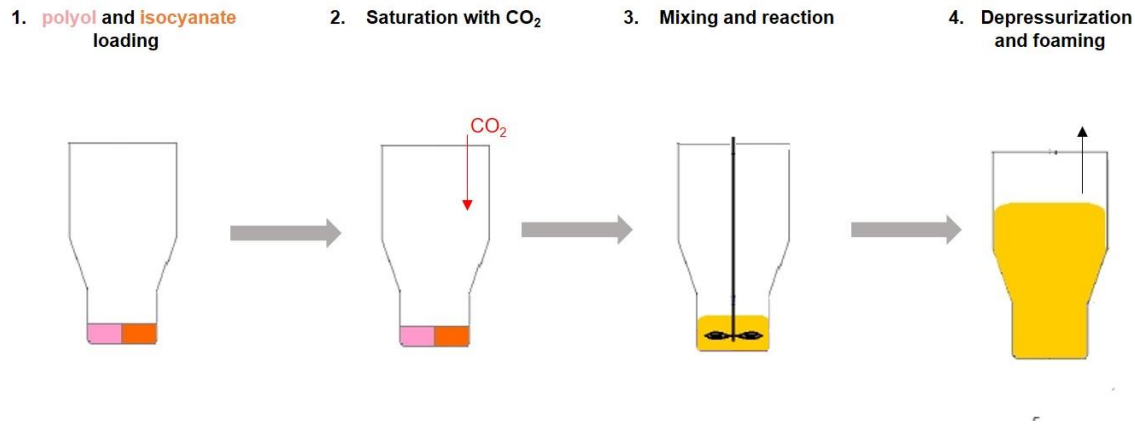

Fig. 7: Steps of batch foaming experiment

Different foaming tests was carried out by changing the CO_2 amount in order to evaluate its influence on the final properties of the polyurethane foam.

In order to meter the CO_2 amount, it is possible change pressure and sorption time. At the present stage, sorption time was changed. The CO_2 amount corresponding to a given sorption time was calculated by assuming one dimensional transport problem (sorption occurs in the two polymers by CO_2 diffusion through the upper surface), sorbed CO_2 amount has been evaluated based on the hypothesis of one-dimensional Fickian behavior (eq. 2.12 Chapter 1) of the polyol/CO_2 mixture and PMDI/CO_2 mixture by using an Excel spreadsheet (Fig. 8). The spreadsheet calculates the CO_2 concentration profile in the thickness at any sorption time, having set the geometry (thickness of the sample), the material properties (the mutual diffusivity, $\overline{D}$ as indicated by coupled sorption-ADSA measurements reported in Chapter 3) and the boundary and initial conditions: i) external CO_2 pressure, which fixes the concentration at the polymer/gas interface, C_s, ii) initial concentration C_0 and iii) the concentration at infinite x (C_0). This classical transport problem has an *analytical* ERF function solution.

$$\frac{C_x - C_0}{C_s - C_0} = 1 - erf\left(\frac{x}{2\sqrt{\overline{D}t}}\right) \qquad (4.1)$$

Integrating the CO_2 concentration profile over the thickness gives the average concentration, which is also the concentration at any point achieved when agitating the mixture (hypothesis of perfect mixing). Finally, it is worth of note that, having set the external CO_2 pressure, fixes the

equilibrium concentration at free surface (x=0) and that this value is calculated based on equilibrium sorption data achieved with the coupled gravimetric/ADSA measurements.

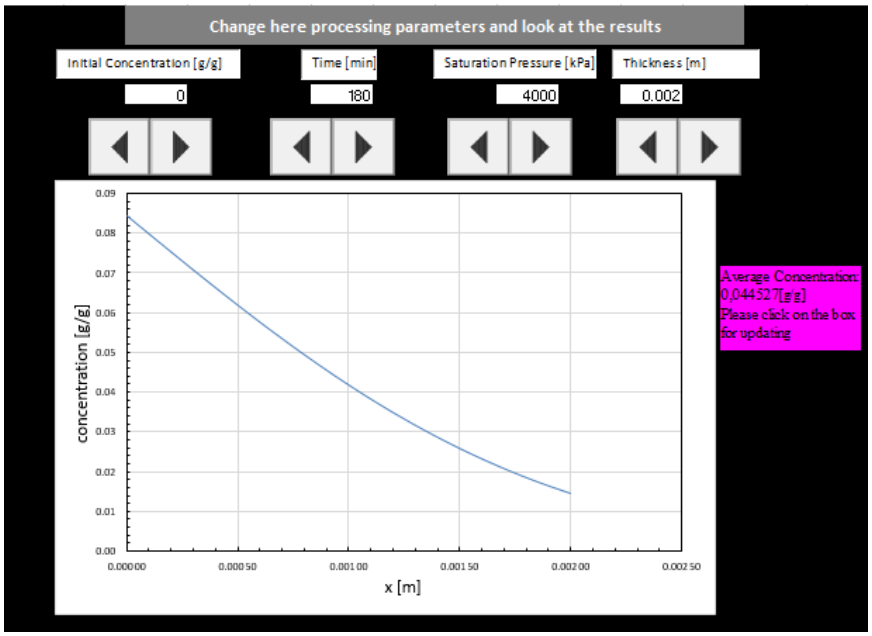

Fig.8: CO_2 mass fraction profile after 3h of sorption in 2 mm of polyol at 4000 kPa.

In Fig. 9a PURs obtained at 35°C and 4000 kPa of CO_2 pressure by changing sorption time (or CO_2 amount) are shown. Curing time was fixed at 1 minute. It is possible to note that by increasing sorption time, PUR change its morphology from an inhomogeneous to more homogeneous one, until to become a compact product characterized by a fine morphology for high sorption time. In particular, the latest foam of this series was obtained pulverized because of the pressure drop rate. In future experiments, this compact foam will be reproduce by changing the pressure drop rate in order to recovery an intact product for a scanning electron microscope (SEM) investigation. A qualitative trend of density and the quality of final morphology is reported in Fig. 9b.

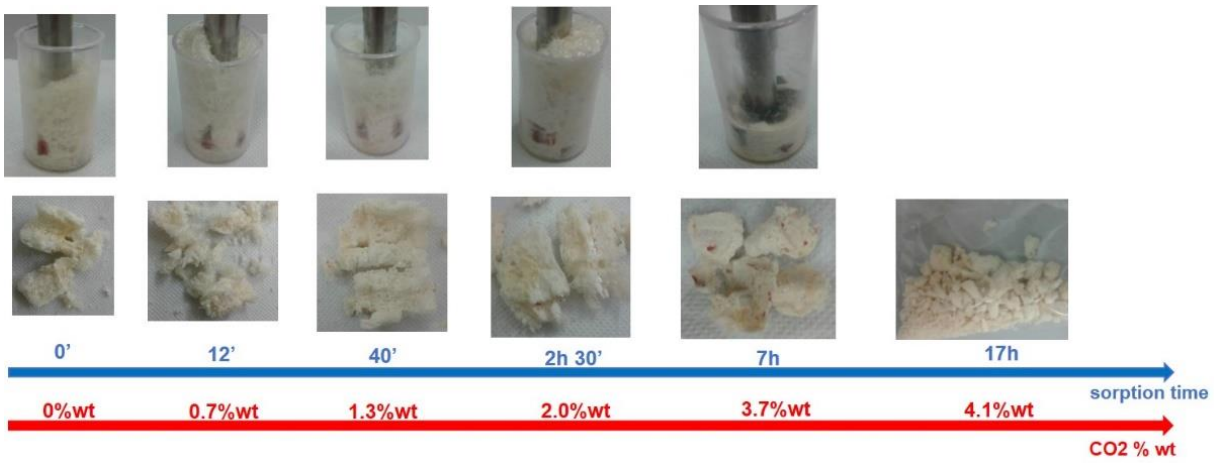

a)

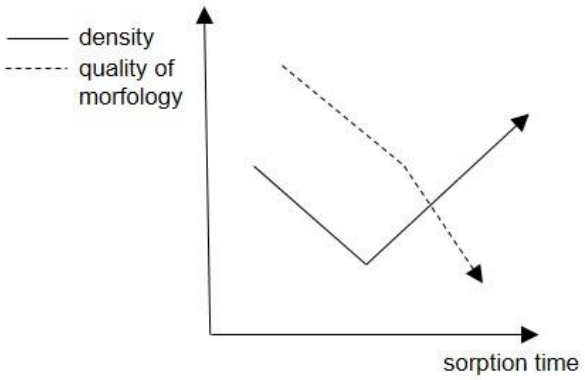

b)

Fig. 9: a) PURs obtained at different sorption times (or CO_2 amount); b) qualitative trend of density and the quality of final morphology.

A middle infrared (MIR) spectroscopy investigation was conducted on a reference foam obtained under at 35°C and atmospheric pressure and on PURs obtained at 2h 30min and 17h of sorption time, to study a possible CO_2 effect on the system. Transmission spectra (Fig.10) were collected at room temperature by using a Nexus-Nicolet apparatus with a wavenumber resolution of 4 cm^{-1}, from 4000 to 400 cm^{-1}, for 64 scans. In the range of 1500-1800 cm^{-1} it is possible to detect the polyurea peak at 1655 cm^{-1}[19] which is not present in the reference foam. It was supposed that in presence of CO_2 the curing reaction is less favorite, therefore at the end of the foaming process

remains an excess of isocyanate that reacts with ambient humidity to give polyurea. Further investigations are need to confirm this aspect.

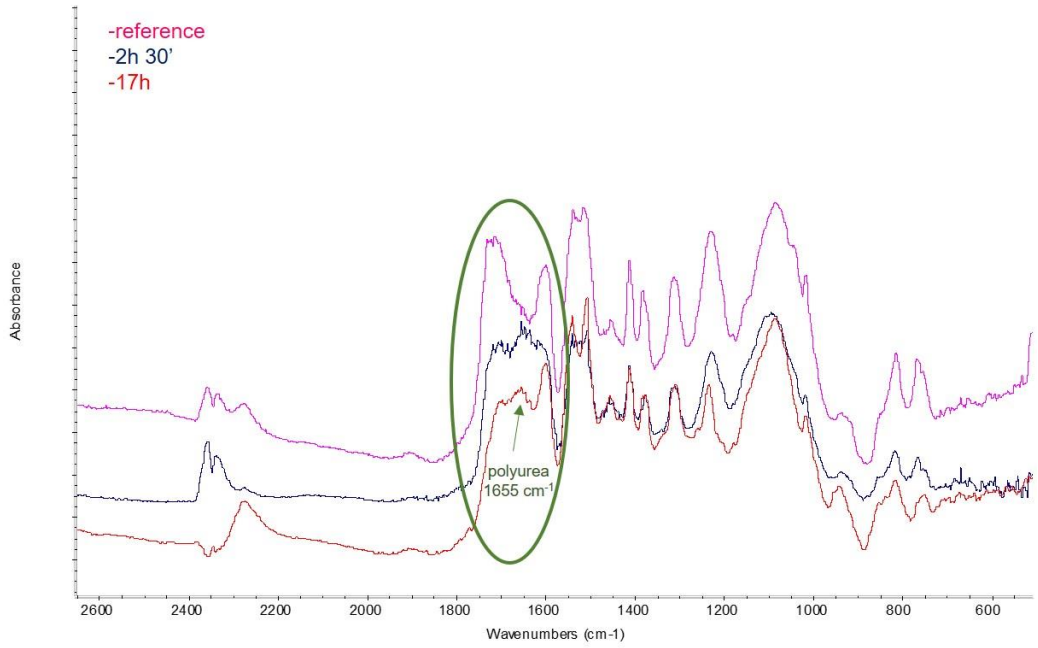

Fig. 10: MIR spectra of reference PUR (pink curve) and of PURs obtained at 2h 30' (blue curve) and 17h (red curve) of sorption time.

In order to study how the extent of curing reaction affects the final morphology of the system, PURs were obtained at 35°C and 4000 kPa of CO_2 pressure by changing the curing time (Fig. 11a). Sorption time was fixed at 2h and 30 minutes, corresponding to an average CO_2 amount of 2%wt/wt. It is possible to note that, also in this case, by increasing curing time, final product shows a different morphology from an inhomogeneous to more homogeneous one until to become a pulverized product because the polymer matrix vitrifies due to the end of curing reaction that happens before the pressure release. A trend of density and the quality of final morphology is reported in Fig. 11b.

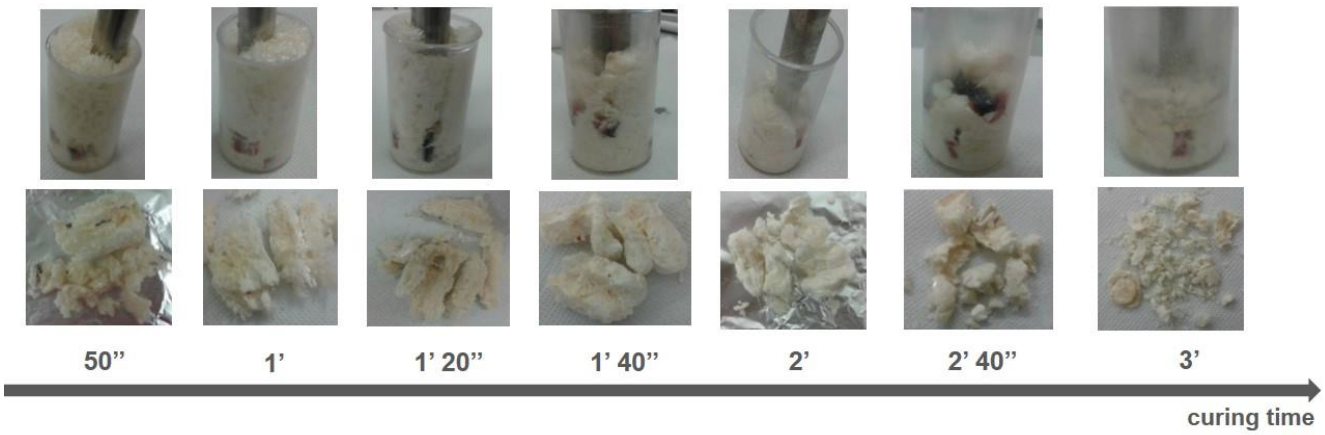

a)

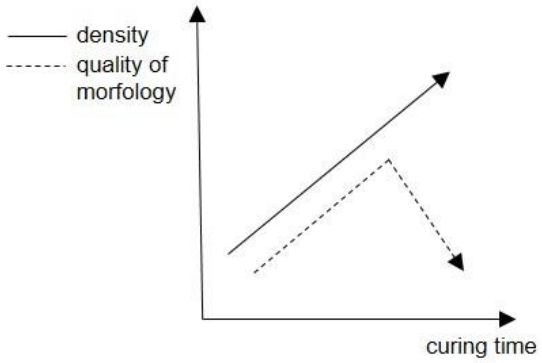

b)

Fig. 11: a) PURs obtained at different curing time; b) qualitative trend of density and the quality of final morphology.

Also per this series of foaming test, middle infrared (MIR) spectroscopy investigation was conducted, to study a possible CO_2 effect on the system, on the reference foam and on PURs obtained at 1 minute and 3 minutes of curing time. Also in this case, transmission spectra (Fig.12) show the polyurea peak at 1655 cm^{-1}[19] which is not present in the reference foam.

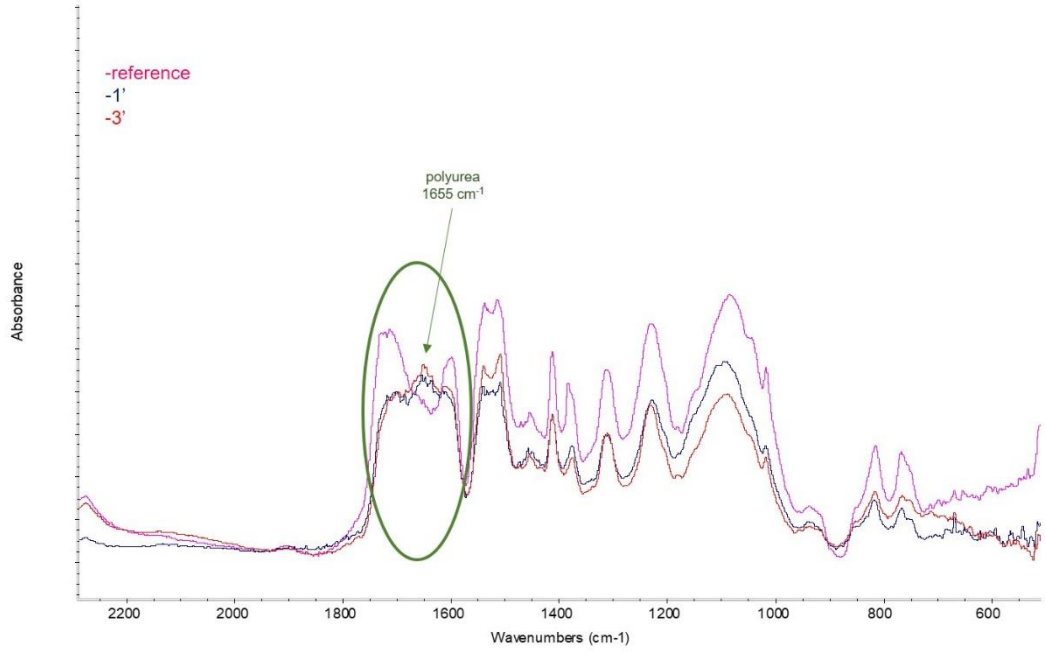

Fig. 12: MIR spectra of reference PUR (pink curve) and of PURs obtained at 1' (blue curve) and 3' (red curve) of curing time.

From the foaming experiments conducted until now, it has been evident that it is necessary to conducted new tests by changing some process variables (e.g. the pressure drop rate) to optimize the final morphology of the foam. For this reason, SEM analysis was not conducted on these foams because their morphology is so coarse.

4.7. From lab-scale to pilot plant start up

The implementation of the foaming process is ongoing at a pilot plant, developed and built by Afros-Cannon. The main scope of the pilot equipment is to scale up and industrialize the steps of batch foaming experiments conducted at lab scale, thus providing metering and sorption of the CO_2 into the polyol side, metering the polyol/CO_2 solution, mixing it with a stoichiometric quantity of isocyanate, accumulating it up to achieve a desired stated viscosity and finally injecting it into a selected mold.

The pilot plant includes (see Fig. 13):

-*High pressure machine* for typical polyurethane foaming injection technology: isocyanate tank is connected to high pressure mixing head, while polyol tank feeds the device for polyol/CO_2 sorption process.

-*Batch device for polyol/CO_2 sorption*. Polyol is fed by high pressure machine, while a carbon dioxide bottle is connected to dose it. The material inside this device can be maintained at a defined pressure up to 210 bar for a certain period of time.

-*High pressure mixing head.* Polyol/CO_2 solution and isocyanate were mixed through high pressure mixing head.

-*Reaction accumulator*. To get microcellular foams it is mandatory to maintain the PUR reactive mixture under pressure to reach a critical reaction conversion or viscosity profile before quickly inject it depressurizing the system. An accumulation and expelling device is used to properly:

- ✓ Receiving the reacting chemicals already mixed
- ✓ Maintaining the mixture under the desired high pressure conditions
- ✓ Holding the reacting mixture for the time necessary to increase the viscosity at desired value.
- ✓ Injecting the so formed reacting mixture into the mold passing through a restriction that should suddenly depressurized the system.

This task is the most challenging to realize as the injection of the reacting mixture into the mold has to be at the right time of polymerization, avoiding the need to perfectly clean the accumulation device after each shot.

-*Mold*. As initial prototyping phase very simple and traditional Lab mold was installed (see Fig.14) to pour the foam in and produce 3D panels.

Fig. 13: Pilot plant for PUR foaming technology at Afros-Cannon facility**.**

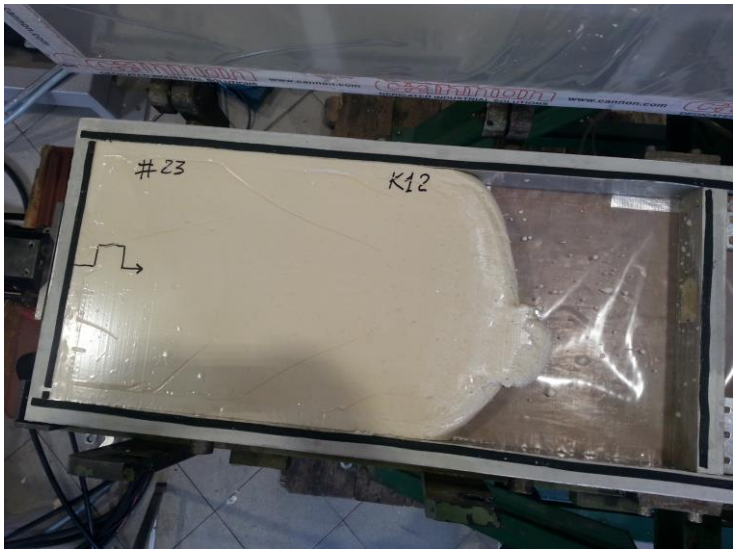

Fig. 14: Example of a PUR foam poured in the mold.

4.8. Conclusions

A new pressure vessel was developed to monitor both the CO_2 sorption in the reactants of PURs, kept separate during this stage, and the curing reaction after mixing of the so-formed reactants/CO_2 solutions, by use of NIR spectroscopy in reflection mode. Furthermore, the new pressure vessel allows for the study of these thermosetting polymers gas foaming. On said equipment, tests were conducted on a polyurethane/CO_2 system at 35°C and at pressures up to 4000 kPa. By following the CO_2 combination band, quantitative data were gathered on the equilibrium CO_2 concentration at each temperature and pressure. After the sorption stage, the reactants were mixed under pressure to induce the polyurethane curing, whose progress has been monitored by same spectroscopic technique by following the NCO band decrease and the NH band formation and increase. Foaming is eventually induced at pressure release and foams showed the remarkable effect of the PBA foaming. These results proved that the introduced apparatus is a powerful analytical as well as processing tool to study the extension of the curing reaction and the gas foaming of thermosetting polymers.

From the foaming experiments conducted by changing sorption time (or CO_2 amount) and curing time, it has been evident that it is necessary to conducted new tests by changing some process variables (e.g. the pressure drop rate) to optimize the final morphology of the foam. For this reason, SEM analysis was not conducted on these foams because their morphology is so coarse.

A pilot plant equipment was designed, realized and installed at Afros-Cannon to scaling up the lab foaming process. Preliminary foaming tests were conducted by using the PUR formulation, studied in this dissertation, in order to validate the foaming technology.

4.8. References

[1] G. E. Fonseca, M. A. Dube´, A. Penlidis. A Critical Overview of Sensors for Monitoring Polymerizations. *Macromol. React. Eng.* 3 (2009) 327.

[2] A. F. Santos, F. M. Silva, M. K. Lenzi, J.C. Pinto. Monitoring and Control of Polymerization Reactors Using NIR Spectroscopy, *Polym Plast Technol Eng*. 44 (2005) 1.

[3] T. Guadagno, S. G. Kazarian. High-Pressure CO_2-Expanded Solvents: Simultaneous Measurement of CO_2 Sorption and Swelling of Liquid Polymers with in-Situ Near-IR Spectroscopy. *J. Phys. Chem. B.* 108 (2004) 13995.

[4] J. P. Dunkers, K. M. Flynn, M. T. Huang, W.G. McDonough. Fourier Transform Near-Infrared Monitoring of Reacting Resins Using an Evanescent Wave High-Index Fiber-Optic Sensor. *Appl. Spectrosc.* 52 (1998) 552.

[5] Q. Wang, B. K. Storm, L. P. Houmøller. Study of the isothermal curing of an epoxy prepreg by near-infrared spectroscopy. *J. Appl. Polym. Sci.* 87 (2003) 2295.

[6] F.A. De Thomas, J. W. Hall, L. S. Monfre. Real-time monitoring of polyurethane production using near-infrared spectroscopy. *Talanta.* 41 (1994) 425.

[7] J. Dupuy, S. Benali, A. Maazouz, G. Lachenal, D. Bertrand. FT-NIR monitoring of a scattering polyurethane manufactured by reaction injection molding (RIM): univariate and multivariate analysis versus kinetic predictions. *Macromol. Symp.* 184 (2002) 249.

[8] E. S. Nogueira, C. P. Borges, J. C. Pinto. In-Line Monitoring and Control of Conversion and Weight-Average Molecular Weight of Polyurethanes in Solution Step-Growth Polymerization Based on Near Infrared Spectroscopy and Torquemetry. *Macromol. Mater. Eng.* 24 (2005) 272.

[9] M. G. Pastore Carbone, E. Di Maio, E. Iannace, G. Mensitieri. Simultaneous experimental evaluation of solubility, diffusivity, interfacial tension and specific volume of polymer/gas solutions. *Polym. Test.* 30 (2011) 303.

[10] M. R. Di Caprio, G. Dal Poggetto, M. G. Pastore Carbone, E. Di Maio, S. Cavalca, V. Parenti, S. Iannace. Polyether polyol/CO_2 solutions: Solubility, mutual diffusivity, specific volume and interfacial tension by coupled gravimetry-Axisymmetric Drop Shape Analysis. *Fluid Phase Equilib*. 425 (2016) 342.

[11] M. R. Di Caprio, B. Immirzi, E. Di Maio, S. Cavalca, V. Parenti, S. Iannace, G. Mensitieri. Mass transport and physical properties of polymeric methylene diphenyl diisocyanate/CO_2 solutions. *Fluid Phase Equilib.* 456 (2018) 116.

[12] C. Marrazzo, E. Di Maio, S. Iannace, L. Nicolais. Process-structure relationship in PCL foaming. *J. Cell. Plast.* 44 (2008) 37.

[13] D. Tammaro, V. Contaldi, M. G. Pastore Carbone, E. Di Maio, S. Iannace. A novel lab-scale batch foaming equipment: the mini-batch. *J. Cell. Plast.* 52 (2016) 533.

[14] M. Buback, J. Schweer, H. Tups. Near infrared absorption of fluid CO and CO_2. *Phys. B&C* 139-140 (1986) 544.

[15] J. Burck, G. Wiegand, S. Roth, H. Mathieu, K. Kramer. Monitoring of technical oils in supercritical CO_2 under continuous flow conditions by NIR spectroscopy and multivariate calibration. *Talanta*. 68 (2006) 1497.

[16] E. Di Maio, G. Mensitieri, S. Iannace, L. Nicolais, W. Li, R.W. Flumerfelt. Structure optimization of PCL foams by using mixtures of CO_2 and N_2 as blowing agents. *Polym. Eng. Sci.* 45 (2005) 432.

[17] M. G. Pastore Carbone, E. Di Maio, P. Musto, A. Braeuer, G. Mensitieri. On the unexpected non-monotonic profile of specific volume observed in PCL/CO_2 solutions. *Polym*. 56 (2015) 252.

[18] M. G. Pastore Carbone, P. Musto, M. Pannico, A. Braeuer, G. Scherillo, G. Mensitieri, E. Di Maio. Raman Line Imaging of Poly(ε-caprolactone)/Carbon Dioxide Solutions at High Pressures: A Combined Experimental and Computational Study for Interpreting Intermolecular Interactions and Free-Volume Effects. *J. Phys. Chem. B.* 120 (2016) 9115.

[19] Z. Piasek, T. Urbanski The Infra-red Absorption Spectrum and Structure of Urea. *B Pol Acad Sci*. 10 (1962) 113.

Chapter 5: FT-NIR spectroscopy investigations

During the last years, the technique of diffuse reflection near infrared NIR spectroscopy has been widely recognized as a versatile technique for the analysis of gas sorption in polymers and of the extent of chemical reactions. The increasing interest in NIR has its origin in improvements in both optronic instrumentation and chemometric data analysis. The near infrared spectral region is 4000–10000 cm-1 and it contains absorption bands corresponding to overtones and combinations of fundamental molecular vibrations, mainly from C-H, O-H and N-H bonds. This means that water and most organic compounds absorb NIR radiation. An NIR analysis can be performed quickly, without pretreatment of the sample, and the use of fiber-optic probes facilitates continuous process monitoring. Near infrared diffuse reflection spectra are the result of both absorption and scattering. The spectra can be considered as multivariate fingerprints of both the chemical and the physical properties of the sample. This multi-sensing property of NIR reflection spectroscopy gives both pros and cons, which must be considered in order to define a strategy for quantitative measurements.

5.1. Near infrared spectroscopy of gaseous CO_2 and CO_2 dissolved in polymers

The NIR absorption spectra of pure sub- and scCO_2 have been thoroughly described and discussed in the literature [1]. The absorption bands occurring in this spectral range are mainly due to Fermi resonance interaction of CO_2 fundamental and overtone modes.

Fig. 1 shows pure CO_2 NIR combination bands until a maximum pressure of 8000kPa in the spectral range 4800-9000 cm^{-1} at 35°C. These spectra were collected by using the pressure vessel with a resolution of 4 cm^{-1} and 32 scans. In particular, in Fig. 2 a zoom of pure CO_2 NIR absorption bands around 5000 cm^{-1} at 35°C is reported. The three components of the absorption around 5000 cm^{-1} are assigned to the Fermi triad band system [1]. An increased of CO_2 pressure, i.e. a higher CO_2 density (concentration), will lead to more intense absorption bands. Additionally, each band shows the transition from P-and R-type contour at lower density to a single band at higher densities and a distinct shift of the absorbance maximum towards lower wavenumbers. These spectral changes and shifts of the absorption band lead to non-linearity in the calibration function if a univariate calibration approach is used. In the literature, calibration with the integrated area of the absorption band between two limiting wavenumbers and to determine the integrated molar absorption coefficient is recommended, which was reported to be quite constant for CO_2 over a certain temperature and pressure range. However, this approach requires a substantial expenditure of measurements and

calculations to correct the optical path length for experimental pressure and temperature [1]. In contrast to this earlier work, recently Burck et al. made a PLS calibration model for determining the $scCO_2$ density is presented, which allows temperature, pressure and optical path length effects to be compensated for within one single calibration procedure [2].

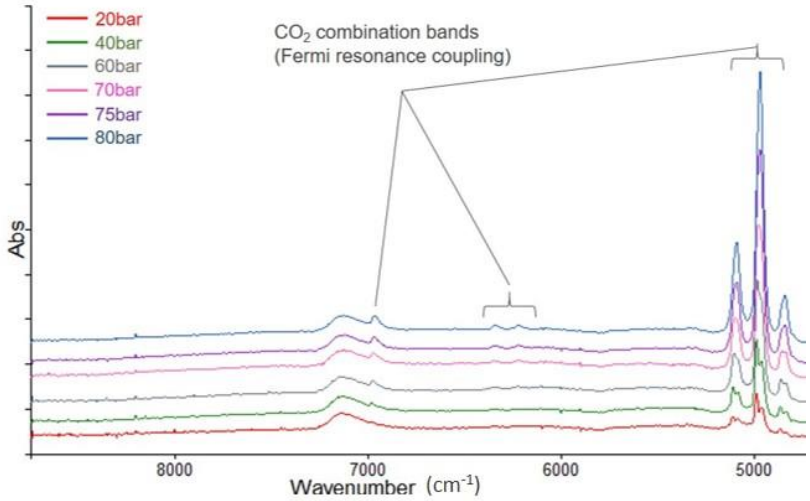

Fig. 1: NIR spectra of pure CO_2 in the range 9000-4800 cm^{-1} at 35°C and different CO_2 pressure.

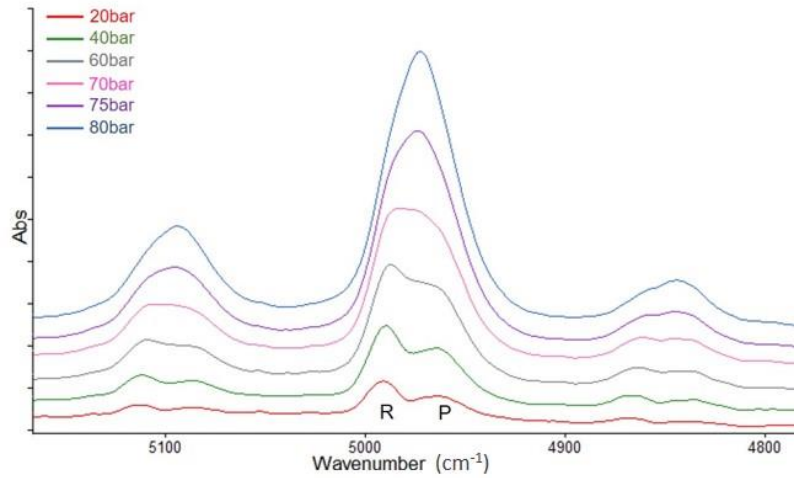

Fig. 2: NIR spectra of pure CO_2 enlarge around 5000 cm^{-1} at 35°C and different CO_2 pressure.

As already reported in 4.5.1 paragraph of Chapter 4, the NIR band of CO_2 dissolved in polymers is located at 4950 cm^{-1} [3,4]. This absorbance peak derives from the combination of symmetric stretching vibrational mode, asymmetric stretching vibrational mode, and first overtone bending vibrational mode of CO_2 [5].

5.2. Effect of CO_2 pressure on the kinetic of curing reaction

In the recent year the use of CO_2 in many chemical reactions, in particular in supercritical condition, as reactant or as a new reaction medium has been largely described in the literature. Stassin et al [6] reported the effect of CO_2 pressure in supercritical conditions on the kinetic of ring-opening polymerization of ε-caprolactone, which is slowed down by a carbonation reaction, resulting in a positive volume of activation and a higher energy of activation as compared to polymerization in a regular hydrocarbon solvent. The tin alkoxide responsible for the growth of the polycaprolactone chains is carbonated by compressed CO_2 as confirmed by the infrared analysis of this initiator. An example of the opportunities that exist to tune reaction rates, equilibrium, and selectivities in scCO_2 reaction media was reported by Paulaitis et. al [7] for Diels-Alder cycloaddition of maleic anhydride and isoprene. In this case was clear that the rate constant is a very strong function of pressure in the critical region and that the effect of pressure is reduced at higher reduced temperatures. In particular, the effect of pressure on reaction rate can occur through the pressure dependence of reacting species concentrations or through the pressure dependence of the rate constant. The latter can be substantial for inert supercritical fluids solvents at conditions approaching the critical point of the solvent. This effect of pressure on reacting systems in supercritical fluids solvents appears to be unique, and consequently pressure represents an additional parameter with which to manipulate reaction kinetics in supercritical fluids. Furthermore, in the field of heterogeneous reaction the work of Tiltscher's group [8] with 1-hexene isomerization on a low-activity macroporous α-Al_2O_3, showed that the initial ratio of cis/truns-2-hexene formed could not be influenced by temperature in the gas phase. There is a modest effect of both temperature and pressure on this ratio for reactions in the liquid phase, but there is a more pronounced effect in the supercritical fluid (SCF) phase. Tiltscher et al. [9] also showed that catalyst deactivation occurred during the gas-phase reaction because hexene oligomers with low volatilities deposited on the catalytically active surface. Performing the reaction at the same temperature, but above the critical pressure prevented the deposition of these oligomers and the ensuing catalyst deactivation. Thus, one advantage of conducting heterogeneous catalytic reactions at supercritical conditions is the possibility of doing in-situ extraction of coke precursors [10].

5.2.1. FT-NIR monitoring of curing reaction at different CO_2 pressures.

In this research activity, the new pressure vessel equipped with the FT-NIR spectrometer was used to monitor in situ the extension of polyurethane curing reaction (below defined as curing time) at different CO_2 pressures in the range 0-10000 kPa. All spectra were collected for

2h automatically at regular time interval of 20s (*fast NIR monitoring)* after 5h of sorption at given CO_2 pressure, in the spectral range 4000-10000 cm^{-1} with a resolution of 4 cm^{-1} and 8 scans. The spectra collection starts just after the stop of the mixing (250 rpm for 10s) until 2 hour to ensure the end of the reaction.

As example, Fig. 3 reports spectra collected just after the mixing of the two components at 250 rpm for 10s (black curve) and at the end of the curing reaction (red curve), at 35°C and 4000 kPa of CO_2 pressure. The main absorption bands of PUR (also reported in Table 1) are assigned with light blue arrows. The orientation of these arrows indicates the disappearing or the formation of the relative band when the curing reaction happens. The CO_2 band is also indicated with a blue arrow. Good signal to noise ratio and reproducibility of NIR spectra were observed.

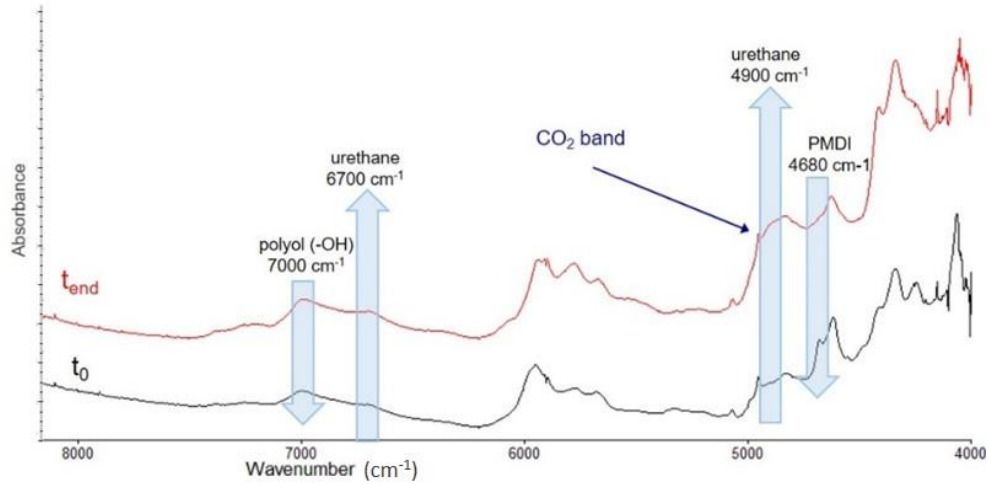

Fig. 3: NIR spectra collected at the beginning t_0 (black curve) and the end t_{end} (red curve) of the curing reaction at 35°C and at 4000 kPa of CO_2 pressure. The polyurethane absorption bands, indicated by the light blue arrows, are assigned according to literature [11] and reported also in Table 1. CO_2 band is also indicated with the blue arrow.

Table 1. Main bands absorption and assignment **[**11]

Wavenumber (cm^{-1})	*Assignment*
4680	Isocyanate
4900	Urethane (-NH combination)
6700	Urethane (-NH overtone)
7000	Polyol (-OH overtone)

For such a polyurethane formulation, the curing reaction leads to an opaque product due to light scattering. This phenomenon can be a problem for the quantitative analysis of FT-NIR spectra because spectra of diffusely transmitting samples are often characterized by poor signal to noise ratio and poor linearity due to deviations from Beer Lambert law [12].

The curing time at different CO_2 pressures, reported in Fig.4 and Table 2, was measured as the time at which the area of NH urethane absorption band at 6700 cm^{-1} does not change anymore. The area of this band was calculated through univariate analysis according to Beer Lambert law by using Perkin Elmer TimeBase software. A quantitative analysis by multivariate chemometric methods will be performed in a future work.

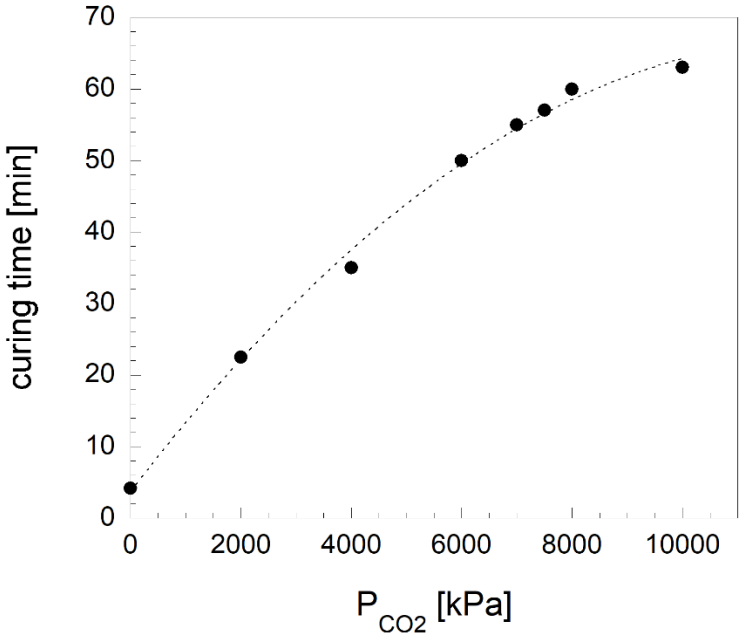

Fig. 4: Curing time as function of CO_2 pressure, measured by following the evolution of the area of NH band at 6700 cm^{-1}.

Table 2. Curing time at different CO_2 pressure and T=35°C.

Pco_2 [kPa]	*curing time [min] (NH band)*
0	4.2
2000	22.5
4000	35.0
6000	50.0
7000	55.0
7500	57.0
8000	60.0
10000	63.0

As reported in Fig.4, the curing time increases by increasing CO_2 pressure according to a polynomial of second order, therefore the curing reaction is slowed down in presence of CO_2.

In the literature, the slowing down of the curing reaction between polyol and PMDI is reported in presence of $scCO_2$ without details about a possible chemical mechanism [13]. This kind of behavior could be attribute to the Lewis acid-base interaction between CO_2, polyol and tertiary amines used as catalysts in the formulation studied in this dissertation. As example, in literature is known the reversible reaction between CO_2 and 1,8-diazabicyclo[5.4.0]undec-7-ene (DBU) tertiary amine in 1-hexanol and 1-propanol (Fig.5) [14].

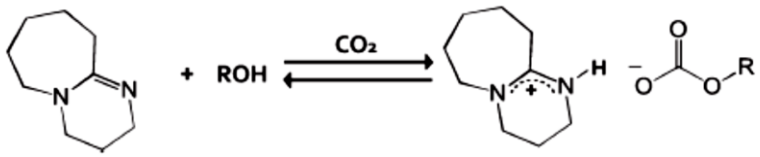

Fig. 5: Reversible binding of CO_2 with DBU in alcohol solution [14].

The mixture of amidine base and an alcohol reacts with CO_2 to create a high polarity ionic liquid with quaternary ammonium cations and alkylcarbonate anions. The reaction can be reversed by removal of the CO_2. The reversible binding between CO_2 and primary, secondary and tertiary amines is well known in literature, in CO_2 capture processes [15-17], but it can be also used in other areas such as in catalytic processes, where CO_2 is used simultaneously as solvent and as a protecting group for amines. Examples include the ring closing metathesis and the hydroaminomethylation of secondary amines [18,19]. The readiness of CO_2 to interact chemically with proton-containing nucleophiles, such as water, alcohols and primary or secondary amines was used to develop

switchable systems. These systems use CO_2 as an external trigger for the switching process and the removal of CO_2 causes the reversal of the process [20]. This is not to be confused with tunable systems, where a change of the external parameter, such as pressure or temperature, causes a continuous change of physiochemical properties [21].

In our case, the CO_2 effect on catalytic deactivation can be used to obtain a right polymer matrix viscosity before the pressure release in order to avoid the collapse of the cellar structure.

5.3. Optimization of foaming experiments

Data related to the extension of curing reaction, obtained from the FT-NIR investigation, were used to conduct a new campaign of foaming experiments at 35°C and 4000 kPa by considering a curing time of maximum 35 minutes (time at which in these conditions of temperature and pressure the curing reaction is completed as reported in Fig.4 and Table 2). The foaming tests were carried out by changing the set-up of the pressure vessel described in Chapter 4 in order to conduct, after CO_2 solubilization in the two reactants and mixing, the pressure release in two steps:

- fast pressure release (40 MPa/s) which helps in the formation of a big number of nuclei
- slow pressure release (0.1 MPa /s) which allows the nuclei growth, avoiding coalescence.

The new tools added to the set-up of the pressure vessel are shown in Figs. 6a and 6b. An aluminum hollow cylinder with a volume of 0.5 L (Fig. 6a) was used in order to reduce the volume of the pressure vessel (1L). Furthermore, a stainless steel double-ended DOT-compliant sample cylinder (0.5 L) (Swagelok, Ohio, USA) was used to conduct the fast pressure release from 4000 kPa to 2000 kPa and then it was evacuated from the top valve by a slow pressure release until to 0 kPa (Fig.6b).

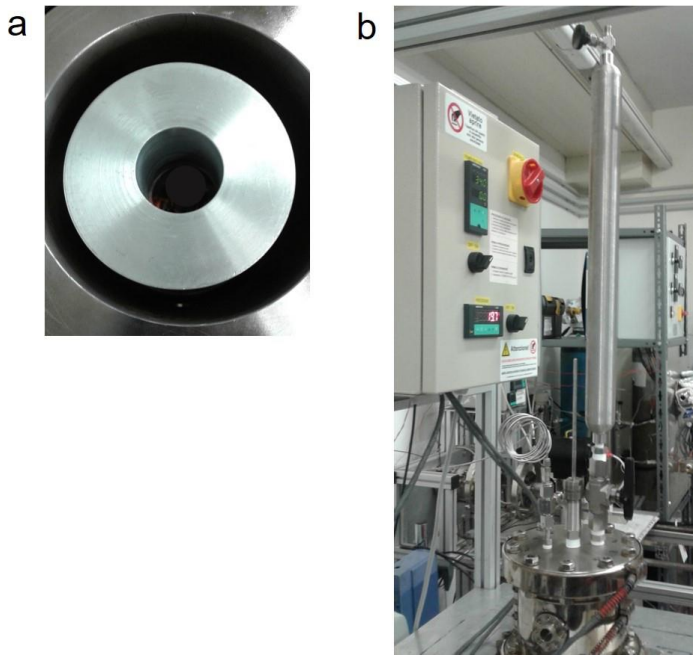

Fig. 6: Images of the modified apparatus. a) Inner of the pressure vessel with the aluminum hollow cylinder; b) assembly with the compliant sample cylinder after the mixing.

In Fig.7a some of PURs obtained by changing the curing time until 35 minutes are shown in order to verify the FT-NIR data. Sorption time was fixed at 2h and 30 minutes, corresponding to an average CO_2 amount of 2%wt/wt and 250 rpm for 10 s was used as the best condition for the mixing. It is possible to note that by increasing the curing time the final product shows a more foamed structure until to become a vitrified polymer matrix due to the end of curing reaction that happens before the pressure release according to the time scale indicated by the FT-NIR investigation. The density of these foams was measured, according to ASTM D792, by using an analytical balance (Mettler Toledo, Columbus, OH, USA). Density values were found in the range of 0.98-0.85 g/cm^3 and a trend of density and of the quality of the foamed structure is reported in Fig.7b. In this series of foaming experiments, the best condition for a good foamed structure (in terms of curing time at which the fast pressure release is conducting) was found at 18 minutes.

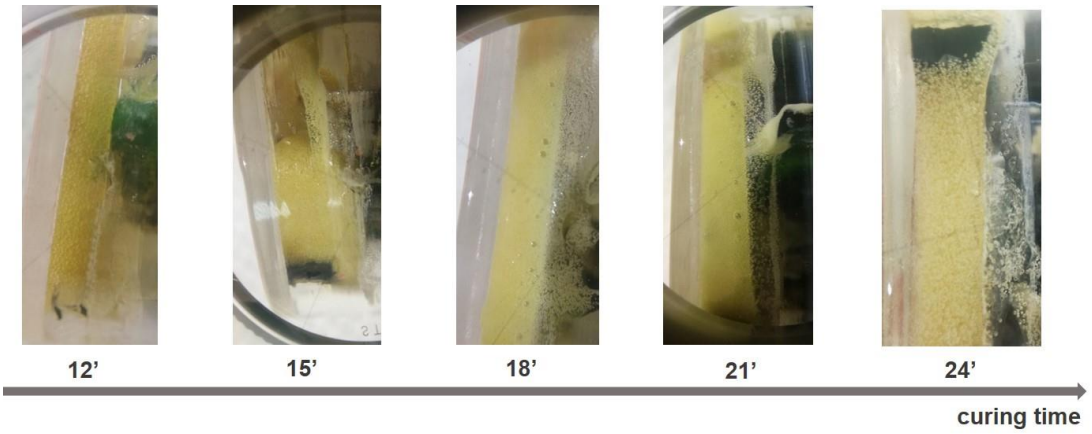

a)

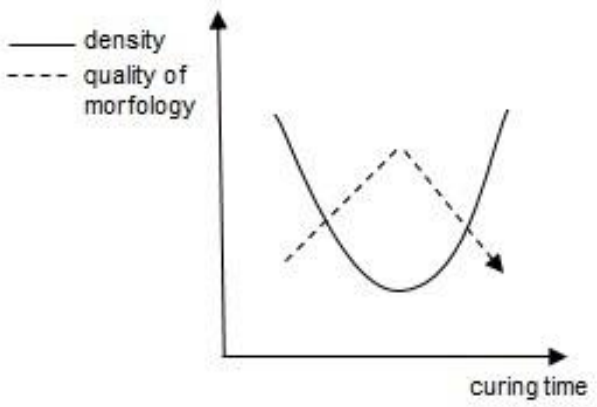

b)

Fig.7: a) PURs obtained at different curing times by two steps of pressure release; b) qualitative trend of density and the quality of final morphology.

In order to study the effect of the sorption time, some PURs were obtained at 35°C and 4000 kPa of CO_2 pressure by fixing the curing time at 18 minutes. In Fig.8 it is possible to note that by doubling the sorption time from 2.5h to 5h, the final product is more foamed and the density decreases from 0.92 g/cm^3 to 0.70 g/cm^3.

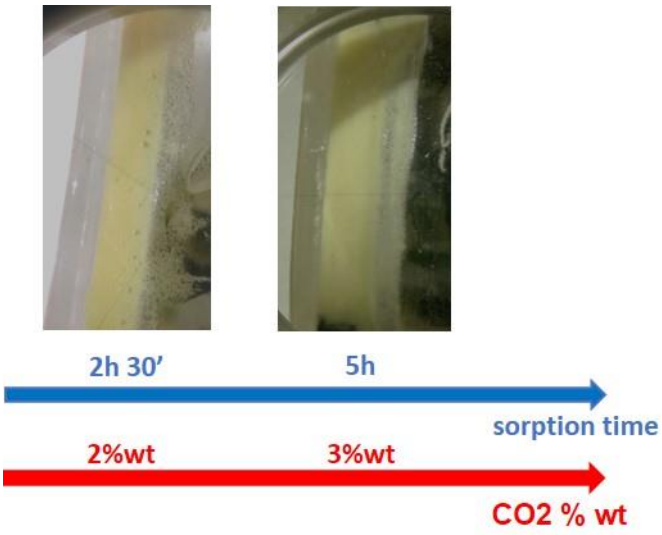

Fig.8: PURs obtained at different sorption times by two steps of pressure release.

The cellular structure of these foams was investigated by using a Scanning Electron Microscope (SEM). The samples were first sectioned with a razor blade and then coated with gold using a sputter coater. As it is possible to observe in Figs. 9a) and 9b), the PUR obtained by using a sorption time of 5h (Fig 9b) shows a finer morphology than by using a lower sorption time (2h 30') (Fig.9a).

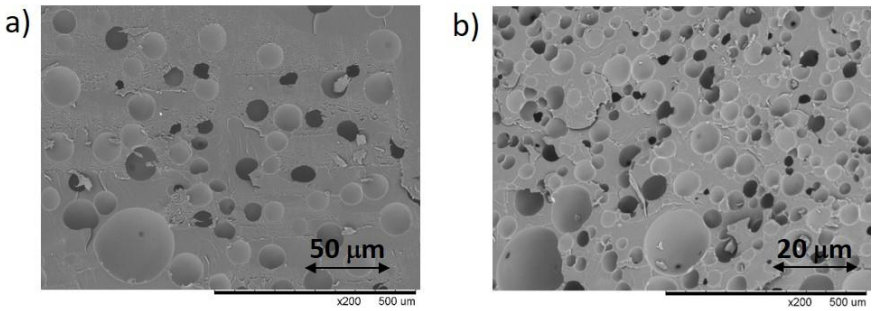

Fig.9: SEM images of PURs obtained by two steps of pressure release at different sorption times: a) 2h 30'and b) 5h.

5.4. Conclusions

The FT-NIR investigation shows that CO_2 is not an inert PBA in the considered chemical system. During polyurethane formation, the curing time increases by increasing CO_2 pressure meaning that the curing reaction is slowed down in presence of CO_2. This kind of behavior could be attribute to the Lewis acid-base interaction between CO_2, polyol and tertiary amines used as catalysts in the formulation object of this thesis. Further investigations are necessary in order to confirm this hypothesis and possible additive effects that can slow down the curing reaction.

A new campaign of foaming tests were conducted by conducting a pressure release in two steps in order to help the formation of a big number of nuclei and to allow the nuclei growth, avoiding coalescence. The results obtained from these foaming tests confirm that it is necessary to control all the process variables (pressure drop rate, curing time and sorption time) in order to improve the final morphology of these PURs.

5.5. References

[1] M. Buback, J. Schweer, H. Tups, Near infrared absorption of fluid CO and CO_2, *Phys. B C* 139-140 (1986) 544.

[2] J. Bürck, G. Wiegand, S. Roth, H. Mathieu and K. Krämer. Quantitative in-line analysis in supercritical CO_2 using fibre-optic NIR spectroscopy and multivariate calibration: a potential method for monitoring continuous flow processes. *J. Near Infrared Spectrosc*. 12 (2004) 29.

[3] T. Guadagno, S. G. Kazarian. High-Pressure CO_2-Expanded Solvents: Simultaneous Measurement of CO2 Sorption and Swelling of Liquid Polymers with in-Situ Near-IR Spectroscopy. *J. Phys. Chem. B.* 108 (2004) 13995.

[4] T. Nagata, M Tanigaki, M. Ohshima. In-Line NIR Sensing of CO_2 Concentration in Polymeric Foaming Extrusion Process. *J. Cell. Plast.* 38 (2002) 11-30.

[5] W. J. Moore. Physical Chemistry, 4th Edt. Prentice- Hall, Inc., Englewood Cliffs, 1972.

[6] F. Stassin, R. Jérome. Effect of pressure and temperature upon tin alkoxide-promoted ring-opening polymerisation of ε-caprolactone in supercritical carbon dioxide. *Chem. Commun.* (2003) 232–233.

[7] M. E. Paulaitis, G. C. Alexander. Reactions in Supercritical Fluids. A Case Study of .the Thermodynamic Solvent Effects on a Diels-Alder Reaction in Supercritical Carbon Dioxide. *Pure Appl. Chem.* 59 (1987) 61.

[8] H. Tiltscher, H. Hofmann. Trends in High Pressure Chemical Reaction Engineering. *Chem. Eng. Sci.* 42 (1987) 959.

[9] H. Tilscher, H. Wolf, J. Schelchshorn. Utilization of Supercritical Fluid Solvent Effects in Heterogeneous Catalysis. *Ber. Bunsenges. Phys. Chem.* 88 (1984) 897.

[10] P. E. Savage, S. Gopalan, T. I. Mizan, C. J. Martino, E. E. Brock, Reactions at Supercritical Conditions: Applications and Fundamentals AIChE Journal July 1995 Vol. 41, No. 7, 1723.

[11] J. Dupuy, S. Benali, A. Maazouz, G. Lachenal, D. Bertrand. FT-NIR monitoring of a scattering polyurethane manufactured by reaction injection molding (RIM): univariate and multivariate analysis versus kinetic predictions. *Macromol. Symp*. 184 (2002) 249.

[12] B. R. Osborn, T. Fearn, P. H. Hindle. Practical NIR Spectroscopy with Applications in Food and Beverage Analysis. 2nd Edt. Addison-Wesley Longman Ltd, 1993.

[13] J. Xiong, D. Li, J. Zhang, D. Hong-Fei. GUO, B. Wang, W. Liu. Surfactants for polyurethane foams. Patent WO 2016095128 A1 June 23, 2016.

[14] M. Ç. Öztürk, Cyril S. Ume, E. Alper. Reaction Mechanism and Kinetics of 1,8-Diazabicyclo[5.4.0]undec-7-ene and CarbonDioxide in Alkanol Solutions. *Chem. Eng. Technol.* 35 (2012) 2093.

[15] A. Dibenedetto, M. Aresta, M. Narracci. Carbon dioxide capture by amines: increasing the efficiency by aminestructure modification. *Fuel Chem. Preprint Papers* 47 (2002) 53.

[16] P. N. Sutar, A. Jha, P. D.Vaidya, E. Y. Kenig. Secondary amines for CO_2 capture: A kinetic investigation using N-ethylmonoethanolamine. *Chem. Eng. J.* 207–208 (2012) 718.

[17] Y. G. Ko, S. S. Shin, U. S. Choi. Primary, secondary, and tertiary amines for CO_2 capture: Designing for mesoporous CO2 adsorbents. *J. Colloid Interface Sci.* 361 (2011) 594.

[18] A. Furstner, K. Langemann. Macrocycles by Ring-Closing Metathesis. *Synthesis* 7 (1997) 792.

[19] K. Wittmann, W. Wisniewski, R. Mynott, W. Leitner, C. L. Kranemann, T. Rische, P. Eilbracht, S. Kluwer, J. M. Ernsting, C. J. Elsevier. Supercritical Carbon Dioxide as Solvent and Temporary Protecting Group for Rhodium-Catalyzed Hydroaminomethylation. *Chem. A. Eur. J.* 7 (2001) 4584.

[20] P. G. Jessop, S. M. Mercer, D. J. Heldebrant. CO_2-triggered switchable solvents, surfactants, and other materials. *Energy Environ. Sci.* 5 (2012) 7240.

[21] W. Leitner, M. Holscher. Regulated Systems for Multiphase Catalysis. Springer, 2008.

Chapter 6: Summary and future developments

In this Chapter, it is reported a summary of the main results obtained in this Ph.D. thesis and possible future developments.

6.1. Summary of the main results

CO_2 sorption measurements in polyol and PMDI

CO_2 sorption in polyol and in PDMI, the two components of the PUR formulation under investigation, was measured by using a fully-experimental, coupled gravimetry-Axisymmetric Drop Shape Analysis. In particular, solubility, mutual diffusivity, specific volume and interfacial tension at 35°C have been measured for polyol/CO_2 solution at CO_2 pressures up to 8000 kPa, while for PMDI/CO_2 solution up to 5500 kPa. The results in the case of polyol/CO_2 solution were shown quite a large CO_2 solubilization (up to 17% ca. in the examined experimental range), in turn responsible for a moderate swelling of the polyol and an extensive effect on the interfacial tension, which reaches vanishing values at the highest investigated pressure. The sorption isotherm for the PMDI/CO_2 solution were shows a monotonic increase of the CO_2 solubility as a function of pressure, up to 6% ca. at a pressure of 5000 kPa. In particular, CO_2 extraction of some lower molecular weight fractions at CO_2 pressure above 5000 KPa was observed in the case of PMDI. For this reason, in order to avoid CO_2 extraction, foaming experiments were conducted at 4000 KPa.

Development of a novel lab-scale batch equipment for spectroscopy monitoring and production of rigid polyurethane foams

A new high-pressure batch equipment to monitor CO_2 sorption and polyurethane synthesis was developed. In particular, the pressure vessel, by its unique design, allows conducting CO_2 sorption, separately in the polyol and isocyanate phases and, at any sorption time (e.g. after attainment of equilibrium), mixing the components under high pressure and, at any stage of the curing reaction, release the pressure. Near infrared spectroscopy monitoring in reflection mode of both sorption and curing stages is possible by using a remote probe housed close to an optical window placed beneath the optical glass sample holder. On said equipment, foaming tests were conducted on a polyurethane/CO_2 system, at 35°C and at CO_2 pressures of 4000 kPa, by changing sorption time (or CO_2 amount) and curing time. From the PURs obtained, it has been evident that it is necessary to

conduct further foaming tests by changing some process variables (e.g. the pressure drop rate) to optimize the final morphology of the foam.

6.2. Future developments

For future developments in the achievement of microcellular polyurethane rigid foams characterized by very low thermal conductivity by using CO_2 as PBA, the following points should be considered:

- Increase the compatibility between polyol and PMDI. In this thesis, the two reactants in use have different viscosity (see Chapter 3 in Materials section), are not miscible and heterogonous nucleation happens at the interfaces generated when the two liquids get in contact due to the mixing;
- increase molecular weight of components in order to avoid CO_2 extraction of low molecular weight fractions of polyol and PMDI and so to have the possibility to conduct foaming experiments at CO_2 pressure higher than 4000 kPa;
- prevent the blowing reaction by changing some catalysts, to have CO_2 as the only blowing agent for bubbles development in the system.
- investigate the effect of different pressure drop rates on the final morphology of the foam.

Acknowledgments

I am grateful to Dow chemical Italy for the LIFE13-EN/IT/001238 project.
http://ec.europa.eu/environment/life ; www.dow.com/k12